NASA CR-72747
LMSC-A974469

FINAL REPORT

THERMAL PERFORMANCE OF MULTILAYER INSULATION

Prepared for

NATIONAL AERONAUTICS AND SPACE ADMINISTRATION

NASA LEWIS RESEARCH CENTER
Contract NAS3-12025

JAMES R. BARBER, PROJECT MANAGER

NOTICE

This report was prepared as an account of Government-sponsored work. Neither the United States, nor the National Aeronautics and Space Administration (NASA), nor any person acting on behalf of NASA:

A.) Makes any warranty or representation, expressed or implied, with respect to the accuracy, completeness, or usefulness of the information contained in this report, or that the use of any information, apparatus, method, or process disclosed in this report may not infringe privately-owned rights; or

B.) Assumes any liabilities with respect to the use of, or for damages resulting from the use of, any information, apparatus, method or process disclosed in this report.

As used above, "person acting on behalf of NASA" includes any employee or contractor of NASA, or employee of such contractor, to the extent that such employee or contractor of NASA or employee of such contractor prepares, disseminates, or provides access to any information pursuant to his employment or contract with NASA, or his employment with such contractor.

Requests for copies of this report should be referred to

National Aeronautics and Space Administration
Scientific and Technical Information Facility
P.O. Box 33
College Park, Md. 20740

NASA CR-72747
LMSC-A974469

FINAL REPORT

THERMAL PERFORMANCE OF MULTILAYER INSULATIONS

by

C. W. Keller

LOCKHEED MISSILES & SPACE COMPANY
Sunnyvale, Ca. 94088

prepared for

NATIONAL AERONAUTICS AND SPACE ADMINISTRATION

20 April 1971

CONTRACT NAS3-12025

NASA Lewis Research Center
Cleveland, Ohio 44135
James R. Barber, Project Manager
LIQUID ROCKET TECHNOLOGY BRANCH

FOREWORD

The Lockheed Missiles & Space Company is submitting this Final Report in partial completion of the requirements of Contract NAS 3-12025, Thermal Performance of Multilayer Insulations, dated 27 June 1968. The total scope of work, data, results, and conclusions pertinent to this program are presented in two report volumes: "Interim Report, Thermal Performance of Multilayer Insulations," NASA CR-72605, dated 20 April 1971, and this Final Report.

CONTENTS

ILLUSTRATIONS

TABLES

ABSTRACT

A composite multilayer insulation system composed of double-goldized Mylar radiation shields alternated with double silk net spacers was installed on a 4-ft-(1.22-m-) diameter tank calorimeter and tested in a vacuum environment. Thermal performance tests were conducted for hot boundary temperatures of 500°R (278°K) and 610°R (339°K), and for cold boundary temperatures of 140°R (77°K) and 37°R (20°K). Each combination of these temperatures was imposed with 20-, 10-, and 5-shield thicknesses of the composite system in place on the tank. Results of these tests were correlated with predictions based on a previously-developed analytical model using measured thicknesses and measured boundary temperatures. The experimental values of heat flux agreed with the analytical predictions within +50 to -30 percent.

Section 1

SUMMARY

The double-goldized Mylar/silk net insulation system, installed and tested on the 4-ft-(1.22-m-) diameter tank calorimeter, was selected as the most promising of four multilayer systems investigated in the analytical and experimental studies conducted earlier in the program. Initially, 20 shields and 20 double net spacers, with a single Dacron net outer layer, were installed on the calorimeter. Each shield and each spacer layer was composed of upper and lower polar caps and cylindrical sections cut to fit the compound curvature of the tank. These shields and spacers were installed one at a time such that the shield joints overlapped slightly and were taped in place, whereas the net spacer joints were butted and sewn together. Thermocouples were installed at four different locations on the tank surface in order to obtain measured temperature profiles through the thickness of the insulation during the tests. At each location, the thermocouples were firmly attached to the outer surface of selected radiation shields.

Subsequent to installation of the insulation and the thermocouples, tangential x-ray exposures were obtained at 22 locations over the tank surface. Local thickness measurements, obtained from these x-rays, were used to determine layer density values for prediction of thermal performance.

Prior to initiation of the first test series, conducted with the 20-shield system, the insulated calorimeter was installed in a large vacuum chamber and leak tested using GHe. Then, additional x-ray measurements were obtained, the chamber was evacuated, and the calorimeter tank was filled with the test cryogen. For each test run conducted, tank pressure and the desired hot boundary temperature values were set to provide a constant heat rate into the tank, once thermal equilibrium had been achieved. Temperatures, pressures, and boiloff flowrate measurements were recorded at discrete intervals

throughout the transient and steady-state periods of each test.

During the test program, four combinations of hot and cold boundary temperatures were imposed for each of 20-, 10-, and 5-shield insulation thicknesses. Hot boundary temperatures of 500°R (278°K) and 610°R (339°K) were achieved by circulating chilled and heated water, respectively, through hot boundary shroud heat exchangers. Cold boundary temperatures of 140°R (77°K) and 37°R (20°K) were achieved by using LN_2 and LH_2 test fluids, respectively.

After completion of the four 20-shield tests, the outer 10 layers of the insulation were removed. Again, after completion of the four 10-shield tests, the outer 5 layers of the insulation were removed. During the final 5-shield test series, a total of five tests were conducted since the results of the initial test conducted for boundary temperatures of 500°R (278°K) and 37°R (20°K) were inconclusive and this test was rerun. Seven different sets of x-ray measurements, which yielded local insulation thicknesses at 22 locations over the tank surface, were obtained during the test program. Of these, three sets were obtained with 20 shields and 21 spacer layers in place on the tank, one set was obtained with 10 shields and 11 spacer layers in place, and the last three sets were obtained with 5 shields and 6 spacer layers in place.

Predictions of the expected heat flux for each test run were made using the analytical model developed earlier in the program. Layer density values, derived from the x-ray measurements, and measured boundary temperatures were used in these predictions.

It was found from analysis of the test results that measured heat flux values could be correlated with the predicted values within +50 to -30 percent. Also, it appears from the test results that insulation layer density values could have been significantly changed between test runs by gas flow forces imposed during evacuation and repressurization cycles. This could not be verified conclusively since the magnitudes of the apparent changes in layer density were within the tolerances associated with the x-ray thickness measurements.

Section 2

INTRODUCTION

This report describes the work performed under Task III of a 24-month analytical and experimental study program conducted to investigate thermal performance of 4 promising multilayer insulations when exposed to a vacuum environment. Descriptions and results of Tasks I and II of the program are presented in the Interim Report, NASA CR-72605 (Ref. 1). This work was sponsored by the Liquid Rocket Technology Branch, Lewis Research Center, National Aeronautics and Space Administration, Cleveland, Ohio.

The overall goal of the program was the development and verification of an analytical technique for accurately predicting the thermal performance of multilayer insulations when applied to an actual cryogen storage tank. The technical approach to the problem was to determine by small-scale laboratory tests the heat transfer characteristics, in a direction normal to the insulation layers, of several candidate insulations as a function of boundary temperatures, compressive loading of the composite, thickness, and number of layers. These data were then used to derive and subsequently to evaluate the accuracy of an analytical expression which describes the one-dimensional thermal performance of each candidate insulation in terms of the above variables. Verification of the usefulness of the expression as a means for predicting tank-installed performance then was accomplished through testing of one selected insulation system on a 4-ft-(1.22-m-) diameter tank calorimeter.

To accomplish the overall program objective, the study effort was divided into three consecutive tasks as noted above. During the initial phase, Task I, the accuracy and repeatability of the experimental apparatus used for heat transfer studies was demonstrated. Also, the degree of sample-to-sample reproducibility was established for two types of multilayer insulation. Task II was directed toward the measurement of heat transfer characteristics

of multiple specimens of four insulations and the derivation and subsequent evaluation of an analytical model describing the thermal conduction and radiation processes for these insulations. Using this model, equations were derived for predicting the thermal performance of the tank test insulation in terms of boundary temperatures, layer density, and total number of layers. Under Task III one insulation system, double-goldized Mylar with double silk net spacers, was applied to the 4-ft-(1.22-m-) diameter tank, and tests were conducted to demonstrate the accuracy of the thermal performance prediction procedure.

The Interim Report describes in detail the approaches taken in Task I to measure thermal performance and to demonstrate measurement accuracy and repeatability. Specifications for the test materials and procedures established for preparation of test specimens are described. Results of heat transfer tests of multiple specimens of two insulations are presented to illustrate the reproducibility of these materials. Tests were conducted with LN_2 and LH_2 cryogens. The two insulations used for these studies were double-aluminized 1/4-mil Mylar with two layers of silk net for each spacer, and crinkled, single-aluminized 1/4-mil Mylar. These were selected as they represent the separate-spacer and integral-spacer concepts in multilayer insulation. The effects of compressive loading and number of layers on thermal performance also were qualitatively evaluated in the Task I work.

A flat plate type of apparatus was chosen for the thermal performance tests since with this device heat transfer rates can be determined as a function of applied compressive pressure and thickness on a single specimen without disrupting the specimen or vacuum or temperature conditions. The "boiloff calorimeter" technique was used for heat-flux measurements. It has good accuracy over the range of the test requirements of this program and is readily adaptable to the flat plate configuration (Ref. 2 and 3. The Lockheed 16-in.-(40.6-cm-) diameter double-guarded flat plate apparatus (Ref. 3) was used for all laboratory heat transfer studies in Tasks I and II.

As thermal radiation plays an important role in certain regimes of multilayer insulation heat transfer (Ref. 4), it is necessary to understand the behavior of the thermal radiation characteristics of the reflective shields as a function of temperature in the analysis of the overall heat transport process. Measurements of the total hemispherical emittance, as a function of temperature, of several samples of each type of reflective shield were initiated in Task I in order that the data would be available for the analytical studies of Task II.

The derivation of the analytical heat transfer model in Task II also is discussed in the Interim Report. The resultant equations for computation of the heat flux through the four insulations are given in terms of temperature, compressive pressure or layer density, number of layers and radiative properties of shields and spacers.

The four multilayer insulations investigated in Task II were:

- Double-aluminized 1/4-mil Mylar with two layers of silk net* for each spacer
- Double-goldized 1/4-mil Mylar with two layers of silk net for each spacer
- Crinkled, single-aluminized 1/4-mil Mylar
- Double-aluminized Mylar with Tissuglas** paper spacers

A detailed description of the tank calorimeter test apparatus and the facilities used to conduct the Task III boiloff tests is presented in Section 3 of this report. Procedures developed and used to install the double-goldized Mylar/silk net composite, to assess its thickness in selected locations over the tank surface, and to conduct the boiloff tests also are presented and discussed.

---

* John Heathcoat Company
** Pallflex Products Company

Section 3

TASK III - INSULATION INSTALLATION VERIFICATION

The primary objective of this program task was to verify the analytical expression developed in Task II for predicting thermal performance of a selected multilayer insulation in a vacuum environment. Of the four multilayer systems investigated during the program, the composite with double-goldized 1/4-mil (0.0064-mm) Mylar shields and two 5-mil (0.13-mm) silk net spacers per shield was selected for this work. This particular system was selected because the flat plate calorimeter data obtained for it in Task II exhibited good reproducibility characteristics and correlated well with the analytical model. In addition, it was found that the Mylar shields and silk net spacers could be fit and installed readily on the compound-curved surfaces of the 4-ft-(1.22-m-) diameter tank calorimeter used for the Task III boiloff tests.

In order to obtain sufficient thermal performance data with which to assess the validity of the analytical expression, twelve boiloff tests plus one test rerun were performed. Results of these tests were compared with predictions obtained from the analysis. The predictions were based on the number of insulation layers in place on the tank, measured layer density and shield emittance values, and measured boundary temperatures. Three different series of four boiloff tests each plus the one test rerun were conducted. Prior to the first series, 20 shields and 20 double silk net spacers with a single Dacron net external layer were installed on the tank calorimeter. Subsequent to this series, the outer layers were removed and the second series was conducted with 10 shields and 11 double silk net spacers still in place on the tank. The third and final series was performed with 5 shields and 6 double silk net spacers remaining on the tank.

Subsequent to installation of the 20-shield system on the tank, and again prior to evacuation of the multilayers for the first 20-shield tests, x-ray measurements were obtained after repressurization following the 20-shield test series, prior to evauation for the 10- and 5-shield test series, and again

after repressurization following the 5-shield test series and the one 5-shield test rerun. Insulation thickness and layer density values were determined from these measurements.

During each test series, four combinations of two hot and two cold boundary temperatures were imposed on the insulated calorimeter tank. Nominal hot boundary temperatures of either 500°R (278°K) or 610°R(339°K) were achieved by circulating either chilled or heated water, respectively, through heat exchanger shrouds mounted external to the insulation envelope. Nominal cold boundary temperatures of either 140°R (77°K) or 37°R (20°K) were achieved by filling the calorimeter tank with either LN_2 or LH_2, repsectively. During each test, the selected cryogen was maintained at constant pressure and the boiloff flowrate was measured to assess the total heat transferred through the insulation.

This section contains detailed descriptions of the Task III test apparatus and the facilities used to accomplish the test program. In addition, the procedures used to obtain and to evaluate the x-ray measurements, the performance predictions, and the boiloff test data are described. Tabulated and graphed data which resulted from these activities are presented and discussed.

3.1 TANK TEST APPARATUS

The appartus that was assembled to accomplish the Task III test program is illustrated schematically in Fig. 3-1. It consists of (1) a 4-ft-(1.22-m-) diameter tank calorimeter and support structure assembly, (2) a multilayer insulation system, (3) a two-piece hot boundary temperature control shroud, and (4) required instrumentation and plumbing system hardware. The general arrangement of these components within the vacuum chamber at Santa Cruz Test Base (SCTB) can be seen in the figure. Additional details concerning the apparatus are presented in the following paragraphs.

Instrumentation Sensors:

PTU-1	-	Tank Ullage Pressure	TGO	-	Cold Guard Outlet Temperature
PTU-2	-	Tank Ullage Pressure	TGI	-	Cold Guard Inlet Temperature
PV	-	Vacuum Chamber Pressure	TB	-	Baffle Plate Temperature
TV	-	Vent Line Temperature	TH-1	-	Hot Boundary Shroud Temperature
TLO	-	Liquid Level Overflow Temperature	TH-2	-	Hot Boundary Shroud Temperature
			TH-3	-	Hot Boundary Shroud Temperature

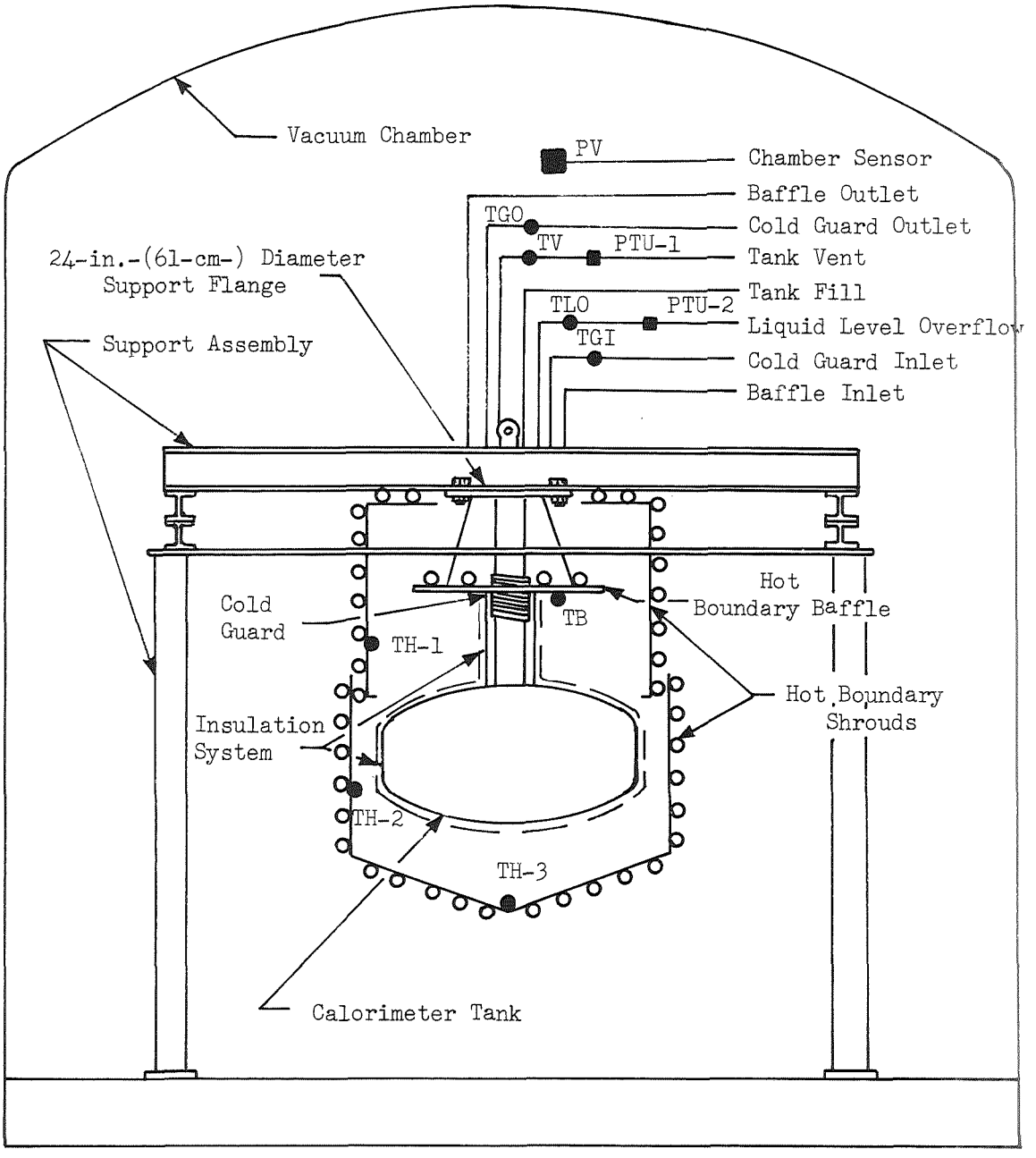

Fig. 3-1 Schematic of the Tank Calorimeters Test Apparatus

3.1.1 Tank Calorimeter and Support Assembly

The uninsulated 4-ft-(1.22-m-) diameter tank calorimeter is shown supported in the handling fixture in Fig. 3-2. The tank assembly consists of two flat elliptical bulkheads joined by a short cylindrical section and supported from a 5-in.-(12.7-cm-) diameter neck approximately 3.0 feet (0.914 meter) in length. The calorimeter shell was fabricated from 1/4-in.-(0.635-cm-) thick copper plate, while the neck and all associated plumbing lines were fabricated from stainless steel. The calorimeter assembly was initially developed and fabricated by Arthur D. Little,Inc., and was used during previous test programs for the NASA Lewis Research Center. It was provided as GFE hardware and modified by Lockheed for use during this contract program. A detailed description of the assembly as used in the previous programs can be found in Ref. 5 through 8.

The calorimeter is supported from a 24-in.-(61-cm-) diameter flange that previously provided an end closure to the vacuum chamber in which it was tested. In the current contract test setup, this flange was used to attach the calorimeter assembly to the support structure within the vacuum chamber at SCTB. As shown in Fig. 3-3, plumbing lines that provide for fill and vent of the calorimeter as well as for cold guard supply and vent and for hot boundary baffle supply and vent penetrate through this flange. The fill line penetrates the calorimeter through the neck support at a point just below the cold guard heat exchanger. The neck support also serves as the vent line in the region just above the tank. The cold guard heat exchanger is brazed to the outside surface of the neck at a point approximately half way between the tank and the support flange. During testing, it intercepts heat that otherwise would be conducted through the neck and into the tank.

Early in Task III, the original calorimeter vent line and the cold guard inlet line fittings were removed and replaced with fittings suitable for sealing cryogenic fluids within a high-vacuum environment. In addition,

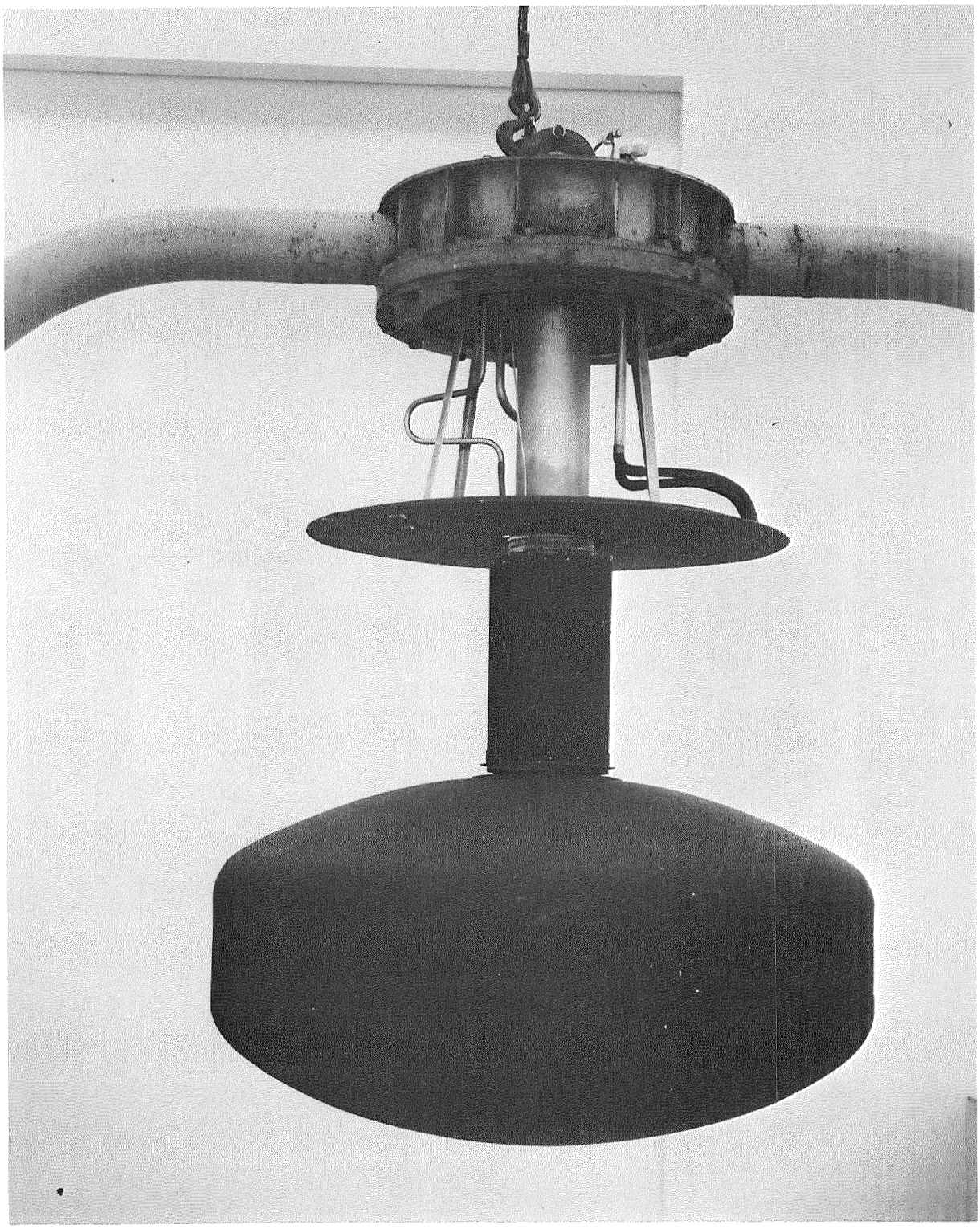

Fig. 3-2 Tank Calorimeter Supported in Handling Fixture

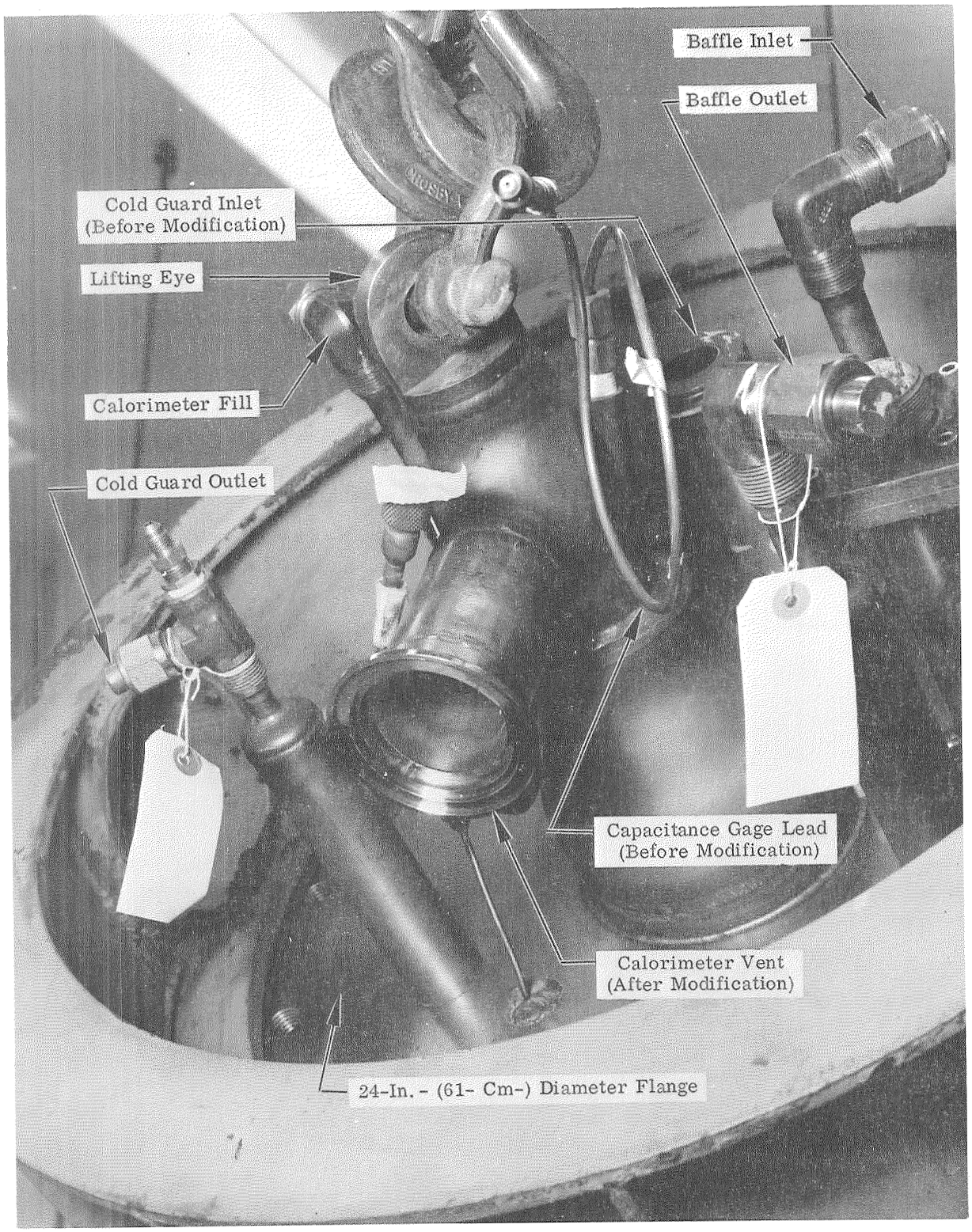

Fig. 3-3 Tank Calorimeter Plumbing Connections

the capacitance gage lead was severed just above the point where it penetrates the calorimeter neck. The 5/16-in.-(0.794-cm-) diameter capacitance gage sheathing tube was then extended and provided with a fitting so that it could be used as a liquid overflow line when the tank was filled. Although the gage lead could not be removed from the sheathing tube, it was determined during the pretest checkout that sufficient clearance existed between the lead and the tube to provide for overflow of the liquid cryogen.

The calorimeter test apparatus was supported within the vacuum chamber by an existing tubular aluminum stand. Aluminum channels were provided to support it within the stand. The 24-in.-(61-cm-) diameter flange from which the calorimeter is suspended was bolted to the cross channels. This attachment was removed, and the calorimeter was lowered together with the lower half of the hot boundary shroud, in order to gain access to the insulation between each of the test series. Fig. 3-4 shows the insulated calorimeter together with the support structure and the hot boundary shrouds just prior to installation in the vacuum chamber.

3.1.2 Multilayer Insulation System

Twenty double-goldized 1/4-mil (0.0064-mm) Mylar reflective shields, separated from the tank and from each other by 20 pairs of silk net spacers, were installed on the external surface of the tank and the lower half of the neck. A single outer layer of Dacron net was then installed to contain the insulation and to provide protection and support during handling and shipment of the insulated assembly from the Sunnyvale shop area to the SCTB test site. Fig. 3-5 is a photograph showing the completed insulation system.

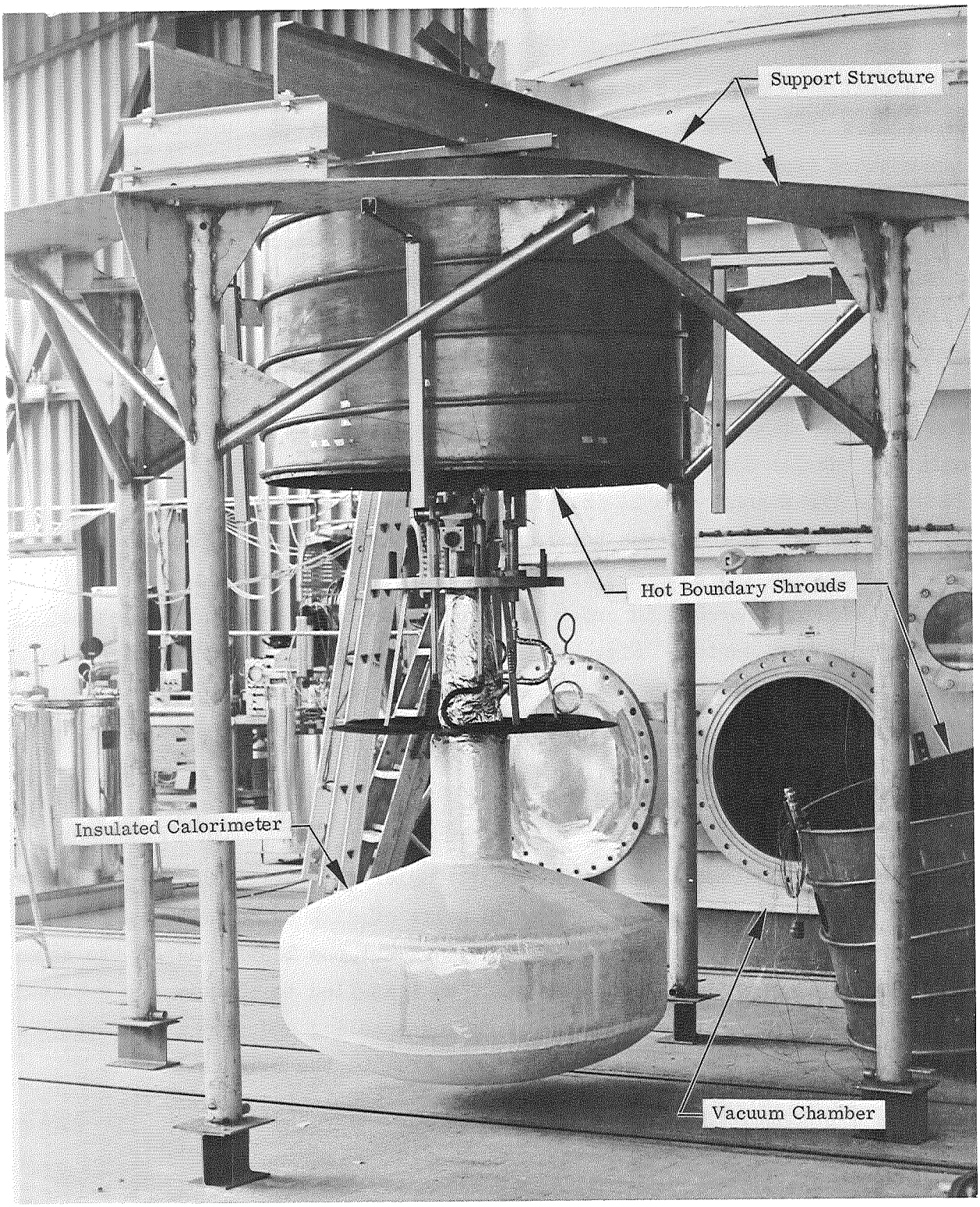

Fig. 3-4 Tank Test Apparatus prior to Installation in the Vacuum Chamber

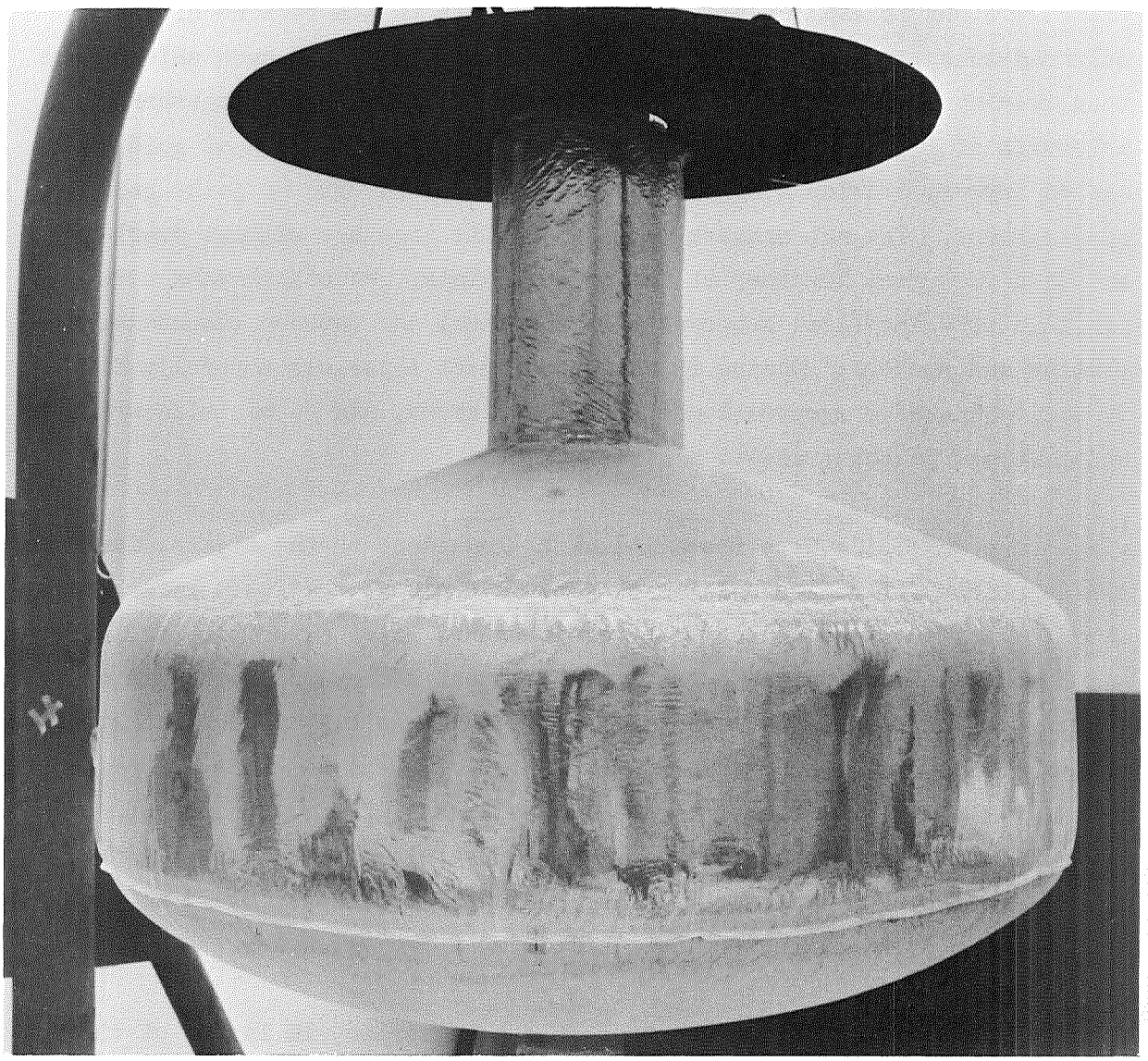

Fig. 3-5 Tank Calorimeter with Insulation Installed

Each of the reflective shields and each of the net spacers consisted of upper and lower polar caps, a tank cylinder segment, and a neck cylinder segment. A gore section was removed from each polar cap segment to allow it to fit smoothly over the double-contoured surfaces of the tank bulkheads. Slits were cut in each of the cylinder segments in the regions of the bulkhead-to-cylinder transitions. The mating segments of each shield were then overlapped from 1 to 2 in. (2.54 to 5.08 cm) and taped together at intervals of 3 to 4 in. (7.62 to 10.16 cm) with small pieces of goldized Kapton tape to provide a continuous integral shield with no joint gaps or penetrations. The net spacers were cut to fit together without overlaps, and then were sewn together at the mating joints. No attachments were provided from the first net spacer to the tank, nor between successive shields and spacers. During installation, each layer was carefully fitted to avoid excessive compression of previous layers, and to minimize wrinkles which formed in the transition areas.

Flat tungsten strips were installed at 21 locations on the eighth, fourteenth, and twentieth reflective shields to provide a visual thickness reference when tangential x-ray photographs were obtained later after the insulation had been installed and again prior to each test series. A schematic of the calorimeter showing these locations is presented in Fig. 3-6. Each strip was approximately 1-mil (0.0254-mm) thick, 0.1-in. (0.254-cm) wide, and 1.0-in. (2.54-cm) long. They were attached to the eighth and fourteenth reflective shields with goldized Kapton tape which completely covered each strip. Clear Mylar tape was used to attach the strips to the twentieth shield so that the locations could be positively identified for x-ray targeting.

Subsequent to completion of the 20-shield test series, 10 layers of the insulation were removed from the assembly to prepare it for the 10-shield test series. Similarly, an additional 5 layers were removed prior to the final 5-shield test series.

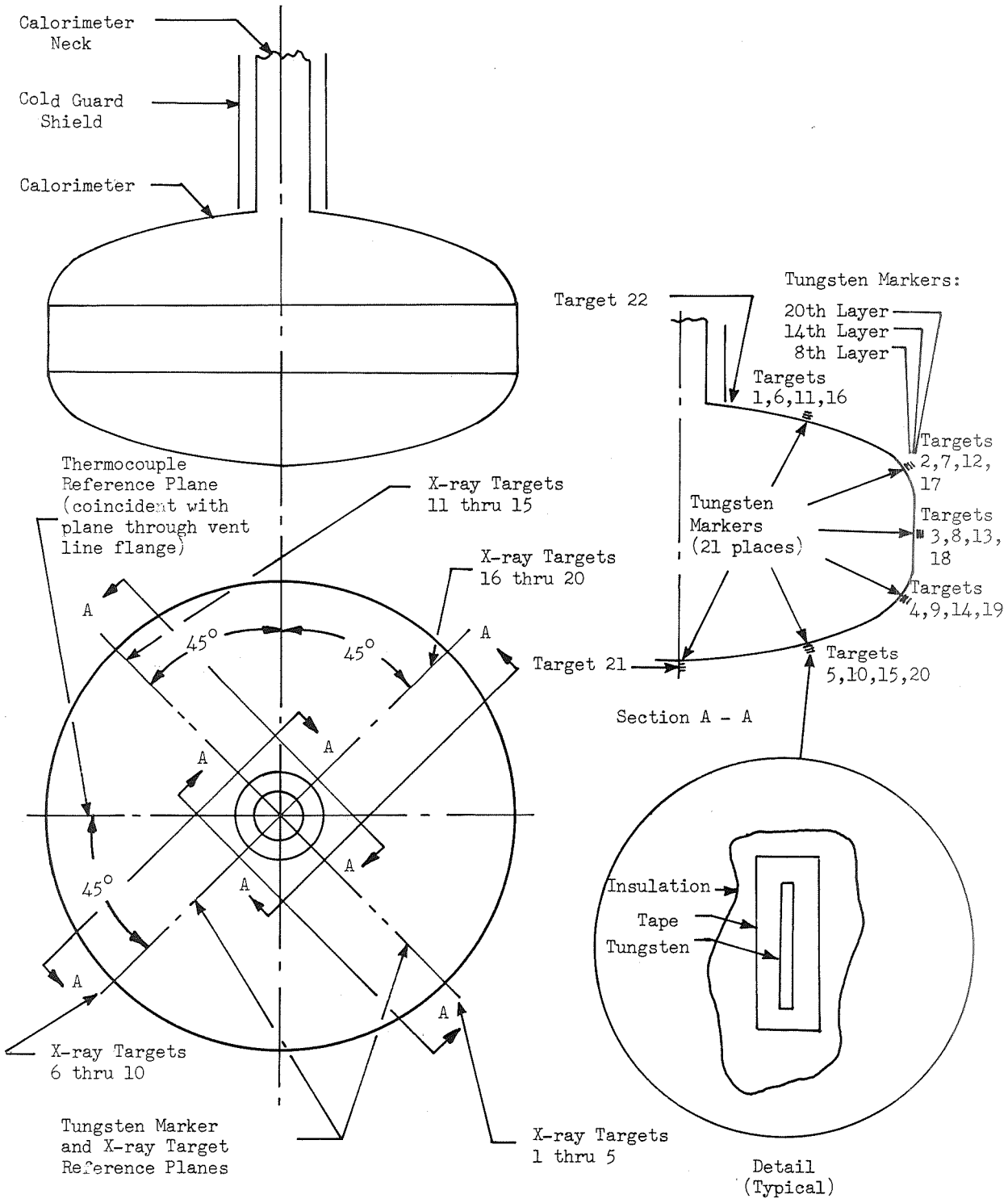

Fig. 3-6 Location of Tank Calorimeter X-Ray Markers and Exposure Targets

3.1.3 Hot Boundary Temperature Control Shrouds

Two overlapping cylindrical hot boundary shrouds were provided as GFE hardware in addition to the calorimeter. These shrouds were installed around the calorimeter during installation in the vacuum chamber. Both were supported from the channel structure to which the calorimeter assembly was attached. Their locations relative to the calorimeter can be seen in Figs. 3-1 and 3.4. Either chilled water or heated water was circulated during alternate runs through the heat exchangers located on the external surfaces of these shrouds to achieve the desired hot boundary temperature.

3.1.4 Instrumentation and Plumbing Components

Instrumentation sensors were installed in the test apparatus and in the vacuum chamber to provide measurements of (1) tank ullage pressure, (2) vacuum chamber pressure, (3) boiloff flowrate, (4) vent and liquid overflow line temperatures, (5) cold guard inlet and outlet temperatures, (6) hot boundary baffle and shroud temperatures, and (7) insulation temperatures. A detailed description of these sensors and the provisions made for acquisition of data from them is presented in Section 3.2.2.

One of the tank ullage pressure transducers was installed in the calorimeter vent line, just outboard of the Conoseal flange above the 24-in. (61-cm-) diameter support flange. The other was installed in the liquid overflow line at the point just outboard of the calorimeter neck where this line was extended. Both of these transducers were installed in tee fittings so that they could sense fluid pressures within the lines and the tank ullage space.

One of three boiloff flowmeters could be selected for any particular test run depending on the magnitude of the flow anticipated. These flowmeters were located in the facility vent line, to which the calorimeter vent line was attached, approximately 30 ft (9.14 m) outside of the vacuum chamber pass-through flange.

The vent line and liquid overflow line temperature sensors also were installed in tee fittings adjacent to the locations where the pressure transducers were installed as described above. These were probe-type sensors selected to provide measurements of fluid temperatures within the lines.

The cold guard inlet and outlet line temperature sensors also were probe-type thermometers which were used to measure fluid temperatures. These sensors were installed in tee fittings located just above the 24-in.-(61-cm-) diameter support flange. Both of the lines were insulated with a double thickness of spirally-wrapped single-aluminized Mylar from the point where the neck insulation was terminated to the vacuum chamber pass-through fittings. This was done to minimize the quantity of cryogen required by the cold guard, and to reduce the operating temperature differential between the inlet and the outlet for better control of the guard temperature and the cryogen flow characteristics. The cold guard and the neck above it also were insulated with 5 layers of single-aluminized Mylar to achieve these same objectives.

Four copper-constantan thermocouples were installed on the surfaces of the hot boundary baffle and shrouds (see Fig. 3-1) to provide measurements of the hot boundary temperatures. These were monitored during the tests so that the water supply temperatures could be adjusted as required.

Twenty-two copper-constantan thermocouples were installed in four groups within the multilayer insulation as the insulation was installed on the tank. The location of these sensors is shown in Fig. 3-7. The thermocouples within each of the three groups of 6 (locations B, C, and D in the figure) were referenced to the tank wall temperature in that respective location. The thermocouples within the single group of 4 (location A in the figure) were referenced to the tank wall temperature at location B. This latter group was used to determine the effectiveness of the insulation transition joint between the upper calorimeter bulkhead and the guarded neck.

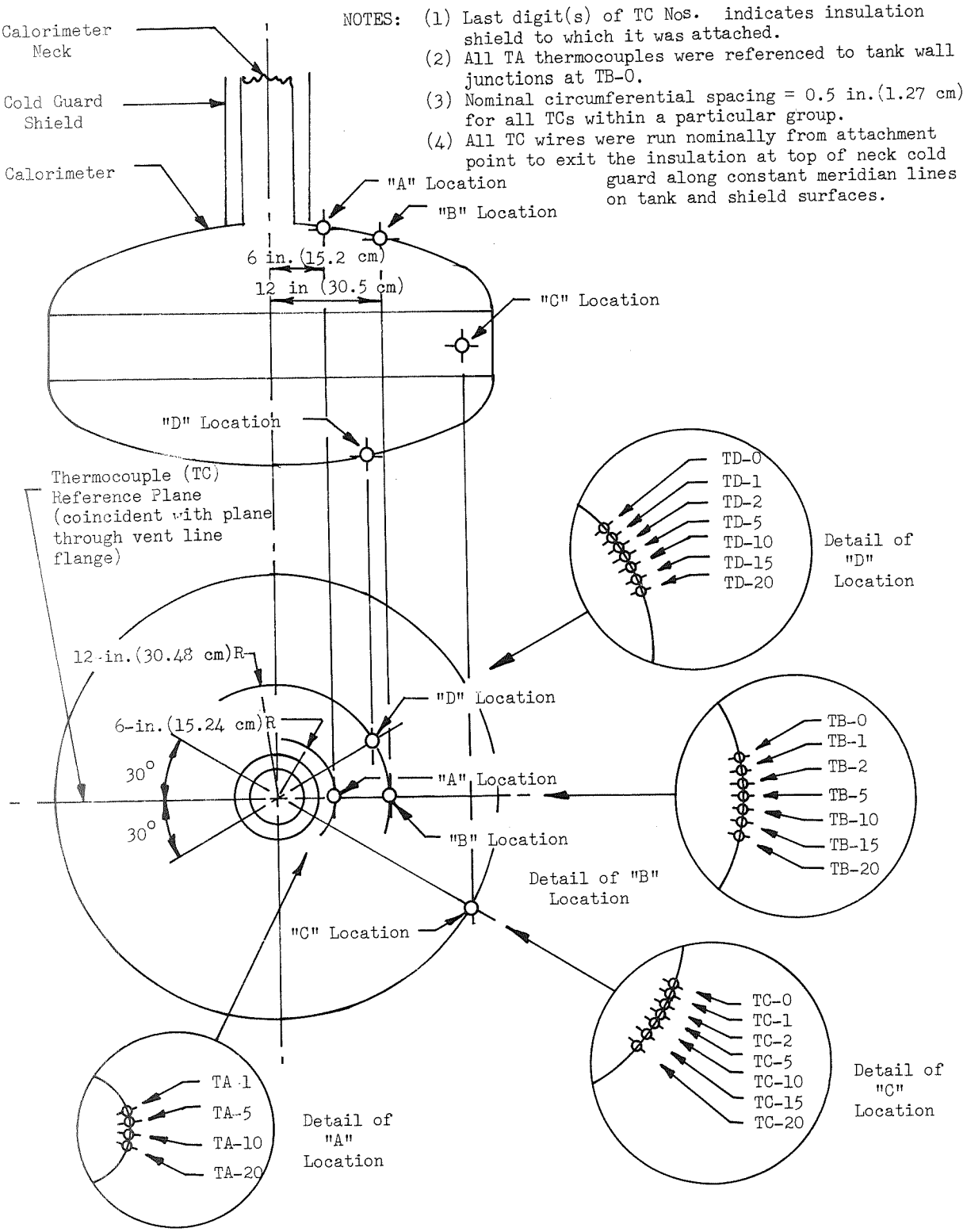

Fig. 3-7 Location of Calorimeter Insulation System Thermocouples

The thermocouples were checked out after fabrication by individually chilling each junction in a bath of LN_2, and by then referencing its output to that of a standard copper-constantan thermocouple maintained at 610°R (339°K) in a controlled environment package. The maximum deviation of the output of any one of the fabricated thermocouples from any other, or from values tabulated in Table A1 of NBS Report 9172, dated July 1968, was approximately 9 microvolts. This deviation corresponds to approximately 0.9°R (0.5°K) at LN_2 temperature, and is representative of the maximum error that was encountered during the Task III tests.

These thermocouples were fabricated from 40-gage, 3-mil-(0.08-mm-) diameter wire which was electrically insulated with a 1/2-mil-(0.013-mm-) thick Nylon coating. Each of the 22 thermocouples was referenced to an individual junction embedded into the calorimeter tank wall. These junctions were installed by inserting the bared ends of 30-gage, 10-mil-(0.25-mm-) diameter constantan wire into No. 80 drill size holes to a depth of approximately 1/8th in. (0.318) cm) and then by peening the copper around the wires to provide good electrical contact. After installation, each wire was bonded to the tank surface with Lefkoweld in the local area of the junction. Each of these reference junction wires then was taped to the calorimeter wall at approximately 12-in. (30.48-cm) intervals as shown in Fig. 3-8. Small pieces of clear Mylar tape were used to hold each wire in place along a constant meridian line from the junction location to a point on the calorimeter neck just above the flat circular radiation baffle where the primary neck insulation was terminated.

During subsequent installation of the insulation reflective shields and spacers, each individual thermocouple junction was attached to the external surface of the appropriate shield with a small piece of double-faced Mylar tape approximately 1/2 in. (1.27 cm) square. The tape was placed between the thermocouple and the reflective shield. The thermocouple wires then were run between adjacent multilayers along constant meridian lines to the area of the radiation baffle on the calorimeter neck. Small pieces of goldized Kapton tape were used

Fig. 3-8 Installation of Thermocouple Reference Wires

to secure the wires to the corresponding reflective shields at intervals. A continuous length of the goldized tape approximately 12 in. (30.48 cm) long and 1/2 in. (1.27) cm) wide was used to cover the thermocouple wires in the vicinity of each junction to ensure that the wire and the junction would operate at the temperature of the reflective shield in this local area.

After all primary insulation multilayers and thermocouples were installed, the individual thermocouple wires were connected to the respective reference junction wires in the local area of the radiation baffle near the calorimeter neck. During installation of each reflective shield and each thermocouple, electrical resistance measurements were made to ensure that the reflective shields were not shorted together and that the thermocouple circuits were continuous. In subsequently insulating the upper half of the calorimeter neck, two layers of single-aluminized Mylar were placed around the neck and the thermocouple wires for the tank reference and the first two reflective shields. Three additional layers were then placed around the previous layers and the remaining thermocouple wires.

3.2 TANK TEST FACILITIES

The Cryogenic Test Complex located at Lockheed's Santa Cruz Test Base (SCTB) was used to perform the calorimeter tank test program. An aerial view of the complex is shown in Figure 3-9. Specific areas of the complex that were pertinent to the program include (1) the test pad area, where the vacuum chamber (flight simulator), vacuum-pumping systems, and other cryogenic test facilities are located, (2) the control and instrumentation building, where the data-acquisition equipment is located, and (3) the cryogen and pressurant storage area, where the 13,000-gal (49.2-m^3) LH_2 storage dewar is located. These areas are described in greater detail in the following paragraphs. Numerous supporting systems that also were significant to the program are integrated throughout the complex. These include systems that provide for LN_2 and GN_2 storage and distribution, LH_2 and GH_2 dump, disposal, and vent, electrical power distribution and control, fire detection and warning, water deluge, closed-circuit television, voice communication, and other pertinent functions.

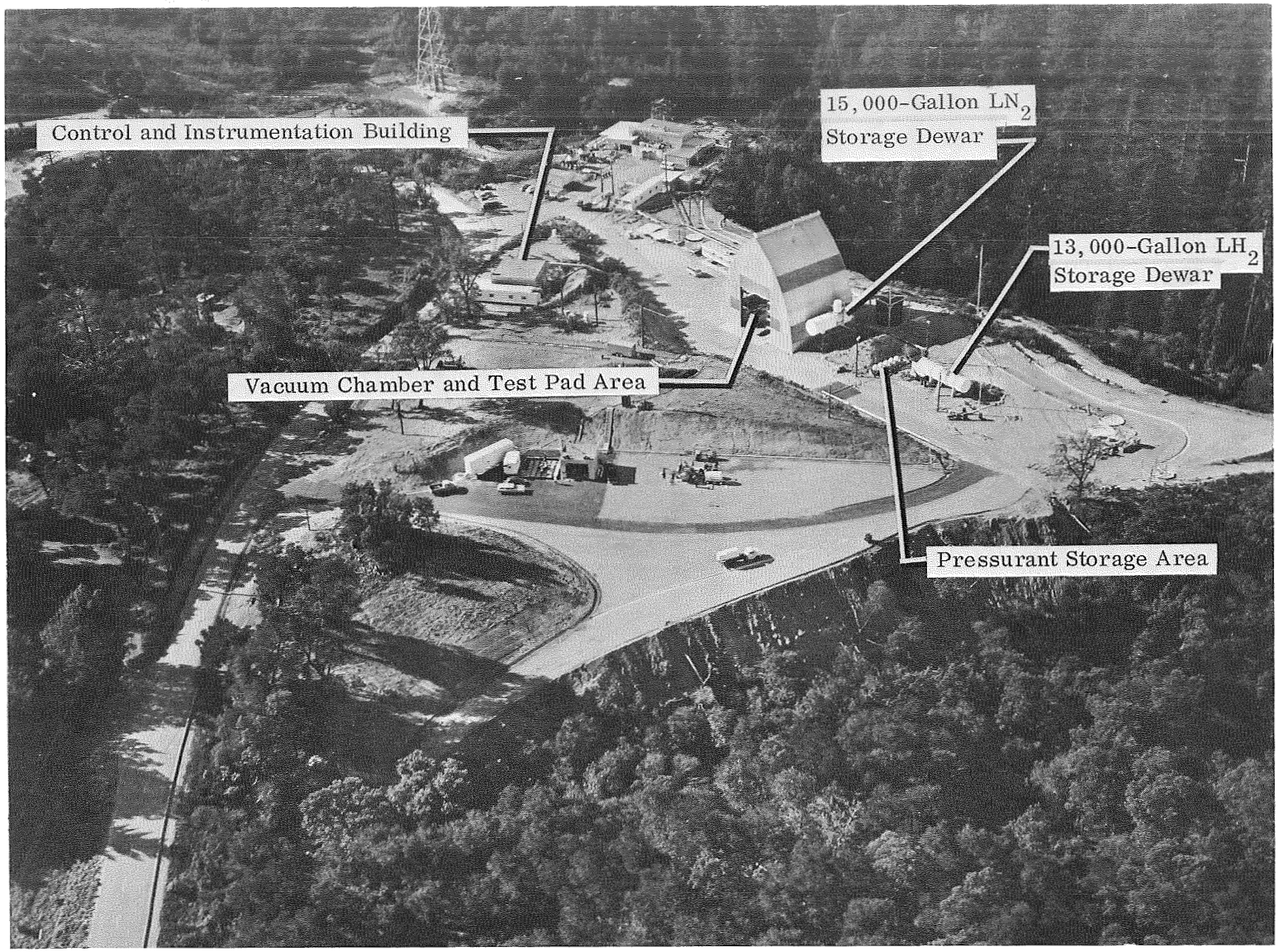

Fig. 3-9 Aerial View of Cryogenic Test Complex

3.2.1 Test Pad Area

The test pad area contains (1) the cryogenic vacuum chamber installation, wherein the 4-ft-(1.22-m-) diameter calorimeter test apparatus was located, (2) the vacuum-pumping systems, and (3) the hot boundary environment fluid transfer and storage system. The area surrounded by a trussed A-frame enclosure 75 ft (22.9 m) in height. The test pad is constructed of reinforced concrete, is approximately 80 ft (24.4 m) in length by 60 ft (18.3 m) in width, and contains tie-down rails, spaced every 3 ft (0.914 m), which run approximately half its length. A 12 ft (3.6 m) by 16 ft (4.9 m) by 18 ft (5.5 m) reinforced concrete blast wall, as well as a 36 ft (11 m) by 69 ft (21 m) by 15 ft (4.6 m) sand and dirt revetment, are located between the pad area and the cryogen and pressurant storage area.

Inside the A-frame enclosure, a 10-ton (9072-kg) capacity hoist with a 63-ft (19.2-m) hook clearance is available to handle test and facility hardware. The hoist is mounted on a monorail and has a 70-ft (21.3-m) traverse. A T-pad of reinforced concrete houses the instrumentation junction box, the controls junction box, and the electrical distribution box.

Cryogenic Vacuum Chamber Installation The cryogenic vacuum chamber, also referred to as the flight simulator, is 16 ft (4.9 m) in inside diameter and approximately 25 ft (7.6 m) in inside height. It can accomodate, in a vertical position, a test specimen 13 ft (4 m) in diameter and 17 ft (5.2 m) in length. The chamber is composed of four sections which include a base, two intermediate sections, and an upper section. The base is cylindrical and has an inside height of 4 ft (11-3/4 in. (1.518 m). This section contains 25 ports for plumbing and instrumentation connections. The two intermediate removable cylindrical sections are each 6 ft 11-1/2 in. (2.121 m) in height. Both of these were installed during reassembly of the chamber after installation of the tank calorimeter test apparatus.

The upper section is composed of a cylindrical segment 2 ft 1 in. (0.635 m) in height and an ellipsoidal head that contains 5 ports for plumbing and instrumentation connections. All chamber sections, including the base floor and all manifolds, flanges, ports, and fittings were fabricated from 304 stainless steel. The surfaces exposed to vacuum conditions were ground and polished to achieve a simulated No. 4 finish. Double O-ring flanges provide sealing between chamber sections, around all instrumentation and plumbing ports, and around the access door located in the base section. The chamber was designed to maintain a minimum pressure of 1.0×10^{-6} torr for extended test periods and a maximum pressure of 0.1 psig (690 N/m^2) without leakage.

The vacuum chamber is located near the center of the test pad area and inside the A-frame enclosure as shown in Fig. 3-10. The 110-in.-(2.794-m-) diameter ellipsoidal tank shown in the figure is one that was fabricated and used for a previously-completed hydrogen test program.

Vacuum-Pumping Systems The vacuum-pumping systems that were installed to service the cryogenic vacuum chamber include a two-stage steam ejector system and a high-vacuum mechanical/diffusion pumping system that can be used either in combination or separately. The steam ejector system can provide sufficient pumping rates to accurately simulate flight vehicle ascent pressure profiles from atmospheric pressure down to approximately 1.5 psia (1.0×10^4 N/m^2), corresponding to approximately 52,000 ft (15,850 m) in altitude. Pressure environments from atmospheric to 1.0×10^{-6} torr can be achieved with use of the high-vacuum system, but require longer pumping times than those that would be needed to simulate the ascent pressure profile for space/vehicles above 52,000 ft (15,850 m) altitude. Only the high-vacuum mechanical/diffusion pumping system was used during this program.

The high-vacuum mechanical/diffusion pumping system consists of two mechanical roughing pumps rated at 250 and 280 cfm (7.08 and 7.93 m^3/min), respectively, a 1300-cfm (36.8-m^3/min) displacement blower, and two 48-in. (121.9-cm) diffusion pumps. The two mechanical pumps can be operated

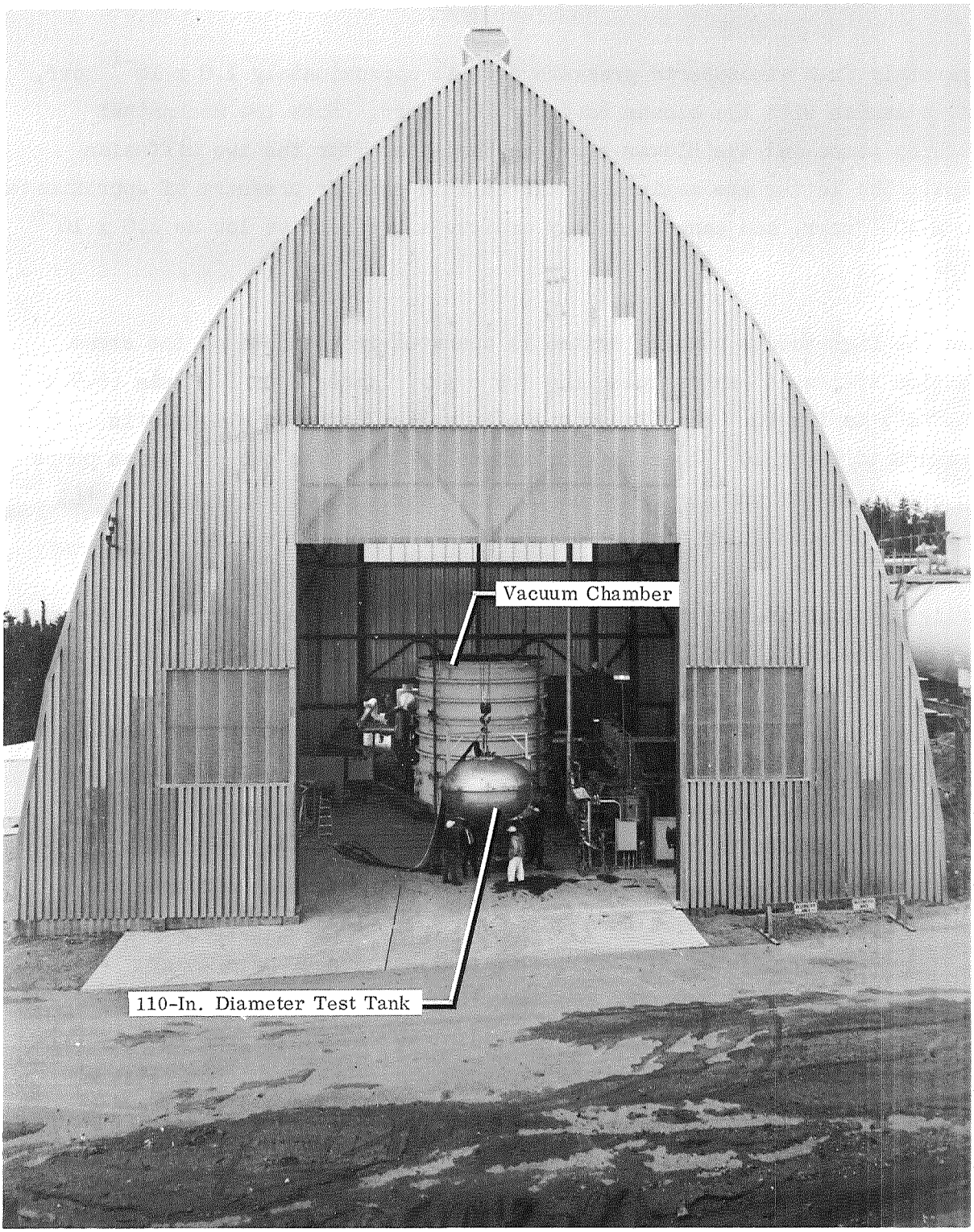

Fig. 3-10 Cryogenic Flight Simulator

separately from atmospheric pressure down to approximately 1.0×10^{-2} torr, and in series with the blower to 1.0×10^{-3} torr. Both the mechanical roughing pumps and the blower serve as fore-pumps for the two diffusion pumps. The latter are nominally started at a chamber pressure of approximately 1.0×10^{-1} torr, and can ultimately achieve a pressure as low as 1.0×10^{-6} torr.

When the high-vacuum pumping system is operated independent of the steam ejection system it can evacuate the dry empty chamber from 1.0 psia (6.9×10^{3} N/m^2) to 1×10^{-4} torr in approximately 2 hr, or from atmospheric pressure to 1.0×10^{-6} torr in approximately 4 hr. The two diffusion pumps can provide a net pumping speed of 1059 ft^3/sec (30,000 liter/sec) at the chamber wall when fully warmed up.

During the calorimeter tank test program, the high-vacuum pumping system was used to evacuate the chamber prior to filling the calorimeter with LH_2 or LN_2 to initiate each test series.

Hot Boundary Temperature Control Systems Hot water was supplied from the boiler to the hot boundary shroud heat exchangers during each of the test runs where a hot boundary temperature of 610°R (339°K) was required. The boiler is equipped with a thermostatic control system that was used to regulate the temperature of the water supply to 615 $\pm$5°R (343 $\pm$3°K). The hot water was circulated through the heat exchangers using a 25-gpm (1.58-liter/sec) pump. During the test runs where a hot boundary temperature of 500°R (278°K) was required, chilled water was supplied from an existing electronic equipment cooler to the shroud heat exchangers. This system also was thermostatically controlled to 495 $\pm$5°R (275 $\pm$3°K. During all test runs, the temperature of the hot boundary shrouds was monitored to ensure that the desired temperatures of 610°R (339°K) and 500°R (278°K) were achieved within $\pm$5°R ($\pm$3°K). Connecting lines from each of the two hot boundary water supplies to the shroud heat exchangers were provided with shutoff valves to permit independent selection of either water supply.

3.2.2 Control and Instrumentation Building

All hazardous tests that are performed in the cryogenic test pad area (described in Section 3.2.1 of this report) can be monitored and controlled remotely from the control and instrumentation building (blockhouse) shown in Fig. 3-9. This building is located approximately 350 ft (106.7 m) from the cryogenic vacuum chamber. It houses the control consoles for the test pad and cryogen storage areas, the data acquisition equipment, and the electrical power supplies, signal-conditioning, and distribution equipment. Control consoles located in the building include those used for (1) handling of liquid and gaseous hydrogen and nitrogen, pressurant gas, and purge gas, (2) the steam ejector and high vacuum pumping systems, and (3) the vacuum chamber thermal environment simulation systems. The control and instrumentation building also contains closed-circuit television monitoring equipment, emergency control system equipment, fire detection and warning system equipment, and other communication and control equipment used to set up, check out, and conduct cryogenic tests.

The data-acquisition equipment located in the building includes (1) a recording digital voltmeter, (2) a number of analog strip chart recorders, (3) various analog and digital display meters, (4) signal conditioning equipment, and (5) valve and equipment control. Table 3-1 identifies the data acquisition equipment that was used for each test function as well as other related information. Fig. 3-11 is a photograph of the interior of the instrumentation and control building and identifies the major elements that were used to accomplish the contract tests.

Recording Digital Voltmeter All primary data for this test program were gathered on the Dymec Model 2010J Recording Digital Voltmeter. This data-acquisition system has a total channel capacity of 400, of which approximately 34 channels were used on this program. The system operates in the following fashion: Analog output voltage levels from instrumentation transducer functions located in the test system are scanned (sampled), converted from

Table 3-1

TEST INSTRUMENTATION AND DATA ACQUISITION EQUIPMENT

Instrumentation Function	Sensor Description				Measurement Range	Estimated System Accuracy
	Code	Type	Mfg	Model No.		
Pressure, Tank Ullage	PTU-1	Strain Gage	Statham	PA285TC	0-25 psia (0-1.7 x 10^5 N/m^2)	± 0.5 psi (± 3450 N/m^2) (a)
Pressure, Tank Ullage	PTU-2	Transducers	Statham	PA285TC	0-25 psia (0-1.7 x 10^5 N/m^2)	± 0.5 psi (± 3450 N/m^2) (a)
Pressure, Vac Chamber	PV	–	Fredricks	3A	10^{-3} to 10^{-6} torr	(b)
Flowrate, Boiloff	FB	Thermal Mass	Rosemont	124AD168B4	0-0.2 lbm/hr (0-0.09 kg/hr)	± 2 percent of full scale
↓	↓	↓	Rosemont	124AD101B5	0-1.2 lbm/hr (0-0.54 kg/hr)	↓
↓	↓	↓	Hastings	AHL25X	0-8.0 lbm/hr (0-3.6 kg/hr)	↓
Temp, Vent Line	TV	Platinum RTB	Rosemont	150MA10	35-180°R (19-100°K)	±0.3°R (LN_2); ±0.6°R
Temp, Liquid Overflow	TLO	↓	↓	↓	↓	↓
Temp, Guard Outlet	TGO					
Temp, Guard Inlet	TGI					
Temp, Baffle Plate	TB	CuCn-TC (150°F)	–	–	500-610°R (278-339°K)	Ave. ±1°R (± 0.6°K) (c)
Temp, Hot Baffle No. 1	TH-1	↓	–	–	↓	↓
Temp, Hot Baffle No. 2	TH-2		–	–		
Temp, Hot Baffle No. 3	TH-3		–	–		
Temp, Insul Location A	TA-1	CuCn-TC (Tank)	–	–	35-610°R (19-339°K)	Ave. ±2°R (± 1.1°K) (c)
↓	TA-5	↓	–	–	↓	↓
	TA-10		–	–		
	TA-20		–	–		
Temp, Insul Location B	TB-1		–	–		
↓	TB-2		–	–		
	TB-5		–	–		
	TB-10		–	–		
	TB-15		–	–		
	TB-20	↓	–	–	↓	↓
Temp, Insul Location C	TC-1	CuCn-TC (Tank)	–	–	35-610°R (19-339°K)	Ave. ±2°R (± 1.1°K) (c)
↓	TC-2	↓	–	–	↓	↓
	TC-5		–	–		
	TC-10		–	–		
	TC-15		–	–		
	TC-20		–	–		
Temp, Insul Location D	TD-1		–	–		
↓	TD-2		–	–		
	TD-5		–	–		
	TD-10		–	–		
	TD-15		–	–		
	TD-20	↓	–	–	↓	↓

NOTES:

(a) Estimated system sensitivity = ± 0.01 psi (± 69 N/m^2)

(b) ±2.0 in each decade

(c) Varies with differential temperature between TC and reference

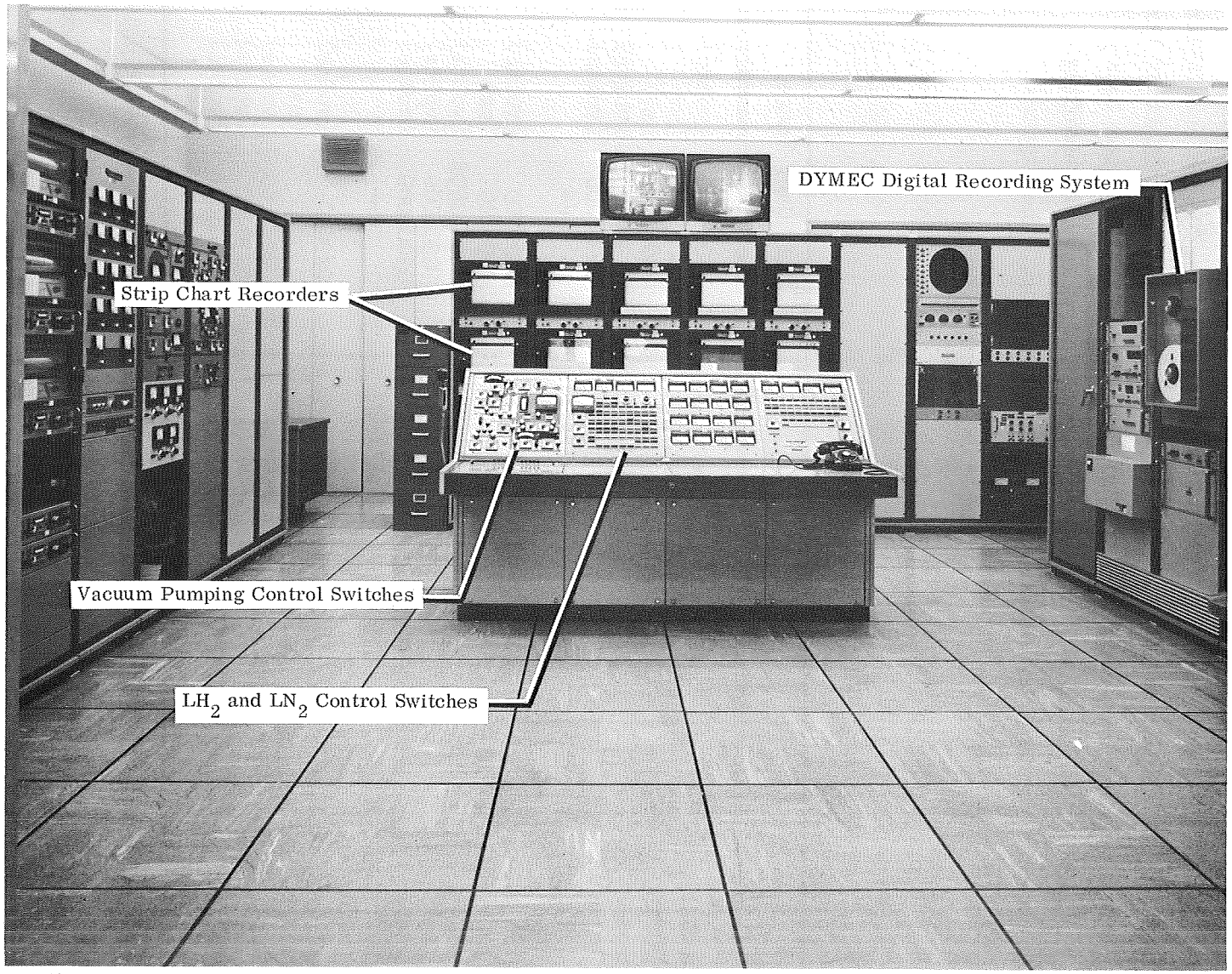

Fig. 3-11 Interior View of the Control and Instrumentation Building

analog to digital format, and printed on paper tape. Overall common mode rejection is 124 db for a 0.1 sec sample period; however, system resolution is affected by the sample period. Table 3-2 summarizes the system resolution for three typical sample periods. Overall system accuracy is ±1 digit of the last digit in the printout recording. Time is recorded on the paper tape from a digital system clock which provides standard time to all recording equipment within the instrumentation and control building. The digital printer tape format is illustrated in Fig. 3-12.

Table 3-2
DYMEC SYSTEM RESOLUTION

Sample Period	Range (Volts)	Full Scale Reading	Max. Over Range Reading
1 sec.	0.01	10.0000 (mv)	300.000 (volts)
	0.1	100.000 (mv)	300.000 (mv)
	1.0	1000.00 (mv)	3000.00 (mv)
	10.0	10.0000 (volts)	30.0000 (volts)
	100.0	100.000 (volts)	300.000 (volts)
	1000.0	1000.00 (volts)	---
0.1 sec.	0.01	010.000 (mv)	0300.00 (volts)
	0.1	0100.00 (mv)	0300.00 (mv)
	1.0	01.0000 (volts)	03.0000 (volts)
	10.0	010.000 (volts)	030.000 (volts)
	100.0	0100.00 (volts)	0300.000 (volts)
	1000.0	01000.0 (volts)	---
0.01 sec	0.01	0010.00 (mv)	00300.0 (volts)
	0.1	00100.0 (mv)	00300.0 (mv)
	1.0	001.000 (volts)	003.000 (volts)
	10.0	0010.00 (volts)	0030.00 (volts)
	100.0	00100.0 (volts)	00300.0 (volts)
	1000.0	001000.0 (volts)	---

Analog Strip Chart Recorders Certain instrumentation functions were selected for visual, analog display on Mosley Model 7100B Stripchart Recorders. Sixteen of these stripcharts are located in the control and instrumentation building in locations of good visual access for the test conductor at the control console.

Column Identification:

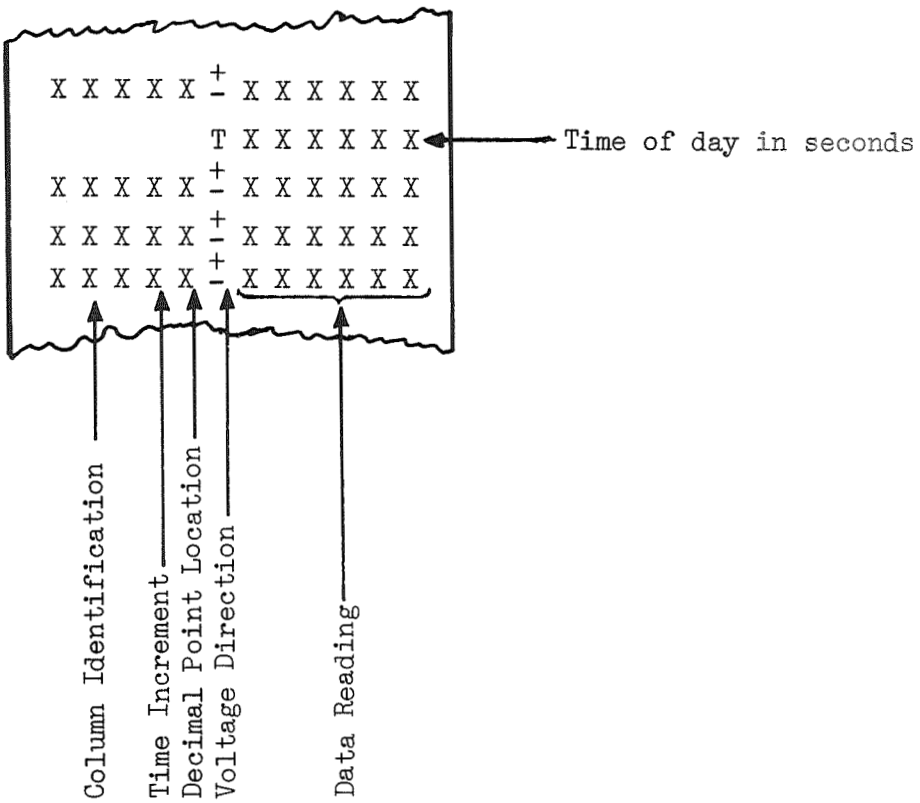

Example:

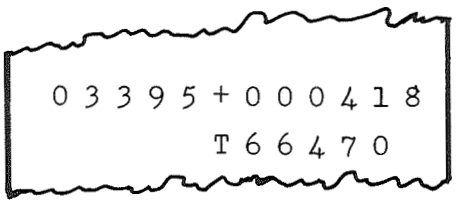

- Function on Channel 33
- Data taken at 66479 sec after midnight
- Transducer output +0.00418 volts

Fig. 3-12 Digital Printer Tape Format

These Mosley recorders incorporate electric writing and have a slewing speed of $\frac{1}{2}$ second full scale. Twelve chart speeds from 1 in./hr (2.54 cm/hr) to 0.1 in./sec (0.25 cm/sec) can be selected from a front panel-mounted selector switch. Each writing element is independently operating from plug-in span modules with sixteen front panel selected spans from 1 mv to 100 v full scale. Inputs are floating, have high common mode rejection, and present a load resistance of 1 megohm at null on all calibrated spans. The accuracy of these recorders is 0.2 percent of full scale with a linearity of 0.1 percent of full scale.

Anlog and Digital Display Meters Various instrumentation functions used for test operations control were displayed on standard analog ammeters, wattmeters, and digital voltmeters. These include, for example, vacuum chamber pressure, tank calorimeter pressure, and valve position indicators.

Signal Conditioning Equipment Instrumentation transducer functions for this program were electrical in nature, and power supplies and amplifiers were required for signal conditioning. These equipment components are located in the instrumentation and control building and include:

210 channels - B&F PC 2400 series power supplies
54 channels - Endevco 4401 power supplies
54 channels - Kintel 111, 112, 114 dc amplifiers
20 channels - Dynamics 7504 dc amplifiers
100 channels - Research, Inc., 150°F (338.8°K) TC reference
200 channels - LMSC liquid nitrogen TC reference

Valve and Equipment Controls During test operations considered potentially hazardous in nature, all equipment was controlled from the instrumentation and control building. Gaseous hydrogen, liquid hydrogen, liquid nitrogen, purge valves, and vacuum pumping equipment were operated by 28 vdc signals. The electrical power was controlled by switches located on the control console and identified in the Fig. 3-11 photograph. On the left hand section of the control console are the vacuum pumping control switches and on the center section are the hydrogen, nitrogen, and purge valve control switches.

3.2.3 Cryogen and Pressurant Storage Area

As shown in Fig. 3-9, all cryogens, pressurant gases, and purge gases used in performing cryogenic tests at the test pad complex are stored in dewars and pressure containers located outside of the A-frame enclosure in the test pad area. Hydrogen and high-pressure storage containers are isolated from the test pad area by the blast wall and earth/sand revetment previously described in Section 3.2.1. The major storage and distrubition components are described in the following paragraphs.

Liquid Hydrogen Storage Dewar The main liquid hydrogen storage dewar has a volume capacity of 13,000 gal (49.2 m^3) and rests on a concrete foundation, with a 20-ft by 50-ft by 2-ft (6.1-m by 15.2-m by 0.61-m) bed of crushed rock to act as a pebble bed flash heater in the event of spillage. The dewar is of dual tank construction, i.e. an inner tank of stainless steel and an outer tank of carbon steel, with an annular space of 12 in. (30.5 cm) between them. The annular space is filled with Perlite insulating material and has a vacuum of less than 5 microns prior to loading with a cryogenic fluid.

The boiloff rate with liquid hydrogen in the dewar does not exceed 1 percent of its volume per day. Other specifics on the dewar are: diameter, 10 ft (3 m); length, 40 ft (12.2 m); and maximum working pressure, 100 psig (6.9×10^5 N/m^2gage). All fittings and valves were fabricated from stainless steel. There is a thermocouple vacuum gage to monitor the vacuum in the annular space, and a carbon resistance probe to measure the liquid level of the cryogen in the dewar.

A vent stack is provided in the dewar area for the safe disposal of boiloff gases. A GN_2 purge capability is available in the vent stack in case of stack fires. A 2-psig (1.4×10^4 N/m^2gage) pressure is maintained in the dewar ullage space by means of a check valve in the vent stack.

Liquid Hydrogen Vaporizer The vaporizer is located below the LH_2 dewar and provides a means of pressurizing the dewar for the purpose of transferring either the liquid or gaseous cryogen from the storage area to the test pad. The equipment will provide a LH_2 flow at the pad of up to 2000 gpm (7.57 m^3/min) for a short duration, and a 500 gpm (1.89 m^3/min) steady flow rate. The unit consists of approximately 68 ft (20.7 m) of 4-in. (10.2-cm) tubing wherein, by environmental heating, the liquid cryogen is vaporized. The liquid cryogen enters the vaporizer from the dewar and is returned from the vaporizer into the ullage space of the dewar. The vaporizer is controlled by a closed-loop electrical pneumatic control system.

Liquid Nitrogen Storage Dewar The dewar has a volume capacity of 15,000 gal (56.8 m^3), and is of dual tank construction. The inner tank is stainless steel, and the outer tank is carbon steel, with an annular space between them. The annular space is filled with Perlite insulating material and has a vacuum of less than 5 microns prior to loading with a cryogenic fluid. The maximum working pressure is 20 psig (1.4×10^5 N/m^2 gage).

Cryogenic Fill Line The facility has a vacuum-jacketed cryogenic fill line which is approximately 160 ft (48.8 m) long. This fill line extends from the LH_2 dewar to the test pad and is in an open horizontal "U" shape to allow for horizontal expansion and contraction of the entire line. The line is made of stainless steel with a 3-in.-(7.6-cm-) diameter hard inner line and a 5-in.-(12.7-cm-) diameter expansion-jointed outer line. The annular space contains static vacuum of less than 5 microns at ambient temperature. There are seven sections of the line individually vacuum-jacketed and containing a pump-down port, a vacuum gage port, and a burst diaphragm. In addition, a relief valve has been connected to the inner line and installed between each shutoff valve on the cryogenic transfer line to prevent an excessive pressure build-up from an entrapment of the cryogen. A cross-connection with isolation valves was installed between the LN_2 storage dewar and this line to provide for filling of the tank calorimeter during the LN_2 test runs.

Dump Line and Disposal Area The dump line, which was not used in this program, runs from the test area to an emergency disposal area of crushed rock. The line is made of 4-in. (10.2-cm) aluminum pipe and has expansion-jointed sections to allow for expansion and contraction. In addition, this line also is connected directly to the LH_2 storage dewar in case it is necessary to dump the dewar for any reason.

The disposal of LH_2 requires that the gases escape at a distance high enough to avoid damage to the facility. For normal disposal of LH_2, a 60-ft (18.3-m) vent stack has been mounted on the dump line, a short distance upstream of the disposal area, to provide a means of discharging the hydrogen gas at a safe elevation.

Gaseous Nitrogen Supply The area has two liquid nitrogen storage tanks, each having a compressor and high pressure receiver. The storage tanks have the capacity to supply 500,000 standard ft^3 (14,160m^3) of nitrogen gas. The compressors deliver gaseous nitrogen at a rate of 40,000 standard ft^3(1133m^3) per hour to a high-pressure gas distribution system.

All of the nitrogen gas passes through a 40-micron filter before entering the distribution system of the cryogenic flight simulator facility. The gaseous nitrogen supplied to the distribution systems may be stored in any of three 3200 psig (2.2×10^7 N/m^2 gage) gas storage spheres. Each sphere has a capacity of 40 ft^3 (1.1 m^3).

Gaseous Helium Supply Gaseous helium is supplied from two high-pressure gas storage spheres. Each sphere has a capacity of 40 ft^3 (1.1 m^3), and can supply gaseous helium at 3200 psi (2.2×10^7 N/m^2).

Gaseous Purge Systems The purge systems installed in the facility have the capability of supplying gaseous hydrogen, helium and nitrogen for purge use.

This system can accommodate purging of the cryogenic lines and test article from an atmospheric air initial condition to an inerted condition containing gaseous hydrogen. This is accomplished by first purgining out the air with gaseous nitrogen, and then by purging out the nitrogen with gaseous hydrogen. An electrolytic hygrometer is employed for measuring water vapor in the purge gases. A water vapor content of 50 parts water vapor per million parts of gas must be achieved before the system is considered dry enough to avoid freezing of the control valves during the transfer of the liquid cryogens during a test.

After a liquid hydrogen flow test, the test hardware and cryogenic lines are inerted to a safe condition for post-test inspection by first purging the tank and cryogenic lines with gaseous hydrogen until they reach a temperature above the freezing point of nitrogen. The gaseous hydrogen is then removed from the system with a gaseous nitrogen purge.

When liquid hydrogen is stored in the dewar, a nitrogen purge is maintained on the dewar vent stack to prevent stack fires, and on all enclosures near the dewar which contain electrical equipment to prevent the collection of gaseous hydrogen in these confined areas. A nitrogen purge is also maintained on electrical equipment boxes near the test pad when LH_2 is present in the pad area.

Check valves are used throughout the purge system to avoid accidental mixing of the purge gases and to prevent air from entering the purged volumes.

3.3 INSULATION THICKNESS MEASUREMENTS

It was shown in the Task I and Task II work (Ref. 1) that the thermal performance of evacuated multilayer insulation is a strong function of mechanical compressive pressures which accrue from forces imposed during installation and evacuation. However, assessment of the compressive pressure values is impractical for any tank-mounted insulation due to the compound curvature of the tank and the insulation surfaces. Consequently, performance predictions must be based on some other property of the insulation system which can be quantitatively evaluated subsequent to installation. In this program, layer density values based on measured insulation thicknesses were used to predict thermal performance with generally good results.

Two techniques to measure insulation thicknesses were investigated in Task III. One of these was an x-ray technique where the measurements were obtained with little or no physical disturbance of the multilayers which might alter the local layer density or thickness. The other was a needle-probe technique where the multilayers were actually penetrated. For the latter case, minor local disturbances of the multilayers caused by the penetration could have occurred; however, results obtained using this technique were in good general agreement with those derived from the x-rays. During the tank test program, 7 different sets of x-ray measurements were evaluated to provide thickness data after the initial installation was completed, after shipment of the insulated calorimeter to the test site, and before and after each test series was performed except that no measurements were obtained after the 10-shield series. Needle-probe measurements were obtained on two different occasions; once just after completion of the 20-shield test series, and again just after completion of the 10-shield test series.

3.3.1 X-Ray Measurements

Using the x-ray measurement technique, tangential exposures were acquired for each x-ray set at each of 22 target locations distributed over the external surface of the tank. The target locations included 5 points in each of 4 radial planes which pass through the tank axis of symmetry (1 for each quadrant

of the tank), plus single points near the centers of the upper and lower domes. The 5 points in each radial plane were located at the midradii points of the upper and lower domes, the midpoints of the upper and lower dome-to-cylinder transitions, and the midpoint of the cylinder. These locations are shown in Fig. 3-6.

Each x-ray exposure shows a cross-sectional view through the insulation thickness for a particular target area. In setting up for the exposure, the x-ray machine was placed so that the centerline of the radiation exposure cone was nominally perpendicular to the radial plane through the tank axis of symmetry and the target point. The x-ray source was spaced approximately 30 in.(76.2 cm) in front of the target point with the film spaced approximately the same distance behind it. The film was oriented parallel to the radial plane through the target and, therefore, perpendicular to the centerline of the exposure cone so that a true projection of the insulation cross-section in the target plane was obtained. Because of the spacing of the machine and the film with respect to the target plane, each exposure obtained was approximately twice actual size. Fig. 3-13 shows typical exposures obtained for one quadrant from the 7th set of x-rays. This set was obtained just subsequent to completion of the 5-shield test series.

During the setup for each x-ray exposure, a gaging wire or scale was placed immediately adjacent to the target point and external to the multilayers. The scaling device was located so that it was nominally in the radial target plane. Consequently, the ratio of the true insulation thickness in the target plane to the projected thickness in the exposure was identical to that of the true scaling dimension (i.e., wire diameter or scale width) to the width of its image in the exposure. During the test program, the scaling devices and techniques were refined several times to increase the accuracy of the resulting measurements. Fig. 3-14 shows the evolution of the scaling devices used.

For the 1st set of x-ray exposures, a relatively long segment of 40-mil-(1.016-mm-) diameter lead wire (solder) was used to provide a scaling reference. The wire was suspended in the radial target plane so that it was adjacent to but not touching the external surface of the insulation. This was done to

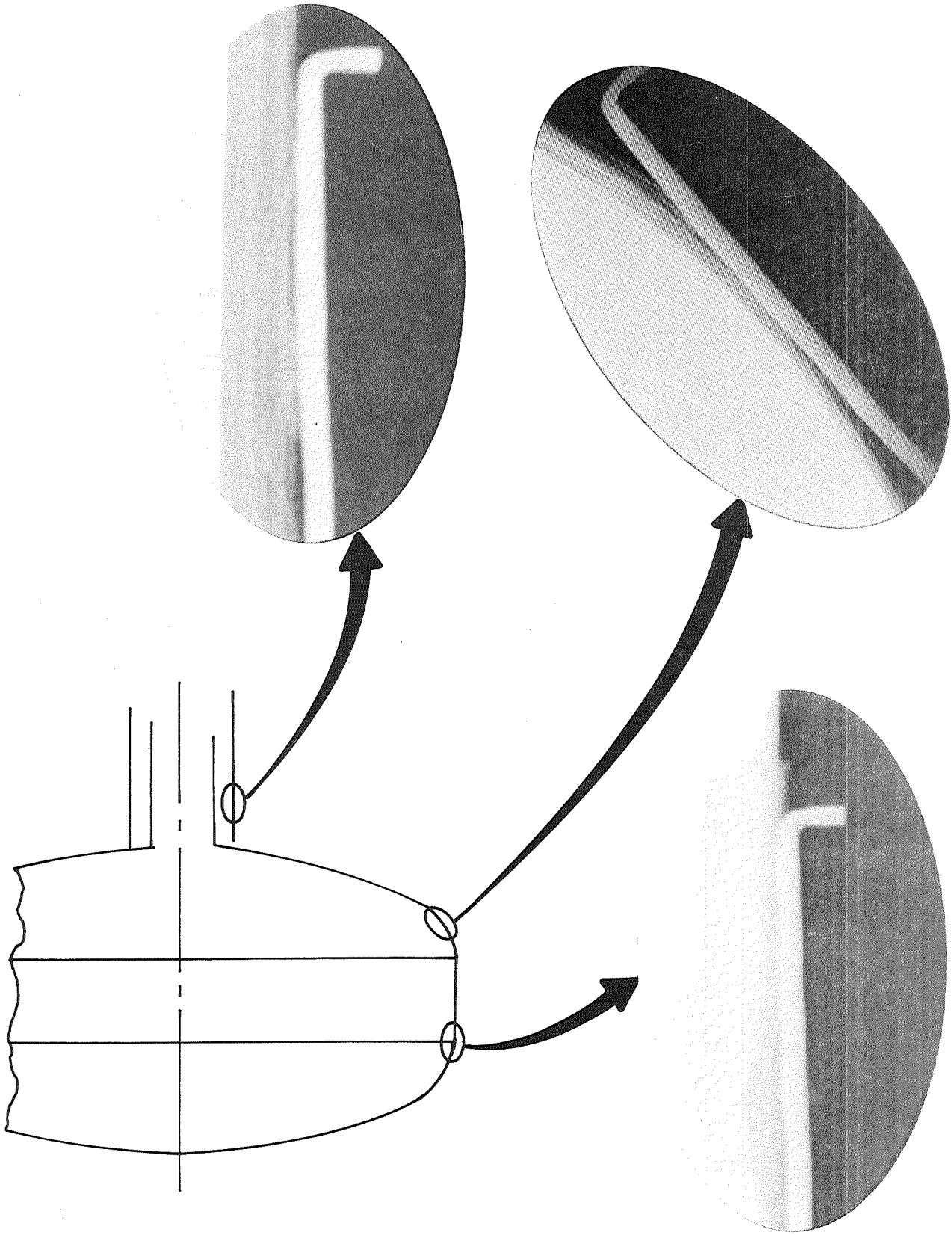

Fig. 3-13 Typical X-Ray Details

X-Ray Set
No. 1

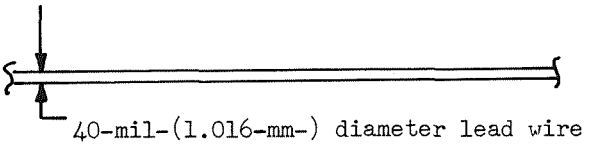

X-Ray Set
Nos. 2 through 6

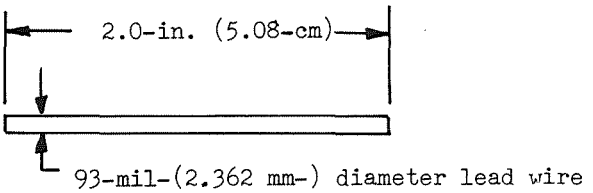

X-Ray Set
Nos. 3 & 4

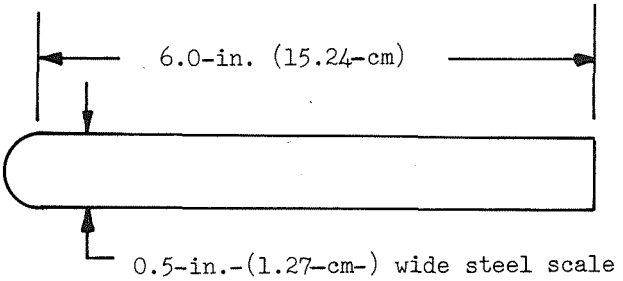

X-Ray Set
No. 7

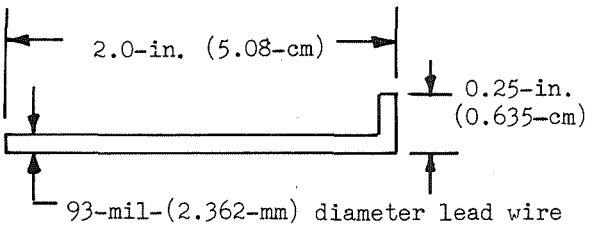

Fig. 3-14 Development of X-Ray Scaling Devices

preclude any local compression of the multilayers in the target area due to the weight of the wire. It was found that use of this wire resulted in significant scaling errors since the edges of the projected image of the wire could not always be pinpointed precisely. Therefore, even slight inaccuracies in measuring the width of the image were large relative to the total width.

For subsequent x-ray sets, a 93-mil-(2.362-mm-) diameter lead wire segment 2 in. (5.08 cm) long was used. The wire segment was taped to the external surface of the insulation in the radial target plane. Local compression (or expansion) forces imposed by this short wire segment due to its own weight were negligible.

In x-ray sets 3 and 4, a 0.5 in.-(1.27-cm-) wide steel scale was taped to the insulation in the radial target plane in addition to the lead wire segment. Again, the local deflection of the multilayers due to the weight of the scaling devices was found to be negligible.

As shown in Figs. 3-13 and 3-14, an L-shaped segment of the 93-mil-(2.362-mm-) diameter wire with a 2-in. (5.08-cm) long leg and a 0.25-in. (0.635-cm) short leg was used to obtain the 7th x-ray set. As before, it was taped to the outer surface of the insulation with the short leg aligned normal to the insulation surface and in the radial target plane.

During the test program, results of each set of x-ray thickness measurements were evaluated and used to compute area-weighted average values of layer density for the total system. These layer density values ranged from approximately 50 to 80 layers/in. (20 to 31 layers/cm). It was concluded that either significant errors resulted from the use of imprecise scaling factors or the forces imposed on the multilayers during each evacuation and subsequent repressurization cycle were significantly affecting the layer density values.

In light of the results discussed above, a post-test evaluation of apparent layer densities for the 20-, 10-, and 5-shield systems were conducted based

on all of the x-ray sets obtained during the tank calorimeter test program. In this evaluation, x-ray scale factors for each exposure were computed and compared based on a reference wire diameter and length, and (where applicable) on a reference scale width. In all cases it was found that the most reliable scale factors obtained were those based on wire diameter and/or scale width where the reference dimension was parallel to the insulation thickness dimension. However, it was found also from this evaluation that the images on the developed x-ray films of the wire diameter or scale width consist of a sharply defined central area of very light intensity and adjacent sharply-defined but very narrow areas of dark intensity on either side. This characteristic is shown schematically in Fig. 3-15. By evaluating and comparing the ratios of known wire length to wire diameter and known scale width to wire diameter, it was found that the true reference dimensions correspond to the external boundaries of the dark-intensity images on the x-rays. In the

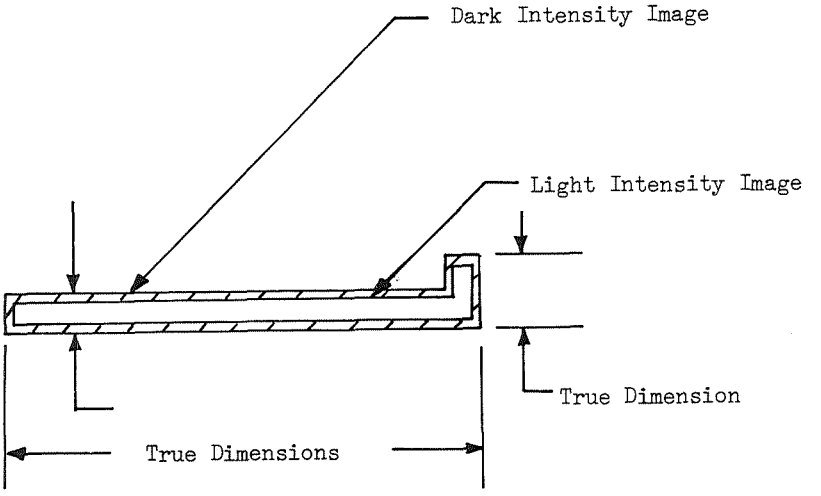

Fig. 3-15 X-Ray Image Characteristics

preliminary evaluations obtained during the tests, reference dimensions corresponding to the external boundaries of the central light-intensity images were used. Consequently, these preliminary evaluations were incorrect and superseded by the data which resulted from the post-test evaluation study.

A summary of the results of the final evaluations is presented in Table 3-3. The value presented for each surface area zone (designated by a letter symbol) represents the arithmetic average of the 4 discrete layer density measurements obtained at the centroids of each quadrant of the tank surface for that zone.

Figure 3-16 shows the zone locations used as well as the incremental surface areas of each zone quadrant. It can be seen by inspection of the Table 3-3 data that significant layer density variations occurred from zone to zone along any particular meridian of the tank as well as from one x-ray set to another.

A review of the x-ray data was conducted to assess the probable accuracy of any particular layer density value presented in the table. An exact error analysis was not possible; however, it was estimated from the review that particular layer density values are accurate within approximately $\pm$ 10 percent and that area-weighted average values for any particular x-ray set are accurate within approximately $\pm$ 5 percent. This estimate was substantiated somewhat by comparing the average values obtained from the x-rays with those obtained from needle-probe measurements for two cases where the latter were obtained. The maximum deviation in these values was found to be approximately 2.5 percent.

During review of the x-ray data, three factors which could have contributed to any inaccuracy of particular layer density values were identified and considered. The first of these was fore-shortening of a true reference dimension caused by inadvertent rotation of a plane through the principal axes of the reference wire or scale during placement so that it was not perpendicular to the x-ray exposure axis. A second factor was inadvertent placement of the reference wire or scale so that its respective distances from the x-ray source and film were not precisely the same as those for the x-ray target plane where the exposure axis was tangent to the tank and insulation surfaces. The third factor was the uncertainty, encountered in only a few cases, of selecting the exact tank and outer insulation surface images in the developed x-ray film. In these cases, the uncertainty was due to local irregularities caused by wrinkles or overlap areas, or by blurring of the images.

Table 3-3

SUMMARY OF INSULATION LAYER DENSITY VALUES OBTAINED
FROM EVALUATION OF X-RAY MEASUREMENTS (No./in. (No./cm)

X-Ray Set	No. of Shields	Test Run Series	Surface Area Zone (Ref. Fig. 3-16) A	B	C	D	E	F	G	H	I	Area-Weighted Averages
1st	20		35.4 (13.9)	65.1 (25.6)	62.7 (24.7)	75.9 (29.9)	103.3 (40.7)	62.5 (24.6)	47.8 (18.8)	53.3 (21.0)	72.3 (28.5)	70.8 (27.9)
2nd [a]	20	1 thru 4 [c][d]	--	--	--	--	--	--	--	--	--	-- 71.5 [e] (28.1)
3rd	20		39.5 (15.6)	62.3 (24.5)	56.5 (22.2)	83.9 (33.0)	105.1 (41.4)	71.8 (28.3)	49.4 (19.4)	52.4 (20.6)	67.8 (26.7)	72.2 (28.4)
4th	10	5 thru 8 [c]	45.9 (18.1)	54.3 (21.4)	46.8 (18.4)	71.2 (28.0)	96.7 (38.1)	51.3 (20.2)	31.0 (12.2)	34.5 (13.6)	49.6 (19.5)	60.4 (23.8) 60.4 [e] (23.8)
5th [b]	5	9 thru 12 [c]	28.0 (11.0)	41.7 (16.4)	35.8 (14.1)	59.7 (23.5)	91.7 (36.1)	50.2 (19.8)	29.7 (11.7)	33.7 (13.3)	49.2 (19.4)	54.0 (21.3) 67.1 [e] (26.4)
6th	5	Rerun of 11 [c]	47.8 (18.8)	63.6 (25.0)	55.2 (21.7)	88.4 (34.8)	133.3 (52.5)	70.8 (27.9)	43.9 (17.3)	49.4 (19.4)	77.8 (30.6)	80.1 (31.5) 72.3 [e] (28.5)
7th	5		33.3 (13.1)	53.0 (20.9)	44.9 (17.7)	67.3 (26.5)	103.8 (40.9)	59.5 (23.4)	38.8 (15.3)	44.6 (17.6)	63.3 (24.9)	64.4 (25.4)

Notes:

(a) No usable data obtained; x-rays blurred by movements during exposure
(b) Where no x-ray data were obtained, underlined values were estimated
(c) Vacuum chamber and insulation evacuated prior to each test series and repressurized after completion of each series
(d) An additional pressurization/evacuation cycle was imposed between test runs 1-2 and 3-4 to permit visual inspection of the insulation
(e) Arithmetic average of pre-test and post-test values used in predictions

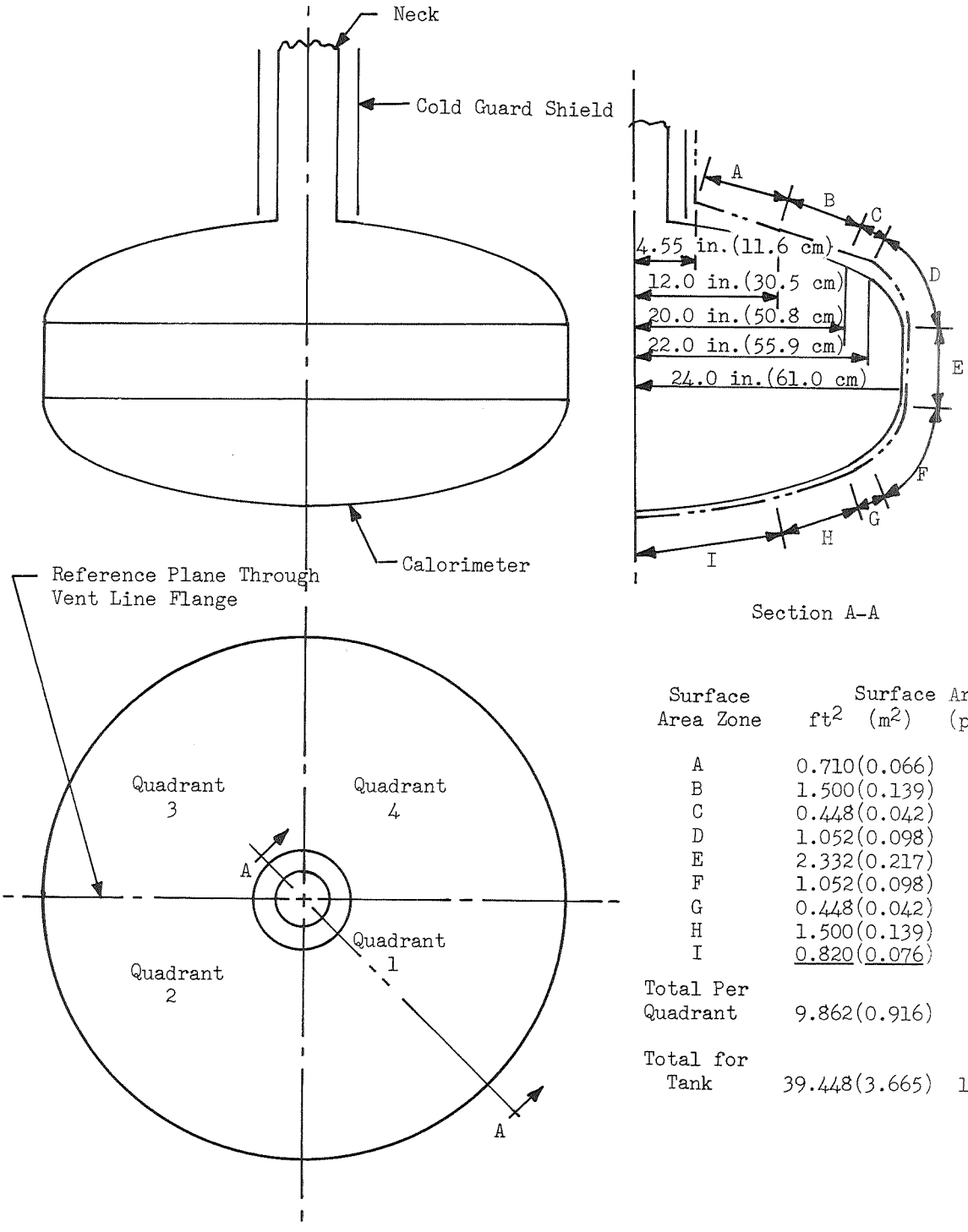

Surface Area Zone	Surface Area ft^2 (m^2)	(percent)
A	0.710(0.066)	1.8
B	1.500(0.139)	3.8
C	0.448(0.042)	1.1
D	1.052(0.098)	2.7
E	2.332(0.217)	5.9
F	1.052(0.098)	2.7
G	0.448(0.042)	1.1
H	1.500(0.139)	3.8
I	0.820(0.076)	2.1
Total Per Quadrant	9.862(0.916)	25.0
Total for Tank	39.448(3.665)	100.0

Fig. 3-16 Tank Calorimeter Insulation Zones and Surface Areas

During evaluation of all of the x-ray sets obtained in the test program, it was found that images of the flat tungsten markers initially installed in the insulation (Ref. Section 3.1.2) were not projected clearly enough to locate in the exposures. It was concluded that thicker markers would have provided sufficient exposure definition to have aided in evaluating layer density variations through the thickness.

3.3.2 Needle-Probe Measurements

Concurrently with the 3rd set of x-rays obtained after completion of the 20-shield tests, measurements of local insulation thicknesses were obtained at 7 locations on the tank surface using a fine sewing needle to probe through the insulation layers normal to the surface. After penetration, the needle was rotated about its longitudinal axis to negate the effect of any local depressions caused by the penetration. It was subsequently marked to indicate the position of the outer insulation surface, withdrawn, and measured.

In general, the deviations in local thickness based on these needle probe measurements were within +0.02 in. (+0.051cm) and -0.04 in.(-0.102cm) of the x-ray measurements.

Thickness data subsequent to completion of the 10-shield test series were obtained also at 9 points on the lower tank dome using the needle-probe technique. As before, the results were in good general agreement with those obtained from the x-rays.

3.4 INSULATION PERFORMANCE PREDICTIONS

The general analytical expression developed early in Task II to characterize the thermal performance of double-goldized Mylar/silk net insulation is

$$q = \frac{a''' P^{m'''} T_m}{N_s + 1}(T_H - T_C) + \frac{2\sigma \epsilon_{TRG}}{(4+a_4)(540)^{a_4} N_s}\left(T_H^{4+a_4} - T_C^{4+a_4}\right)$$

(Ref. 1, Eq. 4.10)

In later Task II analyses, the constants a''' and m''' were evaluated from semi-empirical curve-fits of the flat plate calorimeter test data obtained for 6 specimens of the double-goldized Mylar/silk net composite materials (Ref 1, Section 4.3.2). Numerical values of these constants together with a value for the constant 2σ were substituted into the general expression yielding

$$q = \frac{5.84\text{x}10^{-4}(P-P_o)^{0.422}T_m}{N_s + 1}(T_H - T_C) + \frac{3.426\text{x}10^{-9}\epsilon_{TRG}}{(4+\alpha_4)(540)^{\alpha_4}N_s}\left(T_H^{4+\alpha_4} - T_C^{4+\alpha_4}\right)$$

(Ref. 1, Eq. 4.23)

In this expression, $P-P_o$ equals P from the general expression.

This form of the heat transfer equation was modified in the later Task II analysis to express the solid conduction component of heat flux in terms of layer density, $\bar{N}$, rather than compressive pressure, $P-P_o$. The modification was necessary in order to use the equation to predict thermal performance for a tank-installed insulation* (e.g., the insulation installed and tested in the Task III tank calorimeter study). It was accomplished by evaluating the relationship of $P-P_o$ and $\bar{N}$ from the Task II flat plate calorimeter tests, and by then substituting these results into the general equation. It was found that the desired relationship could be approximated closely by the expression

$$P-P_o = c(\bar{N})^n$$

In the final Task II analysis, values of the constants c and n in the above expression and of the variables ϵ_{TRG} and α_4 in the general heat transfer equation were evaluated both for single specimens and for combined specimens (Ref 1, Section 4.4). Initially, these quantities were evaluated independently for the two 20-shield specimens to illustrate the differences which can result

* Layer density values can be determined from insulation thickness measurements, whereas no practical technique has been found to assess compressive pressure values for a tank-installed multilayer system.

for similar specimens of the same material. Subsequently, they were evaluated independently for the 20-, 10-, and 5-shield specimen pairs. Finally, they were evaluated from all of the flat plate test data obtained for all 6 specimens. The latter evaluation provided the most comprehensive and, therefore, the most reliable fit of all of the data obtained for the double-goldized Mylar/silk net composite system.

The form of the heat transfer equation which resulted from the evaluation of c, n, ϵ_{TRG}, and α_4 based on flat plate and emittance test data for all 6 specimens is given by

$$q = \frac{4.37\times10^{-11}(\bar{N})^{3.27}T_m}{N_s + 1}(T_H - T_C) + \frac{6.70\times10^{-13}}{N_s}\left(T_H^{4.51} - T_C^{4.51}\right)$$

(Ref. 1, Eq. 4.38)

Heat flux values computed from this equation and those measured during the flat plate calorimeter tests were compared in the Task II analysis as functions of layer density and the number of radiation shields in each specimen (Ref. 1, Fig. 4-38 through 4-41). The computed values, shown as the curves in these figures, were used initially in Task III to predict preliminary results of the tank calorimeter tests. Final predictions of the tank calorimeter test results were computed using the evaluated heat flux equation presented above (Ref. 1, Eq. 4.38). The preliminary predictions given by the curves in Figs. 4-38 through 4-41 were approximate only, since they were based on the nominal hot and cold boundary temperatures, whereas the final predictions were based on actual temperatures measured during the tests. The cold boundary temperature for each test was taken as that of the liquid cryogen (i.e., LN_2 or LH_2) saturated at the equilibrium tank pressure recorded during that particular test. The corresponding hot boundary temperature was taken as the average of the temperatures recorded at 3 points on the surface of the outer radiation shield (Ref. Fig. 3-7, locations B, C, and D) after equilibrium conditions had been achieved.

Layer density values used in the final heat flux prediction computations were the area-weighted average values obtained from the evaluation of x-ray thickness measurements (Ref. Table 3-3). The average values used were obtained from the measurements made just prior to and just succeeding each test series, except that no post-test measurements were made for the 10-shield test series. Consequently, average layer density values used in predicting heat flux values for these tests were based on pre-test x-rays only.

The preliminary predictions of heat flux were based on the total number of radiation shields, N_s, and the total number of spacer layers, $N_s + 1$, in place on the tank for any particular test. Different values of N_s and $N_s + 1$ were used in the final computations of predicted heat flux. For example, in the first (conductive) term of the heat flux equation, N_s was taken as the total number of radiation shields then in place less one; i.e., N_s equal to 19, 9, and 4 for the 20-, 10-, and 5-shield tests, respectively. This was done because the outer shield in each case was in fact the hot boundary surface, and neither it nor its encapsulating net spacer contributed to the conductive resistance of the insulation then being evaluated. In the second (radiative) term of the heat flux equation, N_s was taken as the number of radiation shields then in place less one-half; i.e., N_s equal to 19.5, 9.5, and 4.5 for the 20-, 10-, and 5-shield tests, respectively. This was done because the inner surface of the outer shield (which was controlled to the hot boundary temperature) was gold-coated - not black as in the case of the hot boundary surface for the flat plate calorimeter. Consequently, this surface contributed to the radiative resistance of the insulation then being evaluated. These evaluations of N_s for conductive and radiative heat transfer were verified independently by a heat balance analysis.

Preliminary and final predictions of heat flux for each of the 12 tank calorimeter tests conducted in Task III are presented in Table 3-4.

TABLE 3-4

SUMMARY OF PREDICTED HEAT FLUX VALUES FOR THE TANK CALORIMETER TESTS

Test Run Number	Total Number of Shields	Boundary Temperatures (a) ^{o}R T_H (^{o}K)	^{o}R T_C (^{o}K)	Pre-Test Layer Density (b) No./in. (No./cm)	Preliminary Predicted Heat Flux (c) Btu/hr ft^2 (w/m^2)	Average Layer Density (d) No./in. (No./cm)	Final Predicted Heat Flux (e) Btu/hr ft^2 (w/m^2)
1	20	501 (279)	137 (76)	70.8 (27.9)	0.335 (1.056)	71.5 (28.1)	0.345 (1.087)
2	20	615 (342)	137 (76)	70.8 (27.9)	0.552 (1.740)	71.5 (28.1)	0.585 (1.844)
3	20	502 (279)	36 (20)	70.8 (27.9)	0.340 (1.072)	71.5 (28.1)	0.369 (1.163)
4	20	611 (340)	36 (20)	70.8 (27.9)	0.562 (1.771)	71.5 (28.1)	0.597 (1.882)
5	10	499 (277)	137 (76)	60.4 (23.8)	0.422 (1.320)	60.4 (23.8)	0.439 (1.384)
6	10	611 (340)	137 (76)	60.4 (23.8)	0.722 (2.276)	60.4 (23.8)	0.776 (2.446)
7	10	496 (276)	36 (20)	60.4 (23.8)	0.435 (1.371)	60.4 (23.8)	0.458 (1.444)
8	10	612 (340)	36 (20)	60.4 (23.8)	0.732 (2.307)	60.4 (23.8)	0.805 (2.537)
9	5	489 (272)	137 (76)	54.0 (21.3)	0.610 (1.923)	67.1 (26.4)	1.106 (3.486)
10	5	611 (340)	137 (76)	54.0 (21.3)	1.140 (3.593)	67.1 (26.4)	2.003 (6.313)
11 (f)	5	506 (281)	36 (20)	80.1 (31.5)	1.720 (5.421)	72.3 (28.5)	1.571 (4.952)
12	5	615 (342)	36 (20)	54.0 (21.3)	1.140 (3.593)	67.1 (26.4)	2.112 (6.657)

Notes:

(a) Nominal hot boundary temperatures were 500 and 610^{o}R (278 and 339^{o}K); nominal cold boundary temperatures were 140 and 37^{o}R (77 and 20^{o}K); values shown were measured at test equilibrium conditions.

(b) Area-weighted average values obtained from pre-test x-ray measurements (Ref. Table 3-3).

(c) Based on nominal boundary temperatures, pre-test layer densities, and total number of shields (Ref. 1, Figs. 4-38 through 4-41).

(d) Arithmetic average of pre-test and (where available) post-test area-weighted average values obtained from x-ray measurements.

(e) Based on measured boundary temperatures, average layer densities, and corrected number of shields.

(f) Data presented are for rerun of this test.

3.5 INSULATION PERFORMANCE TESTS

Twelve planned boiloff tests plus one additional rerun were conducted during Task III. The primary purpose of these tests was to assess the thermal performance of double-goldized Mylar/silk net insulation as installed on the 4-ft-(1.22-m-) diameter tank calorimeter. A summary of the sequential test operations and boundary conditions is presented in Table 3-5. Four of the planned tests were performed with 20 reflective shields, 20 double silk net spacers, and a single outer layer of Dacron net installed on the tank. An additional 4 tests were performed with 10 reflective shields and 11 double silk net spacers still in place. The remaining 4 planned tests plus the rerun of test 11 were conducted with 5 reflective shields and 6 double silk net spacers in place. Significant test operations are described and results of each test are presented in this section.

As shown in Table 3-5, these tests were conducted with nominal hot boundary temperatures of 500°R (278°K) and 610°R (339°K), and with nominal cold boundary temperatures of 140°R (77°K) and 37°R (20°K). The 500°R (278°K) hot boundary temperature was achieved by circulating cold water through the baffle and shroud heat exchangers from a thermostatically-controlled facility chiller. In a similar manner, the 610°R (339°K) hot boundary temperature was achieved with circulated hot water from a boiler, also controlled by a thermostat. It was found during the tests that the baffle and shroud surfaces could be controlled to the same temperature, as indicated by the attached thermocouples, within approximately ± 1°R (±0.6°K). The resulting average hot boundary average hot boundary temperature (that of the outer insulation radiation shield surface), as indicated by those attached thermocouples, could be controlled within approximately ± 5°R (±2.8°K).

Since it was desired to run the outer reflective shield temperatures at the nominal hot boundary values (Ref. Section 3.4), it was necessary to control the baffle and shroud temperatures at slightly higher values. Approximate

Table 3-5

SUMMARY OF TASK III TANK CALORIMETER TEST OPERATIONS

Pre-Test/Post-Test Operations	Test Run Number	Total Number Of Shields	Nominal Boundary Temperatures T_H,°R(°K)	T_C,°R(°K)
Calorimeter Installation and Check-out; 2nd X-Ray Set; Chamber Evacuated	1	20	500(278)	140(77)
	2	20	610(339)	140(77)
Chamber Repressurization; Visual Inspection; Chamber Reevacuation	3	20	500(278)	37(20
	4	20	610(339)	37(20)
Chamber Repressurization; 3rd X-Ray Set; Removal of Outer 10 layers; 4th X-Ray Set; Chamber Evacuation	5	10	500(278)	140(77)
	6	10	610(339)	140(77)
	7	10	500(278)	37(20)
	8	10	610(339)	37(20)
Chamber Repressurization; Removal of Outer 5 Layers; 5th X-Ray Set; Chamber Evacuation	9	5	500(278)	140(77)
	10	5	600(339)	140(77)
	11	5	500(278)	37(20)
	12	5	610(339)	37(20)
Chamber Repressurization; 6th X-Ray Set; Chamber Evacuation	11(Rerun)	5	500(278)	37(20)
Chamber Represurrization; 7th X-Ray Set; Restoration of Facility				

incremental differences between the temperatures of the shroud and the outer shield were determined from analytical heat balances shown graphically in Figs. 3-17 and 3-18 for the 500°R (278°K) and 610°R (339°K) hot boundaries, respectively.

3.5.1 Twenty-Shield Test Series

Subsequent to installation of the insulation system on the tank calorimeter (Ref. Section 3.1.2) and completion of the first set of x-ray thickness measurements (Ref. Section 3.3), the calorimeter assembly was shipped to the SCTB test site and installed in the vacuum chamber. Then the second set of x-ray thickness measurements was obtained, and plumbing lines and instrumentation sensors were connected to the facility systems. Prior to initiation of the 20-shield test series, the calorimeter and all associated plumbing systems were leak-checked using GHe, and a complete functional checkout of the instrumentation was conducted.

During checkout of the instrumentation, it was found that thermocouples installed within the insulation at locations A-10, A-20, B-1, B-5, B-15, C-15 and D-2 (Ref. Fig. 3-7) were inoperative. A careful inspection of the electrical connections made in the vicinity of the calorimeter neck cold guard between each of the thermocouple leads and the associated reference junction leads (Ref. Fig. 3-8) indicated that these thermocouple circuits were open somewhere within the insulation system. Since replacement of the inoperative thermocouples would have necessitated removal and reinstallation of all of the insulation external to the first reflective shield, a decision was made to proceed with the tests using the remaining thermocouples which were operative.

The 20-shield tests were conducted in two separate series. In the initial series, the 610°R (339°K)/140°R (77°K) test (run number 2) and the 500°R (278°K)/140°R (77°K) test (run number 1) were conducted in that order. Prior to the initiation of run number 2, the vacuum chamber was evacuated and the tank was filled with LN_2 which had been stored at 25 psig ($1.7 \times 10^5 N/m^2$ gage) saturated equilibrium conditions for several days. During the fill and topping

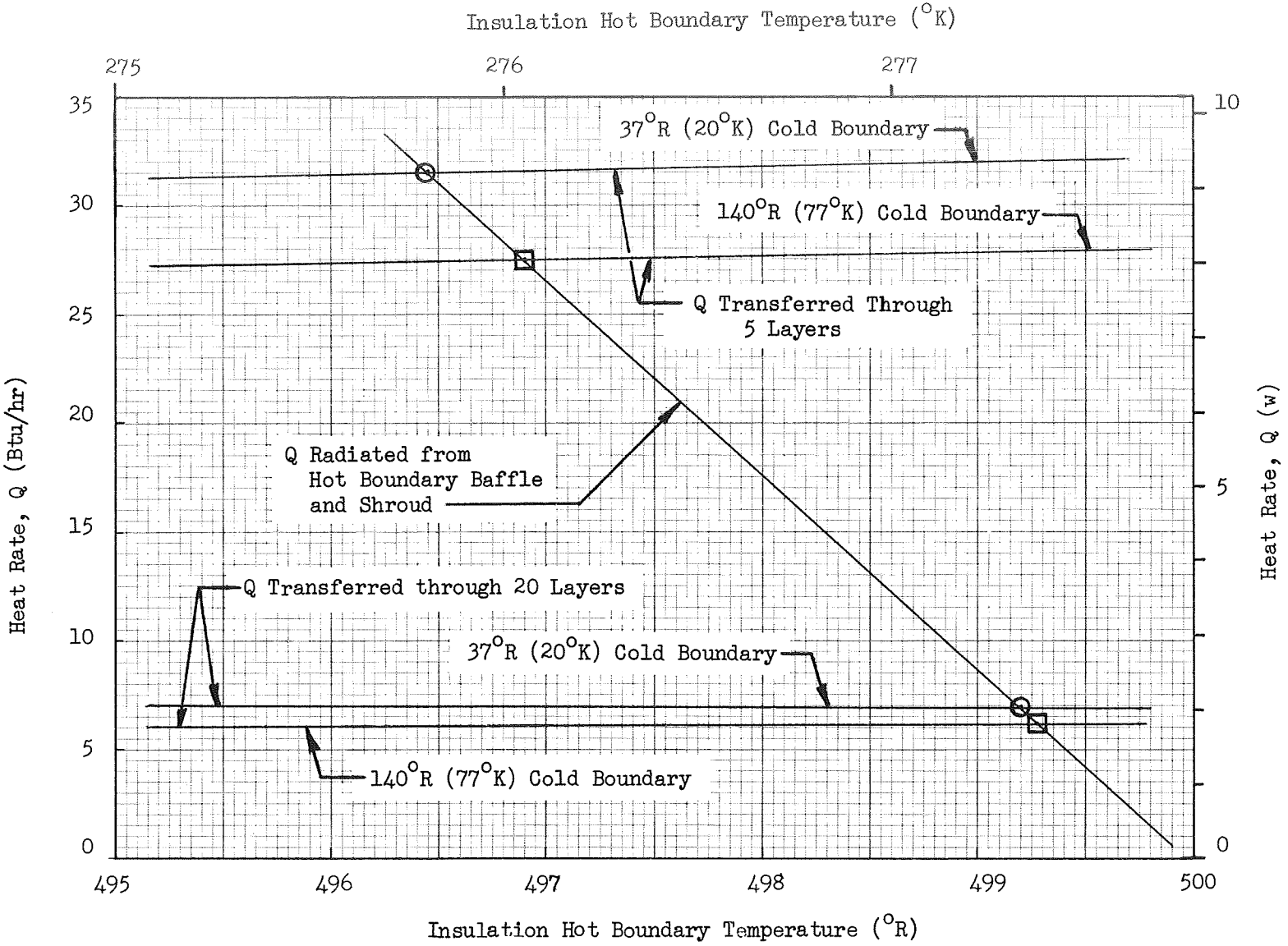

Fig. 3-17 Equilibrium Heat Rate as a Function of Insulation Hot Boundary Temperature for a 500°R (278°K) Shroud Temperature

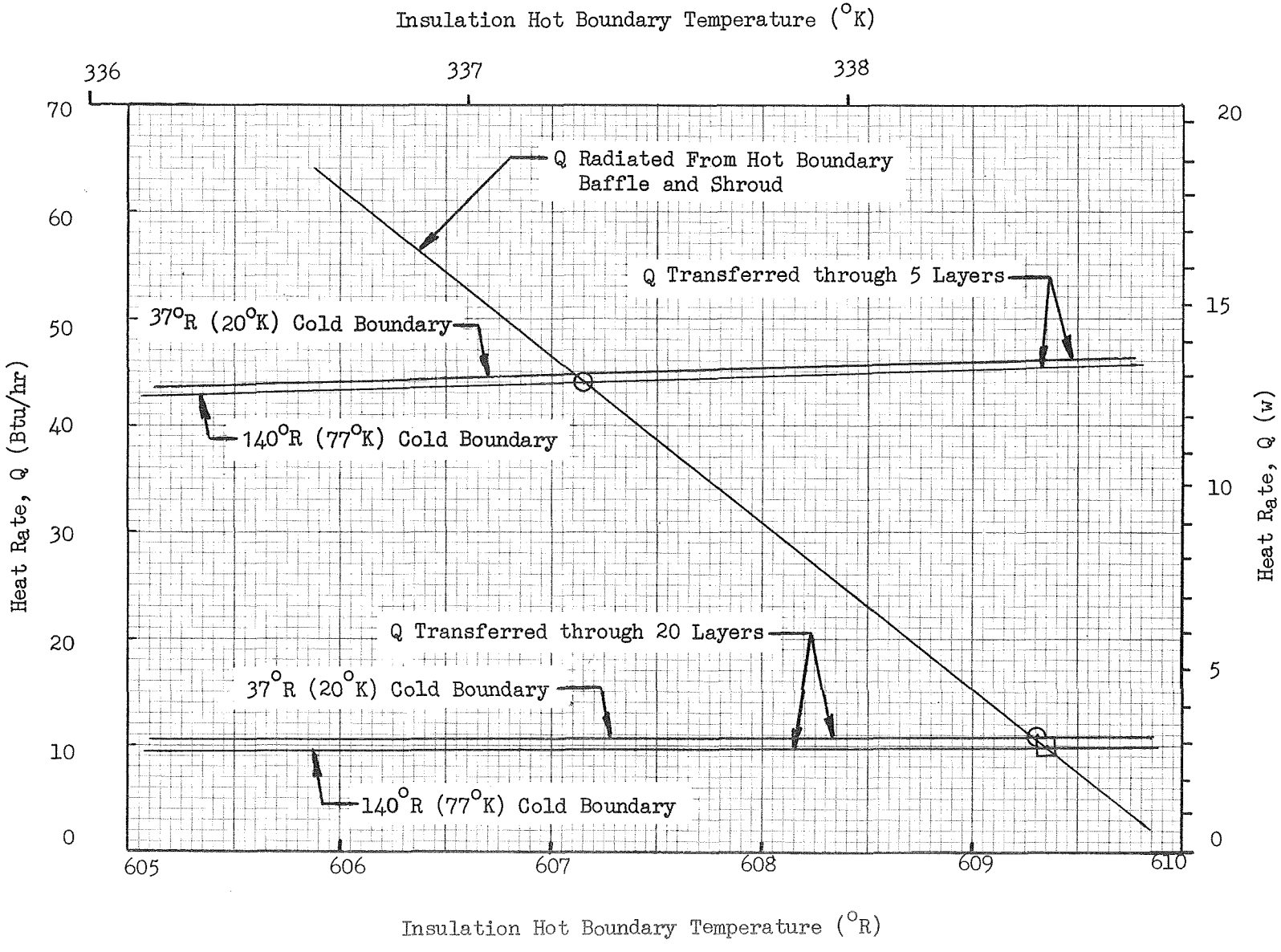

Fig. 3-18 Equilibrium Heat Rate as a Function of Insulation Hot Boundary Temperature for a 610°R (339°K) Shroud Temperature

operation, the tank pressure was controlled to approximately 20 psia (1.3 x $10^5 N/m^2$). When the liquid overflow line temperature sensor (TLO, Fig. 3-1) indicated that the liquid level in the calorimeter neck had risen to the level of the overflow line outlet, the valves in both the fill line and the overflow line were closed thus terminating the fill operation. Subsequently, a vacuum pumping system located in the calorimeter vent line downstream from the back-pressure regulator was operated to reduce the fluid pressure within the calorimeter to a nominal value of 13 psia ($9.0 \times 10^4 N/m^2$). Liquid cryogen within the calorimeter tank and neck flashed off during this operation until the bulk fluid remaining in the tank had reached saturated equilibrium conditions at the test pressure. Calculations showed that the liquid level at this time should be at or slightly below the intersection of the calorimeter neck and the upper tank bulkhead.

Test runs 1 and 2 were conducted in around-the-clock operations during a five day period. Run number 2 required approximately 56 hours of continuous operation to achieve thermal equilibrium of the insulation temperatures and to obtain the boiloff data. Approximately 27 hours of additional time were required to achieve thermal equilibrium and to obtain the boiloff data during run number 1. In the transition from run number 2 to run number 1, only the hot boundary temperature was changed since it was not necessary to refill the tank and thereby disturb the LN_2 equilibrium conditions. Liquid nitrogen was supplied to the calorimeter cold guard continuously during test runs 1 and 2 from the same supply dewar initially used to fill the tank. It was found that the fluid temperature decreased from approximately 156°R (86.7°K), i.e., saturated liquid at 25 psig ($1.7 \times 10^5 N/m^2$ gage), to approximately 154.6°R (85.9°K) average at the guard inlet temperature sensor. An additional decrease in temperature to approximately 149.9°R (83.3°K) average was observed at the guard outlet temperature sensor. The flow was observed to be somewhat unsteady, with an average temperature oscillation on the order of 2-to-5°R (1.1-to-2.8°K). The guard temperature at the neck was taken as the average of the inlet and outlet fluid temperatures, or approximately 152.3°R (84.6°K) during the approximately five hours of apparent steady-state operation when the boiloff for run number 2 was evaluated. Since the tank fluid was in equilibrium

and saturated at 137.4°R (76.3°K) and 12.96 psia ($8.94 \times 10^4 N/m^2$), the average temperature difference across the neck from the guard to the tank was approximately 15°R (8.3°K) during this time. During approximately 13 hours of apparent steady-state operation, when the boiloff for run number 1 was evaluated, the average fluid temperatures at the guard inlet and outlet were found to be 152.9°R (84.9°K) and 145.8°R (81.0°K), respectively. For this run, the average temperature at the guarded neck was 149.4°R (83.0°K) or approximately 12°R (6.7°K) warmer than the tank fluid.

Subsequent to the boiloff evaluation for run number 1, the LN_2 supply dewar pressure was reduced to 17 psig ($1.2 \times 10^5 N/m^2$ gage), i.e., 151.5°R (84.2°K) saturated liquid, in an effort to obtain a lower temperature fluid flow through the cold guard and thus a lower temperature difference across the calorimeter neck. This condition was maintained for approximately nine hours with an average decrease in the guarded neck temperature of approximately 0.7°R (0.4°K), and with no apparent change in boiloff. Then the dewar pressure was reduced to 9 psig ($6.2 \times 10^4 N/m^2$ gage), i.e., 146.3°R (81.3°K) saturated liquid, and maintained for approximately five hours. During this latter period, the average guarded neck temperature increased to 229.3°R (127.4°K), indicating that the flow was insufficient to maintain liquid through this part of the system. As expected, the average total heat rate to the tank, based on measured boiloff, increased by approximately 0.9 Btu/hr (0.26w) during this same time period.

The 500°R (278°K)/37°R (20°K) test (run number 3) and the 610°R (339°K)/37°R (20°K) test (run number 4) were conducted during a subsequent four-day test series. Prior to initiating run number 3, the vacuum chamber was again evacuated, having been pressurized with air in the interim to permit visual inspection of the test apparatus. The tank was filled with LH_2 which had been stored at 25 psig ($1.7 \times 10^5 N/m^2$ gage) for several days. The tank fill and topping operation was performed using the same techniques described previously. Initially in this test series, the cold guard outlet line was connected through a hot water heat exchanger to a vacuum pumping system in an effort to further reduce the temperature of the guard fluid, and consequently

the temperature difference between the guarded neck and the tank. This technique proved to be unsatisfactory, apparently because solids were formed at points of restricted flow within the system causing significant oscillations of the guard inlet and outlet fluid temperatures. The outlet was subsequently reconnected to the facility vent line and allowed to vent to the atmosphere during the remainder of the series.

Test run number 3 required approximately 24 hours of continuous operation to achieve thermal equilibrium of the insulation temperatures and to obtain the boiloff data. Again, it was not necessary to refill the tank, and only the hot boundary temperature was changed in the transition to test run number 4. An additional 39 hours of continuous operation were required to achieve thermal equilibrium within the insulation during this run. However, an electrical power failure occurred which disturbed the equilibrium within the insulation temperatures, and an additional 17 hours of continuous operation were required to achieve equilibrium again and to obtain the boiloff data.

During the LH_2 test series (runs 3 and 4), it was found that the consumption of LH_2 was excessive (approximately 100 gallons or 378.5 liters per hour) when the cold guard was operated continuously. Consequently, in run number 4 the guard was not operated during the long time transient required for the insulation temperatures to reach equilibrium. It was found that this technique works very well, since only 2-to-4 hours of operation were required to achieve system equilibrium after the guard flow was initiated.

It was found also during test number 4 that apparent oscillations in boiloff flowrate, observed during all runs where the guard was operated, were essentially eliminated when the guard flow was shut off. It is not known precisely what caused these apparent oscillations, since tank pressure did not deviate within the sensitivity of the pressure measurement which is 0.01 psi (69 N/m^2). However, boiloff measurements obtained in all of the test runs were based on a large number of flowmeter readings averaged over a period of time when the tank pressure and the insulation temperatures were constant to preclude any inaccuracy due to the oscillations.

During test run number 3, the average guard inlet fluid temperature was found to be approximately 42.5°R (23.6°K), while that at the outlet was approximately 42.2°R (23.4°K). The guarded neck, therefore, was assumed to be operating at an average temperature of 42.35°R (23.5°K). The tank pressure during this run was 12.99 psia (8.96×10^4 N/m^2), corresponding to a saturated liquid temperature of 35.8°R (19.9°K), so that the temperature difference from the guard to the tank was approximately 6.6°R (3.7°K). The average guard fluid temperatures at the inlet and outlet temperature sensor locations were found to be 42.8°R (23.8°K) and 41.3°R (22.9°K), respectively, during run number 4. The average guarded neck temperature, therefore, was assumed to be approximately 42.1°R (23.4°K), resulting in a temperature difference of approximately 6.3°R (3.5°K) between the guard and the tank.

Subsequent to the completion of test run number 4, the supply of LH_2 was exhausted and two additional points of tank heat rate as a function of quasi steady-state guard temperature with cold GH_2 flow through the system were obtained. The average guard temperatures were 88°R (48.9°K) and 105°R (58.3°K), respectively, for these two data points. No increase in total tank heat rate, as measured by the boiloff flowrate, was observed for either point.

A summary of the significant system measurements obtained in the four 20-shield test runs is presented in Table 3-6. Equilibrium temperature profiles through the multilayers, obtained from measurement of particular shield temperatures, are presented in Figs. 3-19 and 3-20. It can be seen from the inspection of these data that the basic profiles are S-shaped for all boundary temperature combinations. However, this effect is significantly greater for the 610°R (339°K) hot boundary tests than for those with a 500°R (278°K) hot boundary. Predicted temperature profiles from the Task II analysis show a convex-upward shape through the entire insulation thickness, and not the S-shape obtained in the tests. Although this effect is not completely understood, it was concluded that it was most likely the result of non-uniform layer density through the thickness. However, it also could have been the result of increased gas conductivity in the outer layers due to insulation outgassing or could indicate that a steady-state condition was not achieved.

Table 3-6

SUMMARY OF SYSTEM MEASUREMENTS OBTAINED AT EQUILIBRIUM FOR THE 20-SHIELD TEST RUNS

Test Run Number	1	2	3	4
Nominal Boundary Temperatures, T_H/T_C, ^oR (^oK)	500/140 (278/77)	610/140 (339/77)	500/37 (278/20)	610/37 (339/20)
Tank Pressure, psia (N/m^2)	12.96 (8.94×10^4)	12.96 (8.94×10^4)	12.99 (8.96×10^4)	12.99 (8.96×10^4)
Tank Temperature, ^oR (^oK)	137.4 (76.3)	137.4 (76.3)	35.8 (19.9)	35.8 (19/9)
Boiloff Flowrate, lbm/hr (kg/hr)	0.211 (0.0957)	0.415 (0.188)	0.0715 (0.0324)	0.150 (0.068)
Av. Guard Temp., ^oR (^oK)	149.4 (83.1)	152.3 (84.7)	42.4 (23.6)	42.1 (23.4)
Hot Baffle Temp. ^oR (^oK)	503 (280)	619 (344)	501 (279)	612 (340)
Hot Shroud Temp., ^oR (^oK)	504 (280)	618 (344)	505 (281)	613 (341)
Av. Hot Boundary Temp. at 20th Shield, ^oR (^oK)	501.4 (278.8)	614.8 (341.8)	501.7 (278.9)	610.6 (339.5)
Vacuum Chamber Pressure (torr)	6×10^{-5}	6×10^{-5}	9×10^{-6}	1×10^{-5}

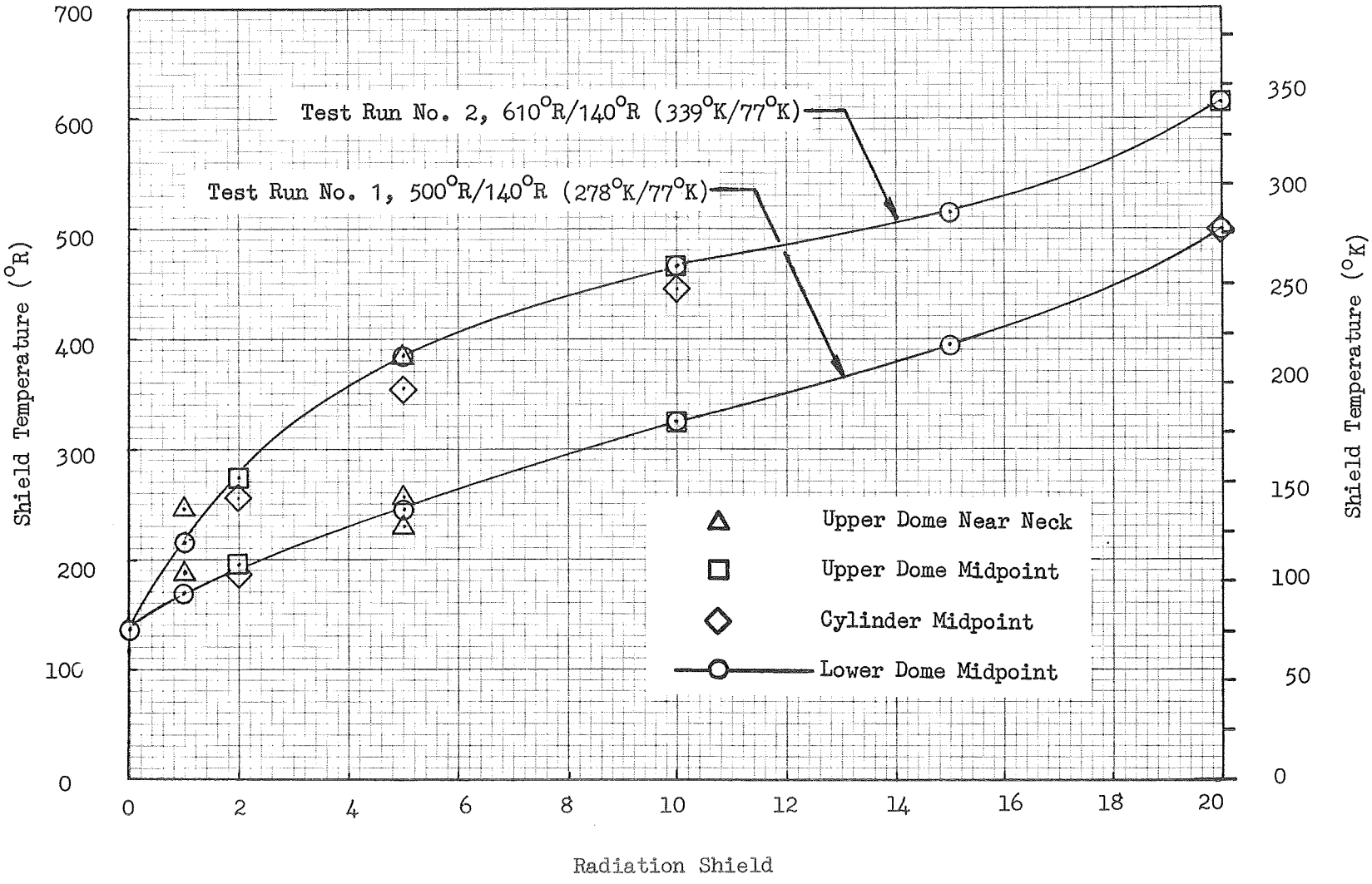

Fig. 3-19 Measured Temperature Profiles Through a 20-Shield DGM/Silk Net Insulation System with T_C = 140°R (77°K)

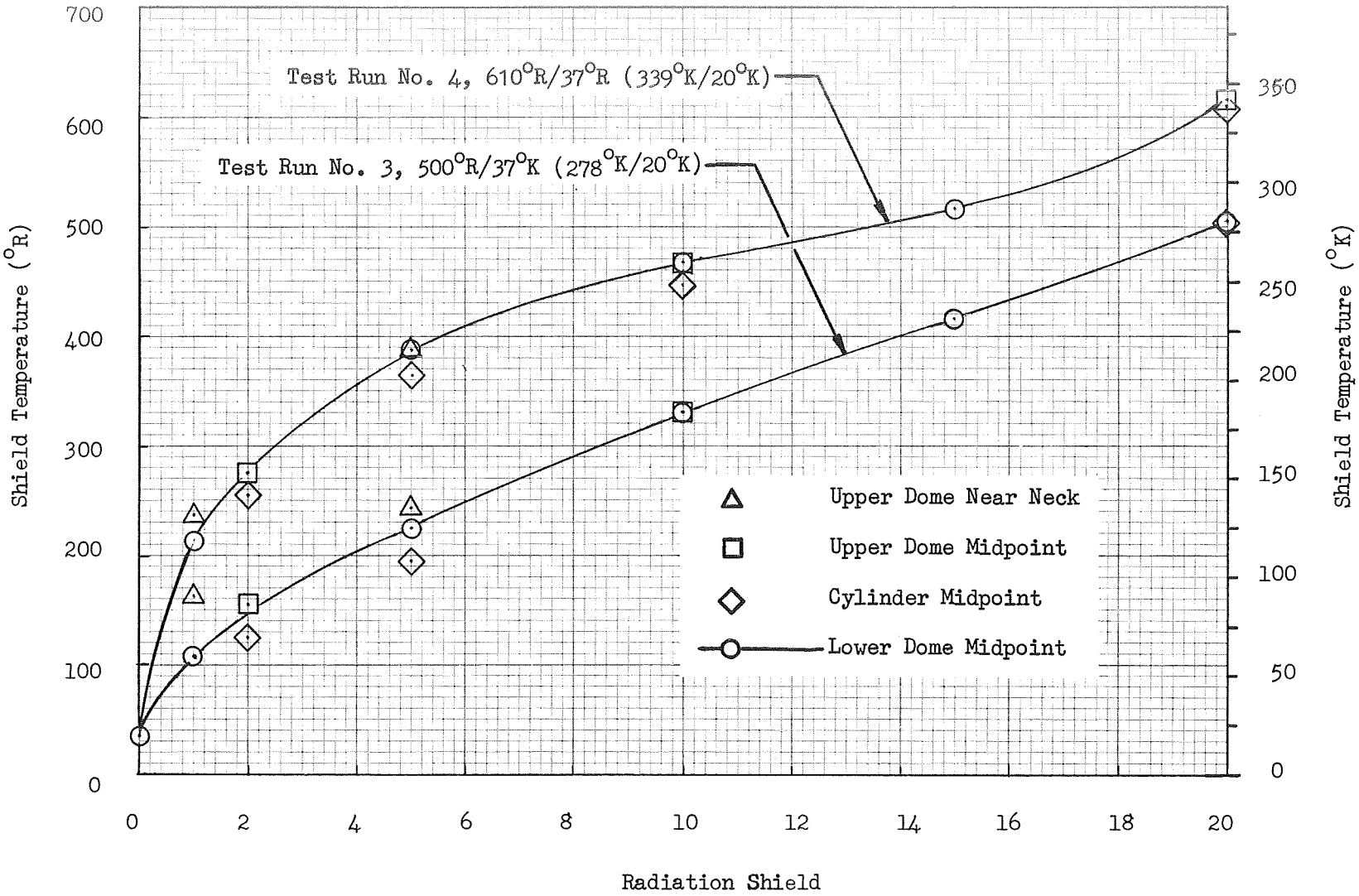

Fig. 3-20 Measured Temperature Profiles Through a 20-Shield DGM/Silk Net Insulation System with $T_C = 37°_R$ $(20°_K)$

During this initial test series, the possibility was considered that the S-shaped temperature distribution might be the result of increased conductivity through molecules of gas within the insulation, caused by small leaks into the vacuum chamber. A small leak apparently did occur during test runs 1 and 2 since the measured vacuum chamber pressure was approximately 6×10^{-5} torr for these runs. During post-test disassembly of the shrouds to gain access to the tank insulation, a cracked O-ring seal was found in the cold guard outlet line connection external to the tank insulation. Consequently, a study of boiloff rate as a function of vacuum chamber pressure was conducted during the 5-shield test series. It was found from results of this study (Ref Section 3.5.3) that no significant increase in boiloff or change in the temperature distribution through the insulation was observed until the vacuum chamber pressure was increased to a value of 1×10^{-4} torr or greater.

After completion of test runs 3 and 4, the vacuum chamber was repressurized with air to permit access for the third set of x-ray thickness measurements and preparation of the insulation for the 10-shield tests. The pressurization cycle was accomplished at a low rate over approximately an 8-hour period to minimize physical compression of the insulation layers.

3.5.2 Ten-Shield Test Series

Subsequent to obtaining the third set of x-ray thickness measurements with the 20-shild insulation system still in place, the outer layer of Dacron net together with ten reflective shields and nine double silk net spacers were removed from the calorimeter tank. The double silk net spacer immediately outboard of the 10th reflective shield was left in place. This served to keep the thermal model consistent for the 20- and 10-shield configurations and also to reduce the temperature difference at equilibrium between the hot boundary shroud and the outer reflective shield.

The fourth set of x-ray thickness measurements was obtained then with 10 reflective shields and 11 double silk net spacers in place on the tank. In addition, the previously inoperative thermocouple at location A-10 and a

second one that malfunctioned at location C-10 (Ref Fig. 3-7) were replaced. Subsequently, the plumbing connections were leak-checked using GHe, all of the instrumentation was functionally checked, and the vacuum chamber was evacuated to prepare the system for the 10-shield test series.

Test runs 5 through 8 (Ref Table 3-5) were preformed as a single continuous series during a four-day period of around-the-clock operations. The 140°R (77°K) could boundary tests (runs 5 and 6 in that order) were conducted first. Prior to initiating test run 5, the calorimeter tank was filled with LN_2 using the same procedure described previously for the 20-shield test series (Ref Section 3.5.1). The time required to achieve thermal equilibrium was approximately 19 hours for run number 5 and approximately 37 hours for run number 6. During the transition between these two tests, only the hot boundary temperature was changed since it was not necessary to refill the calorimeter tank with LN_2. When test run number 6 was completed, the calorimeter tank was pressurixed with warm GN_2, drained, and purged with warm GH_2. Subsequently, it was refilled with LH_2, and test run number 8 was initiated. The hot boundary temperature was maintained at a nominal value of 610°R (339°K) during the draining and refilling operations. Again, the filling and topping procedures described earlier were used. Approximately 25 hours of continuous operation were required to achieve thermal equilibrium for test run number 8. After this test was completed, the hot boundary temperature was changed to the 500°R (278°K) nominal value and test run number 7 was conducted. As before, both test runs were accomplished with a single fill of the calorimeter tank. The time required to achieve thermal equilibrium for test run number 7 was approximately 21 hours.

Each of the 10-shield tests was performed with no flow through the cold guard system until the insulation temperature distributions were approximately constant (i.e., thermal equilibrium was achieved). Subsequently, the test cryogen (liquid) was introduced through the cold guard system and vented to the atmosphere through the facility vent line. For each test, the flow was continued until both the average boiloff flowrate and the insulation temperature distributions again had reached approximately steady-state values. At thermal equilibrium conditions, the average cold guard temperatures and the temperature differences between the cold guard and the calorimeter tank for the 10-shield

tests were similar to the values observed during the 20-shield tests.

A summary of the significant system measurements obtained at thermal equilibrium conditions for the four 10-shield tests is presented in Table 3-7. Equilibrium temperature distributions through the multilayers, based on measured values for particular shields, are presented in Figs. 3-21 and 3-22. Inspection of these data shows that the basic profiles are convex upward, a shape similar to that predicted by the analysis. It appears, therefore, that the physical effect(s) which caused the S-shaped temperature distributions for the 20-shield tests (i.e., non-uniform layer density through the thickness or increased conductivity through gas molecules due to insulation outgassing) was (were) not present for the 10-shield tests.

When test runs 5 through 8 were completed, the vacuum chamber was repressurized slowly with air so that additional x-ray thickness measurements could be obtained and the system could be prepared for the 5-shield tests.

3.5.3 Five-Shield Test Series

Five reflective shields and five double silk net spacers were removed from the calorimeter tank to prepare the system for the 5-shield test series. The double silk net spacer just outboard of the 5th reflective shield was left in place. This provided a consistent thermal model compared to that used for the 20- and 10-shield test series, and served to reduce the equilibrium temperature difference between the hot boundary shroud and the outer reflective shield.

Approximately half of the 5th set of x-ray thickness measurements was obtained before an equipment malfunction occurred which delayed further measurements until after the 5-shield test series was completed. These measurements were obtained with 5 reflective shields and 6 double silk net spacers in place on the tank. Prior to evacuation of the vacuum chamber for the 5-shield test series, the previously inoperative thermocouple at location B-5 (Ref Fig. 3-7) was replaced. As in the previous test series, plumbing connections were leak-checked with GHe and the instrumentation was functionally tested before evacuating the vacuum chamber.

Table 3-7

SUMMARY OF SYSTEM MEASUREMENTS OBTAINED AT EQUILIBRIUM FOR THE 10-SHIELD TEST RUNS

Test Run Number	5	6	7	8
Nominal Boundary Temperatures, T_H/T_C, $^\circ R$ ($^\circ K$)	500/140 (278/77)	610/140 (339/77)	500/37 (278/20)	610/37 (339/20)
Tank Pressure, psia (N/m^2)	13.01 (8.97×10^4)	13.00 (8.96×10^4)	12.97 (8.94×10^4)	12.99 (8.96×10^4)
Tank Temperature, $^\circ R$ ($^\circ K$)	137.4 (76.4)	137.4 (76.4)	35.8 (19.9)	35.8 (19.9)
Boiloff Flowrate, lbm/hr (kg/hr)	0.235 (0.107	0.500 (0.227)	0.135 (0.0612)	0.224 (0.102)
Av. Guard Temp., $^\circ R$ ($^\circ K$)	151 (84)	153 (85)	41 (23)	41 (23)
Hot Baffle Temp., $^\circ R$ ($^\circ K$)	507 (282)	623 (346)	503 (280)	624 (347)
Hot Shroud Temp., $^\circ R$ ($^\circ K$)	509 (283)	623 (346)	506 (281)	623 (346)
Av. Hot Boundary Temp. at 10th Shield, $^\circ R$ ($^\circ K$)	499 (277)	611 (340)	496 (276)	612 (340)
Vacuum Chamber Pressure (torr)	7×10^{-6}	7×10^{-6}	6×10^{-6}	5×10^{-6}

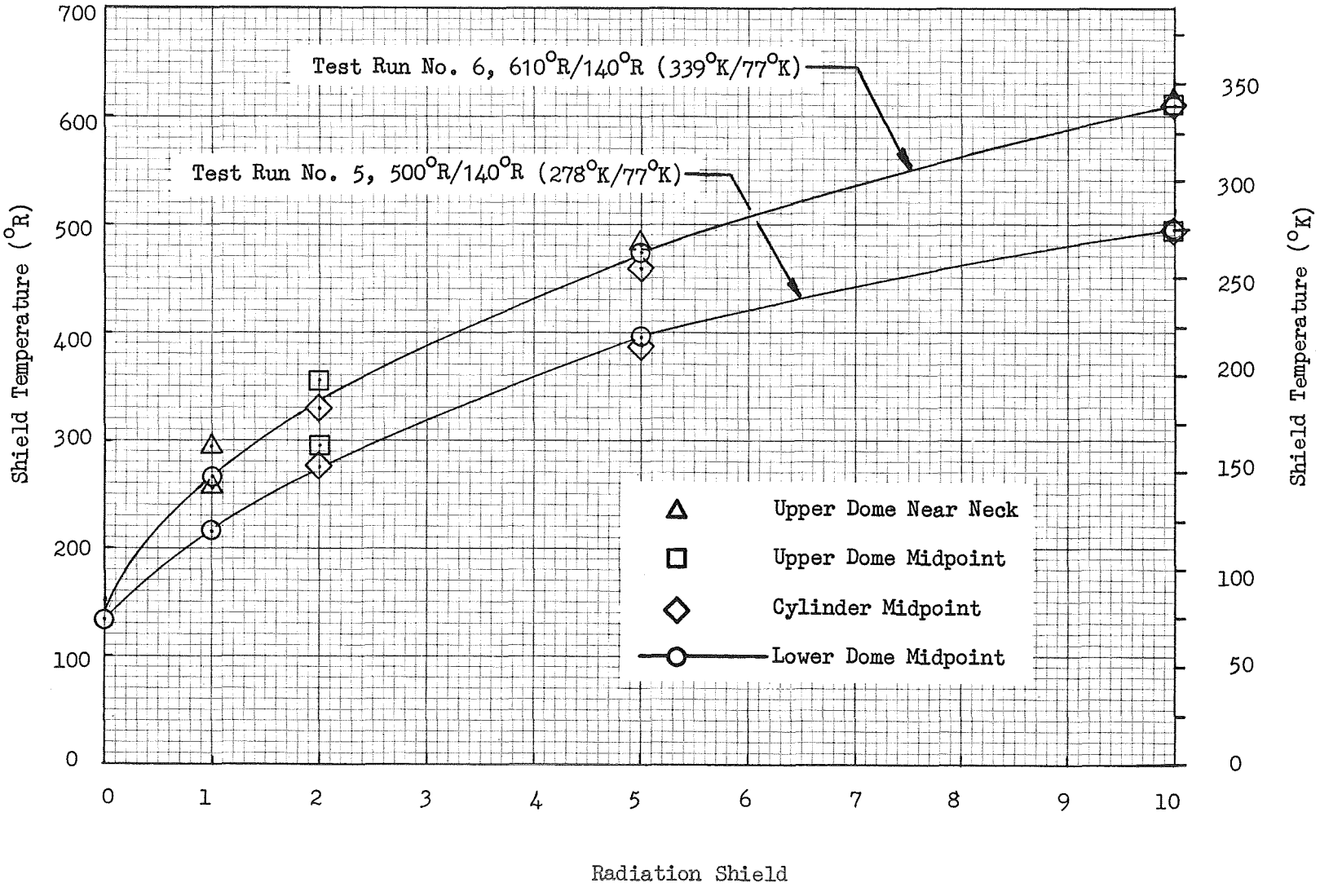

Fig. 3-21 Measured Temperature Profiles Through a 10-Shield DGM/Silk Net Insulation System with T_C = 140°R (77°K)

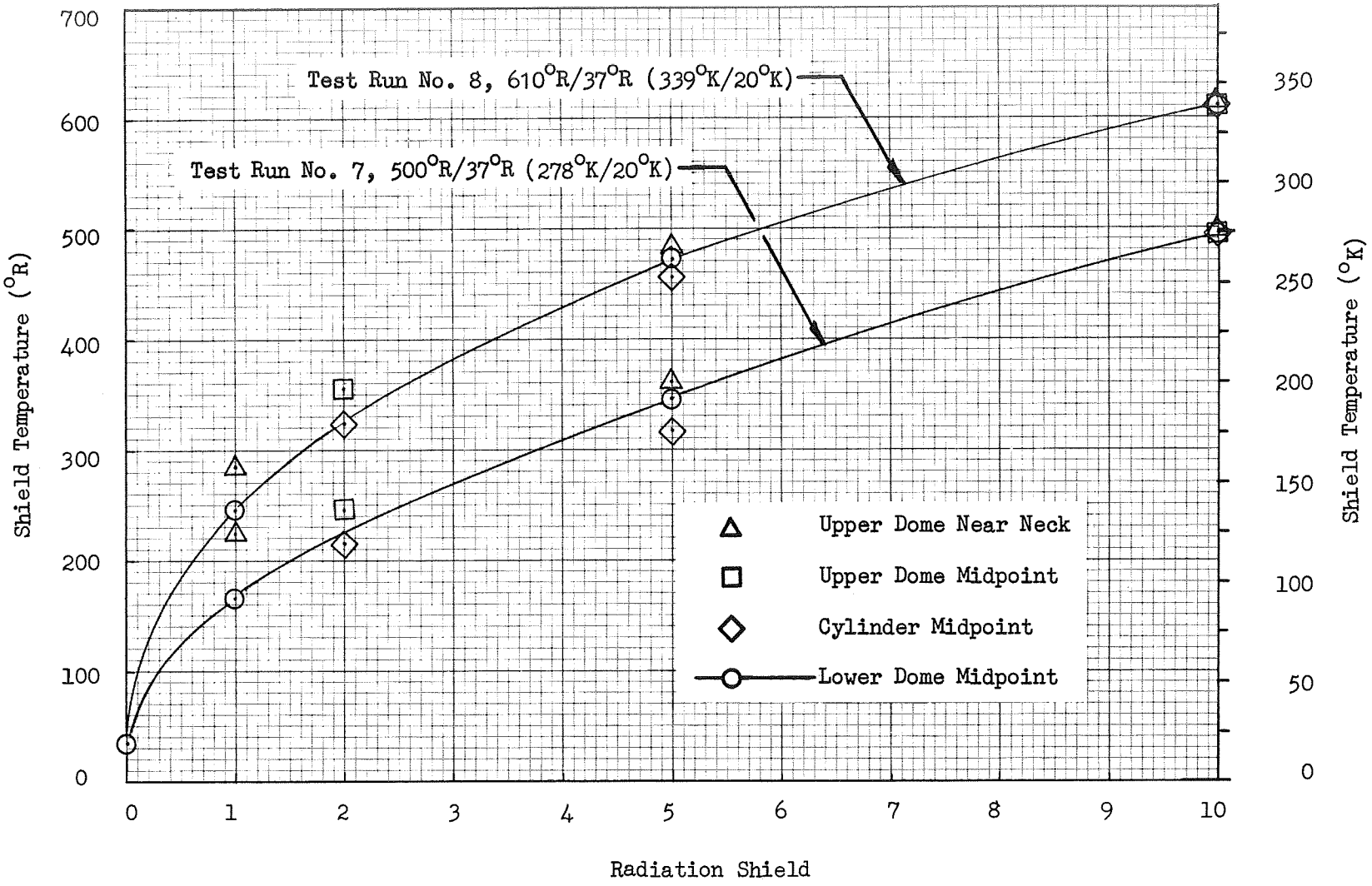

Fig. 3-22 Measured Temperature Profiles Through a 10-Shield DGM/Silk Net Insulation System with $T_C = 37°R$ $(20°K)$

The 5-shield tests were performed in two different series. Initially, test runs 9 through 12 were performed during a $4\frac{1}{2}$-day period of continuous around-the-clock operations. Then, because the data initially obtained for test run number 11 indicated that equilibrium was questionable, this test was rerun during a continuous 2-day operation. In the first series, run number 10 was conducted prior to run number 9. Similarly, run number 12 was performed before run number 11. This particular sequence was selected since results of the 10-shield tests indicated that the transition time to reach equilibrium after a change of the hot boundary temperature was minimum if the $610^{\circ}R$ ($339^{\circ}K$) hot boundary tests were run before those with the $500^{\circ}R$ ($278^{\circ}K$) hot boundary.

The calorimeter tank was filled with LN_2, using the procedure described previously, to initiate test run number 10. During the transition from run number 10 to run number 9, only the hot boundary temperature was changed. After completion of run number 9, the calorimeter tank was pressurized, drained, purged, and refilled with LH_2 to initiate test run number 12. Again, only the hot boundary temperature was changed during the transition from run number 12 to run number 11.

An investigation of the effect of vacuum chamber pressure upon insulation thermal performance was conducted during test runs 9 and 10. Boiloff flowrates were evaluated for vacuum chamber pressures of $9x10^{-6}$, $1x10^{-4}$, and $5x10^{-4}$ torr in test run number 9, and for pressures of $9x10^{-6}$, $1x10^{-4}$, and $1x10^{-3}$ torr in test run number 10. During test run number 10, approximately 34 hours of continuous operation were required to achieve thermal equilibrium at the $9x10^{-6}$ torr vacuum chamber pressure. Approximately 6 and 4 hours of continuous operation were required to achieve thermal equilibrium when the chamber pressure was increased to the $1x10^{-4}$ and $1x10^{-3}$ torr values, respectively. Subsequently, for test run number 9, thermal equilibrium was achieved after approximately 13 hours of continuous operation with the $9x10^{-6}$ torr chamber pressure. For this case, 5 and 4 hours of additional operations were required to achieve thermal equilibrium with the $5x10^{-4}$ and $1x10^{-4}$ torr vacuum chamber pressures, respectively.

In the second test series, the calorimeter tank was purged, chilled, and filled with LH_2, again using the procedures described previously. Then, the rerun of test number 11 was conducted. For this test, operations were continued for approximately 42 hours although thermal equilibrium was achieved somewhat earlier than this.

In all of the 5-shield test runs, flow through the cold guard system was initiated only after apparent thermal equilibrium had been achieved. In each case, however, the cold guard flow then was continued until new equilibrium conditions were achieved. This occurred typically in 2 to 4 hours from the time that the guard flow was initiated. At thermal equilibrium conditions, the temperature differences between the guarded neck and the calorimeter tank for the 5-shield test series were similar to those observed during the 20- and 10-shield test series.

Two additional sets of x-ray thickness measurements were obtained during the 5-shield tests. The sixth set was obtained during the interim between the first test series (runs 9 through 12) and the second series (the rerun of test number 11). The seventh and final set was obtained after completion of the test 11 rerun.

Significant system measurements obtained at thermal equilibrium conditions for test runs 9, 10, 12, and for the rerun of test 11 are summarized in Table 3-8. Measured temperature distributions through the multilayers are presented in Figs. 3-23 and 3-24 for these same test runs. It can be seen by inspection of these figures that the shape of the measured temperature distributions again are similar to those predicted by analysis as they were for the 10-shield tests (Ref. Section 3.5.2).

Data obtained from the investigation of insulation thermal performance as a function of vacuum chamber pressure are summarized in Table 3-9 and in Fig. 3-25. These data show that the increase in heat transfer for a system operating at a chamber pressure of 1×10^{-4} torr, with respect to that obtained at

Table 3-8

SUMMARY OF SYSTEM MEASUREMENTS OBTAINED AT EQUILIBRIUM FOR THE 5-SHIELD TEST RUNS

Test Run Number	9	10	11*	12
Nominal Boundary Temp, T_H/T_C, ^oR (^oK)	500/140 (278/77)	610/140 (339/77)	500/37 (278/20)	610/37 (339/20)
Tank Pressure, psia (N/m^2)	12.97 (8.94×10^4)	13.00 (8.96×10^4)	13.00 (8.96×10^4)	13.02 (8.98×10^4)
Tank Temp, ^oR (^oK)	127.4 (76.4)	137.4 (76.4)	35.8 (19.9)	35.8 (19.9)
Boiloff Flowrate, lbm/hr (kg/hr)	0.413 (0.187)	0.704 (0.319)	0.315 (0.143)	0.315 (0.143)
Av. Guard Temp., ^oR (^oK)	152 (85)	153 (85)	41 (23)	39 (22)
Hot Baffle Temp., ^oR (^oK)	506 (281)	631 (351)	526 (292)	633 (352)
Hot Shroud Temp., ^oR (^oK)	505 (281)	631 (351)	526 (292)	633 (352)
Av. Hot Boundary Temp at 5th Shield, ^oR (^oK)	489 (272)	611 (340)	506 (281)	615 (342)
Vacuum Chamber Pressure (torr)	9×10^{-6}	9×10^{-6}	6×10^{-6}	6.5×10^{-6}

* Data presented were obtained from the rerun of test 11

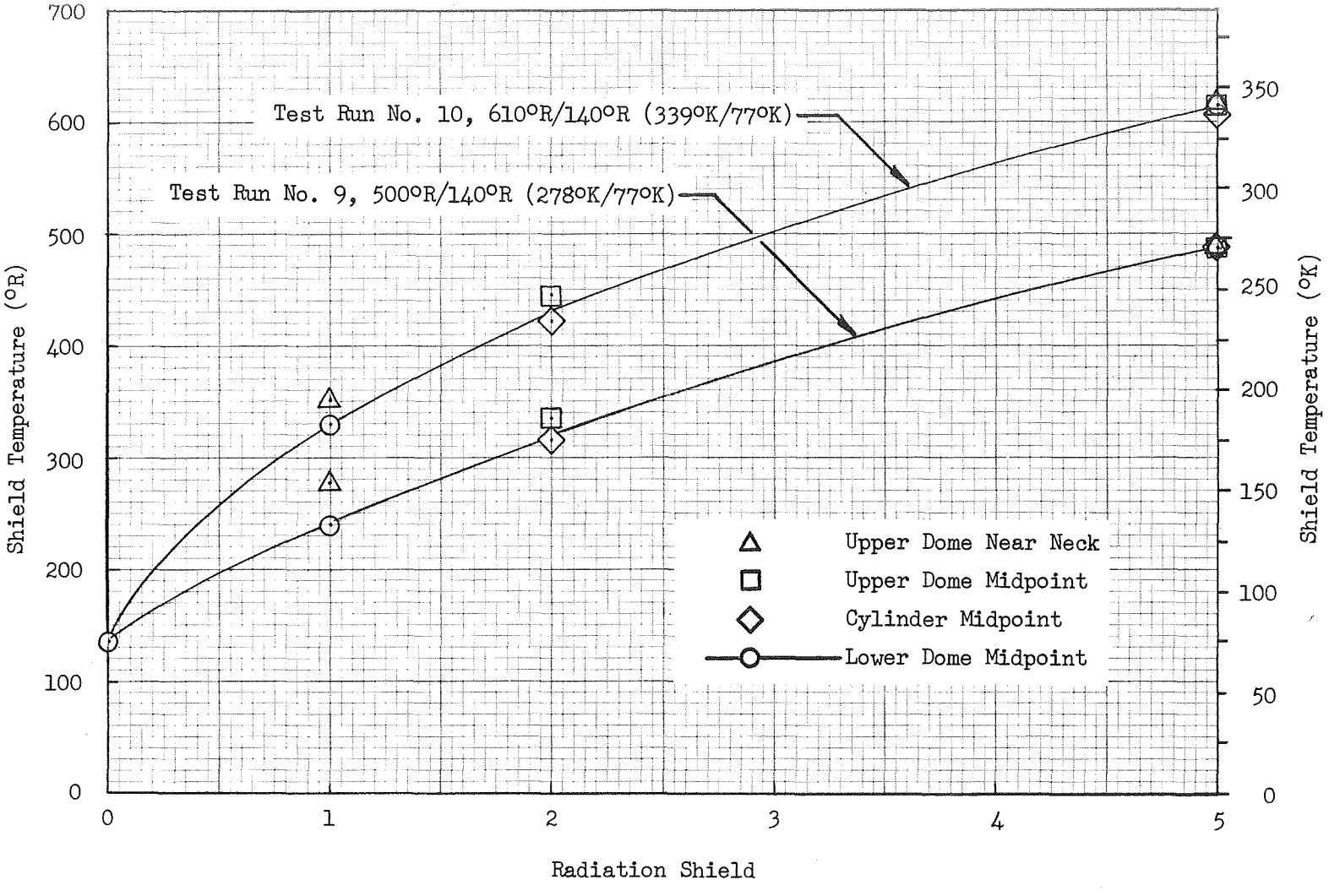

Fig. 3-23 Measured Temperature Profiles Through a 5-Shield DGM/Silk Net Insulation System with T_C = 140°R(77°K)

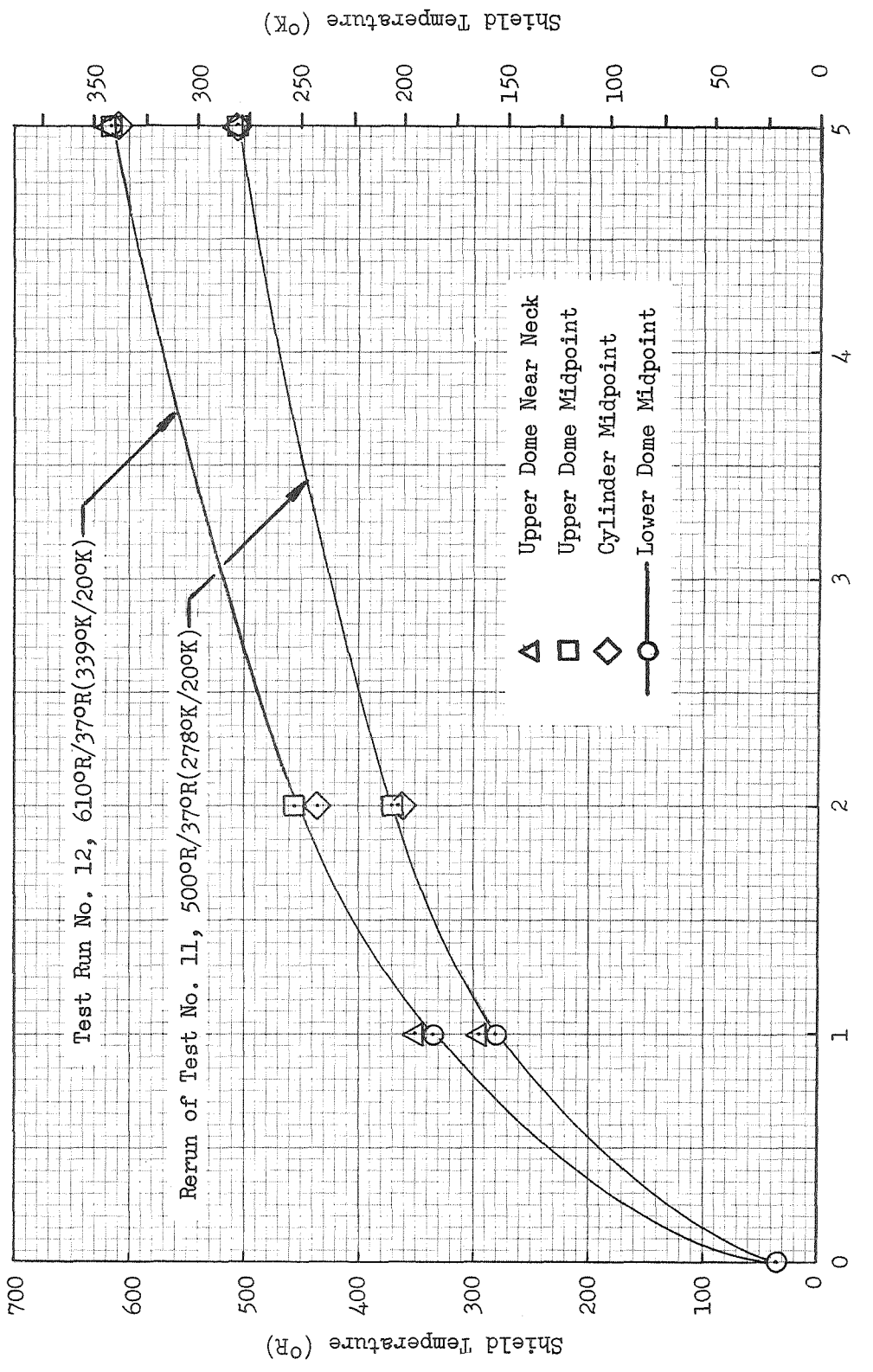

Fig. 3-24 Measured Temperature Profiles Through a 5-Shield DGM/Silk Net Insulation System with T_C = 37°R(20°K)

Table 3-9

VARIATION OF HEAT FLUX AS A FUNCTION OF VACUUM CHAMBER PRESSURE

Test Run Number	9	10
Number of Shields	5	5
Nominal Boundary Temperatures, T_H/T_C, (^oR (^oK))	500/140 (278/77)	610/140 (339/77)
Q_{PC1}/Q_{PC} Ref * for PC Ref = 9×10^{-6} torr and:		
PC1 = 1×10^{-4} torr	1.10	1.003
PC1 = 5×10^{-4} torr	1.43	--
PC1 = 1×10^{-3} torr	--	1.65

* Q values shown were obtained with flow through the cold guard for test run number 9, and with no cold guard flow for test run number 10.

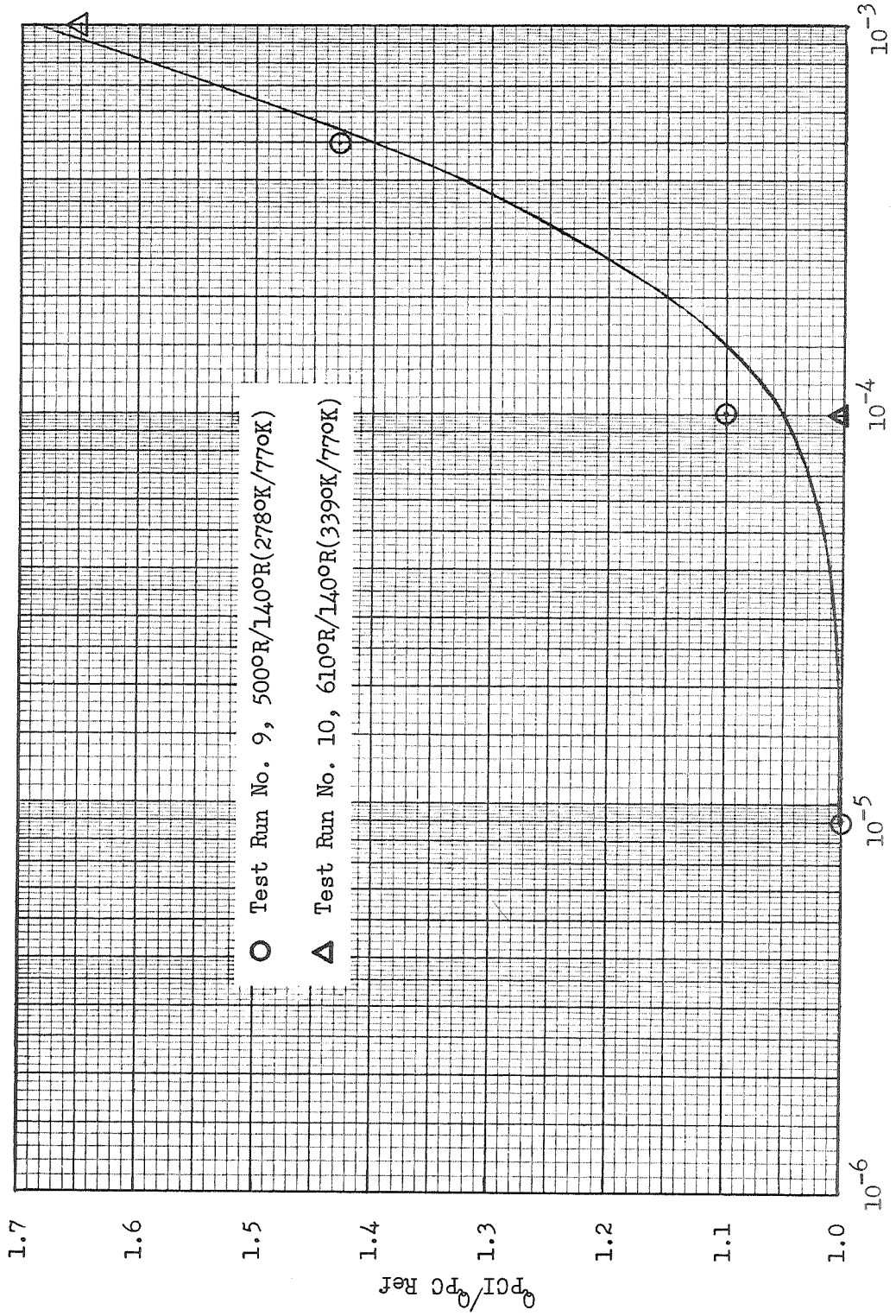

Fig. 3-25 Heat Flux as a Function of Vacuum Chamber Pressure for a 5-Shield DGM/Silk Net Insulation System

$9x10^{-6}$ torr, ranges from approximately 0.3 to 10 percent. However, at vacuum chamber pressures above $1x10^{-4}$ torr, marked increases in heat transfer were observed. Temperature distributions through the insulation thickness are presented in Fig. 3-26 for test run number 9 at vacuum chamber pressures of $1x10^{-4}$, $5x10^{-4}$, and $9x10^{-6}$ torr. Comparison of the temperature distribution at $1x10^{-4}$ torr with that at $9x10^{-6}$ torr (Ref. Fig. 3-23) shows that the effect of chamber pressure on insulation temperatures is negligible for chamber pressures of $1x10^{-4}$ torr or less.

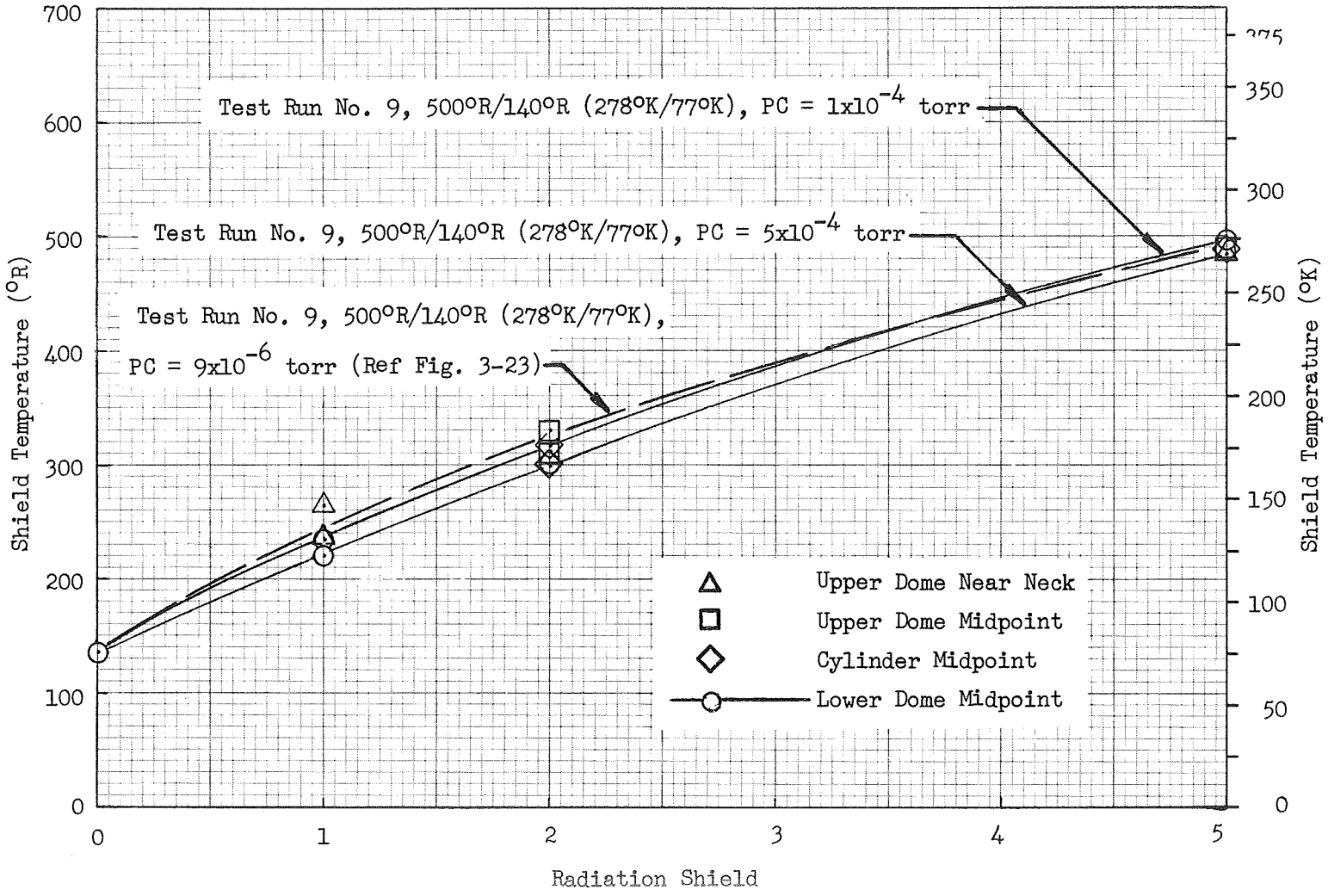

Fig. 3-26 Measured Temperature Profiles Through a 5-Shield DGM/Silk Net Insulation System with Increased Vacuum Chamber Pressures

Section 4

DISCUSSION OF RESULTS

The primary objective of the Task III analysis and test program was to assess the thermal performance of tank-installed double-goldized Mylar/silk net insulation in a high-vacuum environment by correlation of measured heat rates with those predicted by analysis. This objective was achieved. In addition, thermal performance data were obtained for this multilayer composite as a function of vacuum chamber pressure for pressures ranging from 5×10^{-6} torr (high-vacuum conditions) to 1×10^{-3} torr. Also, promising techniques were developed to determine insulation layer density values from measurements of thickness obtained after installation of the insulation on the 4-ft-(1.22-m-) diameter calorimeter tank.

Results of the tank calorimeter tests, together with comparisons of measured and predicted heat flux values, are presented in Table 4-1. In the table, the measured average heat flux is compared with both the preliminary and the final predicted values (Ref Section 3.4). The preliminary predictions were based on nominal boundary temperatures, layer density values determined from the pretest x-rays only, and the total number of shields on the tank for each test. Inspection of the table shows that the data scatter from this comparison ranges from +59 percent for test run number 2 to -12 percent for the rerun of test number 11. The final predictions shown were based on measured boundary temperatures, the average layer density values from both pretest and (where available) post-test x-rays, and the number of shields actually effective in resisting conductive and radiative heat transfer for each test. From this comparison, the data scatter ranges from +50 percent for test run number 2 to -28 percent for test run number 12.

A post-test analysis of the results presented above was conducted to determine why the final predictability range obtained for the tank tests (i.e., +50 to -28 percent) was somewhat greater than that obtained for the Task II flat plate calorimeter tests (i.e., $\pm$25 percent, Ref 1, Section 4.3.2).

TABLE 4-1

COMPARISON OF MEASURED AND PREDICTED HEAT FLUX VALUES FOR THE TANK CALORIMETER TESTS

Test Run Number	Total Number of Shields	Boundary Temperatures[a] T_H °R (°K)	T_C °R (°K)	Preliminary Predicted Av. Heat Flux[b] q_{P1} Btu/hr ft^2 (w/m^2)	Final Predicted Av. Heat Flux[c] q_{P2} Btu/hr ft^2 (w/m^2)	Measured Av. Heat Flux[d] q_M Btu/hr ft^2 (w/m^2)	Preliminary Comparison $100(q_M/q_{P1}-1)$ (Percent)	Final Comparison $100(q_M/q_{P2}-1)$ (Percent)
1	20	501(279)	137(76)	0.335 (1.056)	0.345 (1.087)	0.447[e] (1.409)	+33	+30
2	20	615(342)	137(76)	0.552 (1.740)	0.585 (1.844)	0.879[e] (2.771)	+59	+50
3	20	502(279)	36(20)	0.340 (1.072)	0.369 (1.163)	0.343 (1.081)	+ 1	- 7
4	20	611(340)	36(20)	0.562 (1.771)	0.597 (1.882)	0.719 (2.266)	+28	+20
5	10	499(277)	137(76)	0.422 (1.330)	0.439 (1.384)	0.510 (1.608)	+21	+16
6	10	611(340)	137(76)	0.722 (2.276)	0.776 (2.446)	1.085 (3.420)	+50	+40
7	10	496(276)	36(20)	0.435 (1.371)	0.458 (1.444)	0.650 (2.049)	+49	+42
8	10	612(340)	36(20)	0.732 (2.307)	0.805 (2.537)	1.078 (3.398)	+47	+34
9	5	489(272)	137(76)	0.610 (1.923)	1.106 (3.486)	0.900 (2.837)	+48	-19
10[f]	5	611(340)	137(76)	1.140 (3.593)	2.003 (6.313)	1.532 (4.829)	+34	-24
11	5	506(281)	36(20)	1.720 (5.421)	1.571 (4.952)	1.522 (4.797)	-12	- 3
12	5	615(342)	36(20)	1.140 (3.593)	2.112 (6.657)	1.520 (4.791)	+33	-28

Notes:

(a) Nominal T_H values were 500 and 610°R (278 and 339°K); nominal T_C values were 140 and 37°R (77 and 20°K); values shown were measured at equilibrium test conditions

(b) Based on nominal boundary temperatures, pre-test layer densities, and total number of shields (Ref Table 3-4)

(c) Based on measured boundary temperatures, average pre-test and post-test layer densities, and corrected number of shields (Ref Table 3-4)

(d) Based on measured boiloff flowrates and the insulation surface area at mid-thickness

(e) Data shown were corrected for effect of vacuum chamber pressure above 1×10^{-5} torr (Ref Table 3-9 and Fig. 3-25)

(f) Data shown are for rerun of this test

It was found from this analysis that the higher tolerances associated with measured thicknesses and corresponding layer density values for the tank-installed insulation, compared to those for the flat plate specimens, could account entirely for the increased heat flux scatter observed for the tank tests. To illustrate this point, the final prediction equation (Ref 1, Equation 4.38) was used to compute the theoretical layer density values which would be required for the predicted and measured flux values to match exactly (i.e., zero data scatter) for each of the tank test runs. Results of these computations are presented in Table 4-2. It can be seen from these results that an uncertainity range in layer density values of +17 to -14 percent is equivalent to heat flux data scatter of +50 to -28 percent. The estimated uncertainity of the layer density values obtained from 7 sets of x-rays in Task III ranges from ± 5 to ± 10 percent (Ref Section 3.3.1). Based on results of the analysis described above, a ± 10 percent uncertainity in layer density would be approximately equivalent to ± 25 percent scatter in heat flux values. Therefore, the heat flux scatter observed for the flat plate calorimeter tests was much smaller than that observed for the tank calorimeter tests primarily because the layer density values measured for the flat plate calorimeter tests were significantly more accurate than those measured for the tank calorimeter tests. This result illustrates the high influence of layer density on thermal performance, and clearly indicates that more development work is needed to further improve layer density control during installation, and assessment of insulation after installation, if the predictability range is to be narrowed from the +50 to -28 percent values obtained in this program.

A critical factor that must be given careful consideration in any test program to measure insulation thermal performance based on the boiloff flowrate of a cryogen is that of maintaining the test fluid at constant pressure and the corresponding saturated temperature during the test period. The procedure used to load the calorimeter tank and to conduct the boiloff tests in Task III were carefully selected to achieve constant pressure and saturated conditions within the calorimeter tank. During loading of the tank, the cryogenic test

Table 4-2

CHANGE IN MEASURED LAYER DENSITIES REQUIRED
TO ACHIEVE ZERO HEAT FLUX DATA SCATTER

Test Run Number	Total Number of Shields	Measured Layer Density[a] $\bar{N}_M$ No./in. (No./cm)	Computed Layer Density[b] $\bar{N}_C$ No./in. (No./cm)	$\Delta\bar{N}$ Required for Zero Scatter 100 ($\bar{N}_C/\bar{N}_M$-1) (Percent)
1	20	71.5 (28.1)	78.4 (30.9)	+ 9.7
2	20	71.5 (28.1)	83.3 (32.8)	+16.5
3	20	71.5 (28.1)	69.6 (27.4)	- 2.7
4	20	71.5 (28.1)	76.7 (30.2)	+ 7.3
5	10	60.4 (23.8)	64.0 (25.2)	+ 6.0
6	10	60.4 (23.8)	69.7 (27.4)	+15.4
7	10	60.4 (23.8)	68.9 (27.1)	+14.1
8	10	60.4 (23.8)	68.4 (26.9)	+13.2
9	5	67.1 (26.4)	62.0 (24.4)	- 7.6
10	5	67.1 (26.4)	59.5 (23.4)	-11.3
11[c]	5	72.3 (28.5)	71.5 (28.1)	- 1.1
12	5	67.1 (26.4)	57.9 (22.8)	-13.7

Notes:

(a) Average values from pre-test and (where available) post test x-rays

(b) Computed from final heat flux equation assuming predicted heat flux values are equal to measured heat flux values

(c) Data shown are for rerun of this test

fluid was allowed to reach thermal equilibrium (i.e., saturated conditions) quickly by controlling the tank pressure to approximately 5 psia ($3.4 \times 10^4 N/m^2$) less than the previous saturated storage pressure. This resulted in vigorous bulk boiling and thorough mixing of the fluid during the fill process. Further bulk boiling and mixing was induced after the tank was filled when the calorimeter tank pressure was lowered to the desired operating pressure (nominally 13 psi or $8.96 \times 10^4 N/m^2$) by vacuum pumping of the vent line. After the initial test conditions were established, constant tank pressure was achieved during the test period by throttling the boiloff vapor flow through an adjustable orifice provided by the back-pressure regulator. The orifice size and the magnitude of the differential pressure from the calorimeter tank to the partially-evacuated vent line were such that the vapor flow was choked throughout the test duration.

During each test, all of the data including tank pressure were recorded nominally at 1600-second intervals. Critical parameters such as the tank pressure were also displayed continuously on stripchart recorders. When thermal equilibrium within the tank and the insulation was achieved, as indicated by nominally-constant insulation shield temperatures and boiloff flowrates (with the cold guard in operation) test data were recorded at 1-sec intervals for two 10-min periods approximately 30 minutes apart before the test was terminated. In reducing the measured data for each test run, boiloff flowrate values were obtained both by averaging the 1600-sec interval data for approximately 2 to 4 hours at the equilibrium conditions and by averaging 300 to 600 of the 1-sec interval data points for each of the two 10-min periods. Values obtained by these independent computations were generally consistent within ± 2 percent; however, the average values obtained from the 1-sec interval data were considered to be the most valid statistically and were used in the data comparisons presented in this report.

It was found from results of the test data analysis described above that the average boiloff flowrate values obtained using these procedures were accurate even though the boiloff flowrate appeared to oscillate in magnitude whenever

the cold guard was operated (Ref Section 3.5.1). Since fluid temperatures measured at the cold guard inlet and outlet sensor locations also oscillated during operation of the cold guard, it was concluded that the flowrate oscillations were in fact induced by the guard fluid temperature oscillations. However, these oscillations had no measurable effect on tank pressure since the pressure sensing equipment used was sensitive to pressure fluctuations as low as 0.01 psi (69 N/m^2) and since no pressure fluctuations were observed.

An analysis was conducted in conjunction with the 20-shield test series to predict theoretical neck heat leak values as a function of cold guard temperatures, and to correlate the predictions with test data. Results of the analysis are presented in Figs. 4-1 and 4-2 for operation of the system with LN_2 and LH_2, respectively. The curves shown in the figures represent calculated neck heat leaks based on (1) radiation only down the neck cavity, (2) radiation plus solid conduction down the neck, and (3) the approximate net effect of interacting the radiation and conduction heat transfer components. The interaction coefficient of 1.29 (Ref. 9) neglects any cooling due to boiloff gas outflow.

The data points shown in the figures were obtained from the 20-shield test series. The temperature of the cold guard for each data point was taken as the average of the guard fluid temperatures measured at the guard inlet and outlet temperature sensor locations, except for points 4a and 4b in Fig. 4-2. The temperatures shown for the latter points were calculated upper and lower limits, since no direct measurements were made at this location and since there was no fluid flow through the guard system at the time these data points were obtained. Point 4a represents the lowest possible neck temperature at the guard. It is based on the conservative assumption that a straight-line temperature gradient existed between the support flange, assumed to be at the $610^{\circ}R(339^{\circ}K)$ hot boundary temperature, and the $35.8^{\circ}R(19.9^{\circ}K)$ tank fluid. Point 4b, on the other hand, represents the highest possible neck temperature at the guard, assuming that it is thermally shorted directly to the guard inlet line flange, since this is a relatively short copper line.

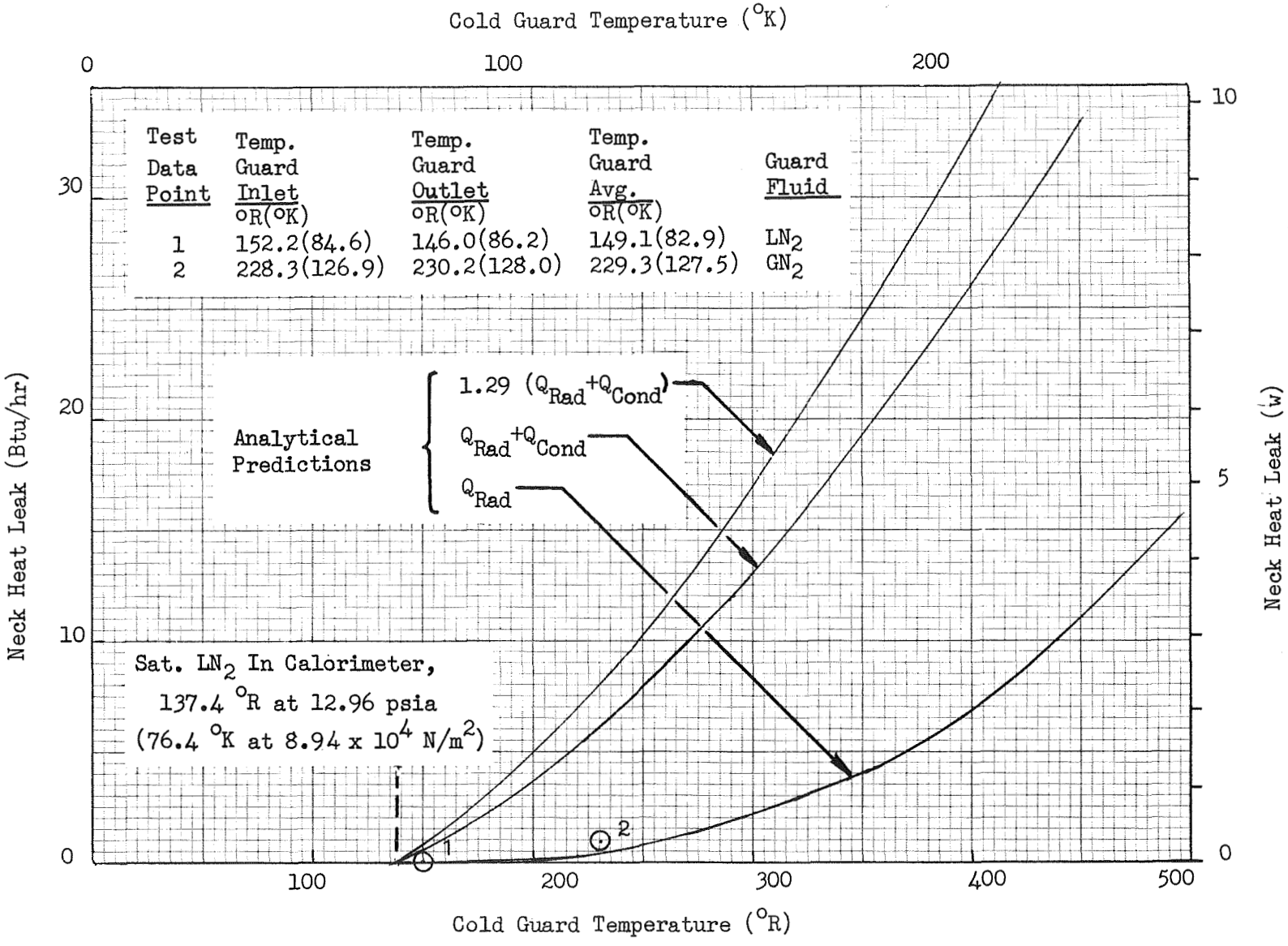

Fig. 4-1 Tank Calorimeter Neck Heat Leak as a Function of Cold Guard Temperature for Operation with LN_2

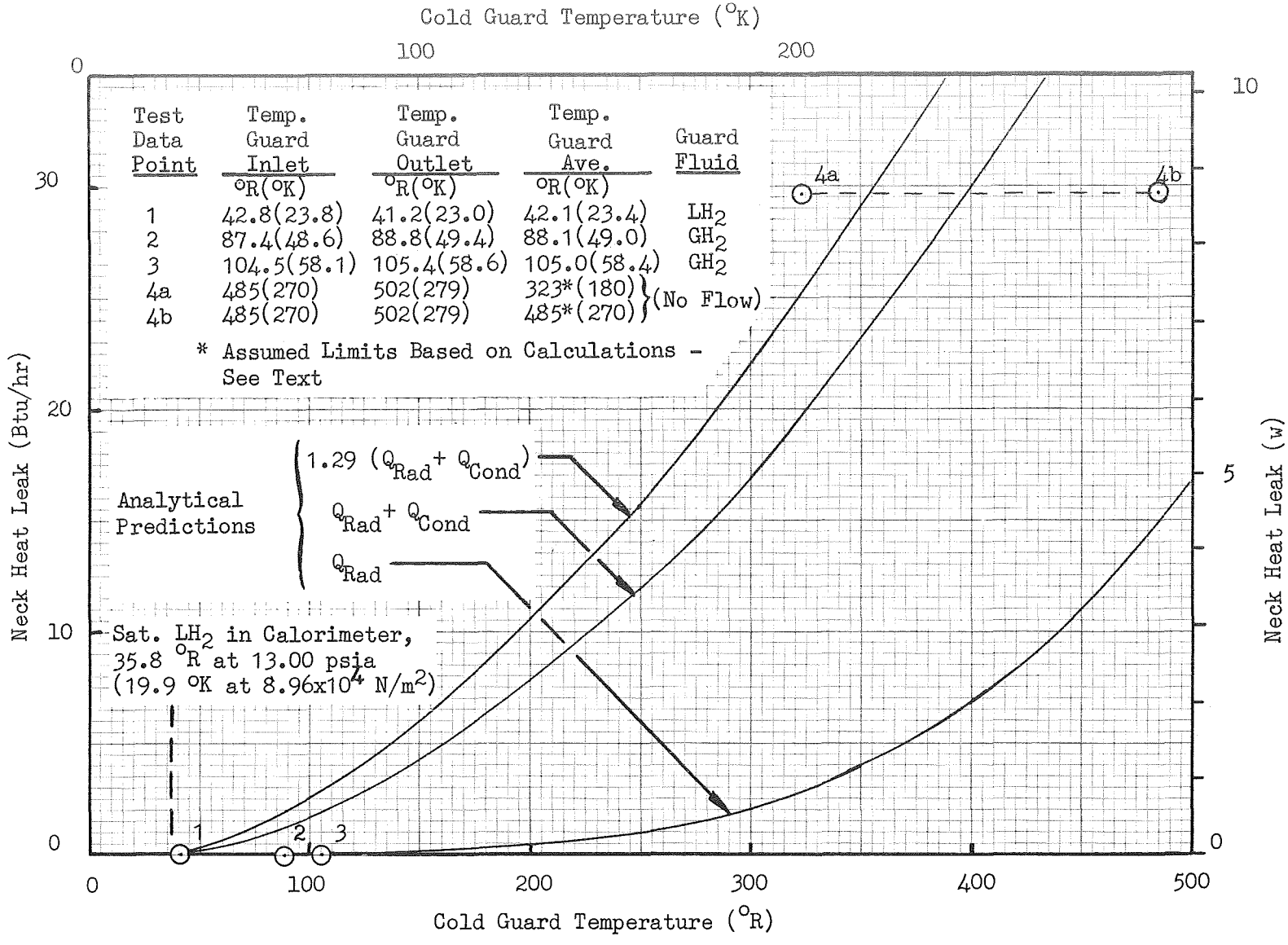

Fig. 4-2 Tank Calorimeter Neck Heat Leak as a Function of Cold Guard Temperature for Operation with LH_2

In this case, it was assumed to be equal to the measured guard inlet temperature, T_{G1}.

The neck heat leak value for data point 1 shown in Fig. 4-1 was taken as the zero reference for operation of the system with LN_2. The heat leak value for data point 2 was then computed as the difference between the total measured heat rates to the tank for points 1 and 2. Based on these two data points, the net neck heat leak as a function of guard temperature correlates well with the radiation-only prediction. This indicates that the neck wall between the tank and the guard could have been cooled by the outflowing boiloff gas to the extent that the conduction heat transfer component was negligible. In any case, it appears from these data that the net effect of the neck heat leak was negligible for guard temperatures below approximately $160^{\circ}R$ ($89^{\circ}K$).

A similar conclusion was reached regarding operation of the system with LH_2. In this case, the neck heat leak value for data point 1 shown in Fig. 4-2 was taken as the zero reference point. The heat leak values for data points 2, 3, 4a, and 4b were then computed as the respective differences between the total measured heat rates to the tank for those points and for point 1. Based on the data for points 1, 2, and 3, the radiation-only prediction again appears to be valid. Since points 4a and 4b do not correlate well with the radiation-only prediction, it appears that for this case the cooling effect of the outflowing boiloff gas was insufficent to balance the conduction heat transfer at this high guard temperature. There also may have been an additional secondary effect at this high guard temperature due to two-dimensional heat transfer through the neck and upper dome insulation. For operation of the system with LH_2, it appears that a negligible neck heat leak was incurred for guard temperatures up to approximately $120^{\circ}R$ ($67^{\circ}K$).

The effect of vacuum chamber pressure on the thermal performance of double-goldized Mylar/silk net insulation was investigated in the 5-shield test series. During test run numbers 9 and 10, the chamber pressure was varied to achieve steady-state values ranging from approximately 9×10^{-6} torr (high

vacuum) to $1x10^{-3}$ torr by injecting a controlled bleed flow of GHe from a bottled source into the chamber through a needle valve. Initially, for each of these test runs, equilibrium boiloff flowrates were obtained for a chamber pressure value of $9x10^{-6}$ torr with no bleed flow of GHe. Then equilibrium boiloff flowrates were obtained at the higher chamber pressure values with the required flow of GHe. The degradation effect of chamber pressure on heat rate can be seen in Fig. 3-25 where the ratio of measured heat rate at a particular vacuum chamber pressure to that for the reference chamber pressure value of $9x10^{-6}$ torr is plotted as a function of the chamber pressure value. These data show that no significant degradation occurred until the chamber pressure was increased to values of $1x10^{-4}$ torr or greater.

Seven different sets of x-ray thickness measurements were obtained during the tank calorimeter test program. Thickness values obtained from these measurements were used to compute the corresponding layer density values at particular target locations. A total of 22 target locations distributed over the entire calorimeter tank surface were used. Scaling techniques were developed and improved during the program to obtain more accurate thickness measurements. Area-weighted average values of layer density for each x-ray set were computed using local layer density values and the corresponding incremental surface areas for each target point. The resulting area-weighted averages were used to predict the thermal performance of the calorimeter tank insulation. A summary of the area-weighted averages obtained from the analysis of x-ray data is presented in Table 4-3.

Based on the data shown in the table, it appears that the layer density values for the double-goldized Mylar/silk net insulation system evaluated in Task III actually were changing due to forces imposed during the evacuation and repressurization cycles. However, this apparent behavior could not be conclusively verified since the magnitude of the changes are within the uncertainity of the x-ray thickness measurements. These results indicate that additional test data should be obtained to determine whether such changes in

Table 4-3

SUMMARY OF AREA-WEIGHTED AVERAGE LAYER DENSITY VALUES OBTAINED FROM X-RAY THICKNESS MEASUREMENTS

X-Ray Set	Total Number of Shields	Test Run Series	Area-Weighted Average Layer Densities No./in. (No./cm)
1st	20		70.8 (27.9)
2nd	20		(a)
		1 through 4 (b) (c)	71.5 (d) (28.1)
3rd	20		72.2 (28.4)
4th	10		60.4 (23.8)
		5 through 8 (b)	60.4 (d) (23.8)
5th	5		54.0 (21.3)
		9 through 12 (b)	67.1 (d) (26.4)
6th	5		80.1 (31.5)
		Rerun of 11 (b)	72.3 (d) (28.5)
7th	5		64.4 (25.4)

Notes:

(a) No usable data obtained due to target movements

(b) Vacuum chamber and insulation evacuated prior to each test series and repressurized after each series

(c) An additional repressurization/evacuation cycle imposed between test runs 1-2 and 3-4

(d) Arithmetic average of pre-test and post-test values used in predictions

layer density do occur in fact. If they do, additional development of layer density control and assessment techniques also are needed to further improve the predictability and usefulness of this or any multilayer insulation.

Section 5

CONCLUSIONS

Results of analytical and experimental studies conducted under Task 1, Insulation Repeatability and Calorimeter Checkout, and of Task II, Multilayer Insulation Performance, are presented and discussed in the Interim Report (Ref. 1). Results of Task III, Insulation Installation Verification, are presented and discussed in this Final Report.

Based on results obtained in Task III, the thermal performance for a single installation of double-goldized Mylar/silk net insulation on a 4-ft-(1.22-m-) diameter tank was found to be analytically predictable within approximately ±50 percent. However, achievement of even this degree of predictability required assessment of reflective shield emittance values and the temperature dependency of emittance as well as area-weighted average layer density values within approximately ±10 percent. Good results were achieved in Task III using an x-ray thickness measurement technique to assess layer density values within this required accuracy.

It appears from evaluation of the Task III x-ray and boiloff test data that insulation layer density values could have been significantly changed between test runs by gas-flow forces imposed during evacuation and repressurization cycles. This result could not be verified conclusively since the magnitudes of the apparent changes were within the accuracy of the layer density values based on x-ray thickness measurements. It is significant to note, however, that the gas flow rates imposed in the test program were much lower than those which would be realized during ascent and/or reentry flight of an actual space vehicle. Consequently, the impact on thermal performance of the insulation from such changes could be great considering the strong influence of layer density on heat rate shown by the analysis and test data. In any case, it is clear that layer density control is perhaps the single

most important requirement in the application and use of multilayer insulations. It is also clear that improved accuracy in assessing as-installed thicknesses must be developed if the ± 50 percent predictability range observed in this program is to be narrowed further.

The conclusions which resulted from evaluation of the Task III work are:

1. Thermal performance of tank-installed double-goldized Mylar/silk net insulation in a high-vacuum environment can be predicted within approximately ± 50 percent by using the analytical techniques and data developed in this program.

2. Gas-flow forces which are imposed on multilayer insulation during evacuation and repressurization cycles appear to result in significant changes to the as-installed layer density. This should be conclusively verified by additional testing. For DGM/silk net insulation, a change in layer density of ± 10 percent will result in a corresponding change in thermal performance of approximately ± 25 percent.

3. Additional work is needed to further develop insulation layer density control and thickness assessment techniques.

4. Advanced studies conducted by various investigators have indicated that from 100 to 200 layers of insulation may be required to achieve long-duration storage for some future missions. Additional tests should be performed on the DGM/silk net or other selected insulation systems to assess the temperature dependency of shield emittance and solid conduction heat transfer, and to assess thermal performance and outgassing characteristics for specimens of up to 100 layers or more. Data which could be obtained from such tests are needed to evaluate the applicability of the analytical prediction techniques developed in this program to installations of greater thickness.

NOMENCLATURE

DGM = double-goldized Mylar insulation

FB = boiloff gas flowrate from tank calorimeter vent, lbm/hr (kg/hr)

$\bar{N}$ = layer density of an insulation system, No./in. (No./cm)

$\Delta\bar{N}$ = increment of change in insulation layer density, dimensionless

$\bar{N}_C$ = computed value of insulation layer density, No./in. (No./cm)

$\bar{N}_M$ = measured value of insulation layer density, No./in. (No./cm)

N_s = number of radiation shields in an insulation system, dimensionless

P = total compressive pressure acting on an insulation system per unit area, psi (N/m^2)

PC = vacuum chamber pressure, torr

PC1 = vacuum chamber pressure with GHe bleed flow, torr

PC Ref = vacuum chamber pressure with no GHe flow (i.e., high-vacuum), torr

P_o = compressive pressure acting on an insulation system per unit area due to its own weight, psi (N/m^2)

PTU = measured tank ullage pressure, psia (N/m^2)

PV = measured vacuum chamber pressure, torr

Q = heat rate, Btu/hr (w)

Q_{cond} = heat rate due to solid conduction, Btu/hr (w)

Q_{rad} = heat rate due to radiation, Btu/hr (w)

Q_{PC1} = heat rate into tank calorimeter with a degraded vacuum chamber pressure, Btu/hr (w)

$Q_{PC\ Ref}$ = heat rate into tank calorimeter with a reference vacuum chamber pressure, Btu/hr (w)

R = radius, in. (cm)

TA = tank calorimeter thermocouple installed at location A (Ref. Fig. 3-7)

TB = tank calorimeter thermocouple installed at location B (Ref. Fig. 3-7)

= absolute temperature of the tank calorimeter hot boundary baffle, ^{o}R (^{o}K)

TC = thermocouple

= tank calorimeter thermocouple installed at location C (Ref. Fig. 3-7)

TD = tank calorimeter thermocouple installed at location D (Ref. Fig. 3-7)

T_C = absolute temperature of the tank calorimeter cold boundary, ^{o}R (^{o}K)

TH = absolute temperature of the tank calorimeter hot boundary shroud, ^{o}R (^{o}K)

T_H = absolute temperature of the tank calorimeter insulation hot boundary, ^{o}R (^{o}K)

TGI = absolute temperature of the tank calorimeter cold guard inlet, ^{o}R (^{o}K)

TGO = absolute temperature of the tank calorimeter cold guard outlet, ^{o}R (^{o}K)

TLO = absolute temperature of the tank calorimeter liquid overflow, ^{o}R (^{o}K)

T_m = absolute mean temperature of an insulation system (i.e., average of the hot and cold boundary surface temperatures), ^{o}R (^{o}K)

TV = absolute temperature of the tank calorimeter vent gas, ^{o}R (^{o}K)

a''' = a constant correlation coefficient of compressive pressure that characterizes solid conduction heat transfer for DGM/silk net insulation

c = a constant coefficient, dimensionless

m''' = a constant correlation exponent of compressive pressure that characterizes solid conduction heat transfer for DGM/silk net insulation

n = a constant exponent, dimensionless

q = total heat flux through an insulation system, Btu/hr ft^2 (w/m^2)

q_M = measured average heat flux through the tank calorimeter insulation based on boiloff flowmate, Btu/hr ft^2 (w/m^2)

q_{P1} = predicted average heat flux through the tank calorimeter insulation based on preliminary data, Btu/hr ft^2 (w/m^2)

q_{P2} = predicted average heat flux through the tank calorimeter insulation based on final data, Btu/hr ft^2 (w/m^2)

α_4 = a constant correlation exponent that relates absolute temperature to the total hemispherical emittance of a radiation shield surface

ϵ_{TRG} = total hemispherical emittance of a double-goldized Mylar radiation shield at room temperature, dimensionless

σ = Stefan-Boltzmann constant = 1.713×10^{-9} Btu/hr ft^2 $^oR^4$ (5.669×10^{-8} w/m^2 $^oK^4$)

REFERENCES

1. NASA-CR 72605, "Thermal Performance of Multilayer Insulations," Interim Report for Contract NAS 3-12025, Lockheed Missiles & Space Company, Sunnyvale, California, April, 1971.

2. Black, I. A. and Glaser, P. E., "The Performance of a Double-Guarded Cold Plate Thermal Conductivity Apparatus," Advances in Cryogenic Engineering (Plenum Press, N. Y., 1964), Vol. 9, page 52.

3. Coston, R. M. and Zierman, C. A., "Cryogenic Thermal Conductivity Measurements of Insulating Materials," Special Technical Publication No. 411, ASTM, 1967.

4. Caren, R. P. and Cunnington, G. R., "Heat Transfer in Multilayer Insulation Systems," Chemical Engineering Progress Symposium Series, Vol. 64, No. 87, 1968, page 67.

5. NASA-CR 55864, "Liquid Propellant Losses During Space Flight," Final Report for Contract NASw-615, Arthur D. Little, Inc., Cambridge, Mass., October, 1963.

6. NASA-CR 54191, "Basic Investigations of Multilayer Insulation Systems," Final Report for Contract NAS 3-4181, Arthur D. Little, Inc., Cambridge, Mass., October, 1964.

7. NASA-CR 54929, "Advanced Studies on Multilayer Insulation Systems," Final Report for Contract NAS 3-6283, Arthur D. Little, Inc., Cambridge, Mass., June, 1966.

8. NASA-CR 72368, "Advanced Studies on Multilayer Insulation Systems," Final Report for Contract NAS 3-7974, Arthur D. Little, Inc., Cambridge, Mass., January, 1968.

9. LMSC-A742593-1, "Design of High-Performance Insulation Systems," Summary Report for NASA contract NAS 8-11347, August 1965.

DISTRIBUTION LIST FOR FINAL REPORT, NASA CR-72747,
THERMAL PERFORMANCE OF MULTILAYER INSULATIONS

		Copies
National Aeronautics and Space Administration Lewis Research Center 21000 Brookpark Road Cleveland, Ohio 44135		
Attention:	Contracting Officer, MS 500-313	1
	Liquid Rocket Technology Branch, MS 500-209	8
	Technical Report Control Office, MS 5-5	1
	Technology Utilization Office, MS 3-16	1
	AFSC Liaison Office, MS 4-1	2
	Library	2
	D. L. Nored, MS 500-209	1
	Office of Reliability & Quality Assurance, MS 500-111	1
	E. W. Conrad, MS 100-1	1
	W. E. Roberts, MS 3-17	1
	R. Knoll, MS 501-2	1
	J. Kennard, MS 3-14	1
National Aeronautics and Space Administration Washington, D.C. 20546		
Attention:	Code MT	1
	RPX	2
	RPL	2
	SV	1
	RV-2	1
Scientific and Technical Information Facility P. O. Box 33 College Park, Marylard 20740		
Attention:	NASA Representative Code CRT	6
Office of the Director of Defense Research & Engineering Washington, D. C. 20301		
Attention:	Dr. H. W. Schulz, Office of Asst. Dir. (Chem. Technology)	1

	Copies
Defense Documentation Center Cameron Station Alexandria, Virginia 22314	1
RTD (RTNP) Bolling Air Force Base Washington, D. C. 20332	1
Arnold Engineering Development Center Air Force Systems Command Tullahoma, Tennessee 37389 Attention: AEOIM	1
Advanced Research Projects Agency Washington, D. C. 20525 Attention: D. E. Mock	1
Aeronautical Systems Division Air Force Systems Command Wright-Patterson Air Force Base, Dayton, Ohio Attention: D. L. Schmidt, Code ASRCNC-2	1
Air Force Missile Test Center Patrick Air Force Base, Florida Attention: L. J. Ullian	1
Air Force FTC (FTAT-2) Edwards Air Force Base, California 93523 Attention: Col. J. M. Silk	1
Air Force Office of Scientific Research Washington, D. C. 20333 Attention: SREP, Dr. J. F. Masi	1
National Aeronautics and Space Administration Ames Research Center Moffett Field, California 94035 Attention: Library	1
National Aeronautics and Space Administration Goddard Space Flight Center Greenbelt, Maryland 20771 Attention: Library W. C. Lund, Code 623	1 1

	Copies
National Aeronautics and Space Administration John F. Kennedy Space Center Cocoa Beach, Florida 32931 Attention: Library	1
National Aeronautics and Space Administration Langley Research Center Langley Station Hampton, Virginia 23365 Attention: Library R. R. Heldenfels	1 1
National Aeronautics and Space Administration Manned Spacecraft Center Houston, Texas 77001 Attention: Library Merlyn Lausten (EP-2)	1 1
National Aeronautics and Space Administration George C. Marshall Space Flight Center Huntsville, Alabama 35812 Attention: Library Keith Chandler, S & E-ASTN Clyde Nevins E. H. Hyde I. G. Yates J. M. Stuckey	1 1 1 1 1 1
Jet Propulsion Laboratory 4800 Oak Grove Drive Pasadena, California 91103 Attention: Library Lou Toth	1 1
U. S. Air Force Washington 25, D. C. Attention: Col. C. K. Stambaugh, Code AFRST	1
Bureau of Naval Weapons Department of the Navy Washington, D. C. Attention: J. Kay, Code RTMS-41	1
Commanding Officer Office of Naval Research 1030 E. Green Street Pasadena, California 91101	1

	Copies
Director (Code 6180) U. S. Naval Research Laboratory Washington, D. C. 20390 Attention: H. W. Carhart	1
Picatinny Arsenal Dover, New Jersey Attention: I. Forsten, Chief Liquid Propulsion Laboratory	1
Aerojet-General Corporation P. O. Box 296 Azusa, California 91703 Attention: Librarian	1
Aerojet-General Corporation P. O. Box 1947 Sacramento, California 95809 Attention: Technical Library 2484-2015A	1
Aeronutronic Division Philco Corporation Ford Road Newport Beach, California 92600 Attention: Library	1
Aeroprojects, Incorporated 310 East Rosedale Avenue West Chester, Pennsylvania 19380 Attention: C. D. McKinney	1
Aerospace Corporation P. O. Box 95085 Los Angeles, California 90045 Attention: J. G. Wilder, MS-2293 Library-Documents	1 1
Air Products and Chemicals, Inc. Allentown, Pennsylvania Attention: A. Lapin	1
Arthur D. Little, Inc. 20 Acorn Park Cambridge, Mass. 02140 Attention: R. B. Hinckley F. Gabron	1 1

	Copies
Atlantic Research Corporation Shirley Highway & Edsall Road Alexandria, Virginia 22314 Attention: Security Office for Library	1
Battelle Memorial Institute 505 King Avenue Columbus, Ohio 43201 Attention: Report Library, Room 6A	1
Beech Aircraft Corporation Boulder Facility Box 631 Boulder Colorado 80302 Attention: J. H. Rodgers R. L. Reed	1 1
Bell Aerosystems, Inc Box 1 Buffalo, New York 14205 Attention: T. Reinhardt W. M. Smith	1 1
Autonetics 3370 Miraloma Avenue Anaheim, California 92803 Attention: Dr. Edward Lax Dept. 447, Bldg. 202	1
The Boeing Company Space Division P. O. Box 3868 Seattle, Washington 98124 Attention: Library C. F. Tiffany	1 1
The Bendix Corporation Instruments and Life Support Division P. O. Box 4508 Davenport, Iowa 52808 Attention: Wm. Carlson	1
Chemical Propulsion Information Agency Applied Physics Laboratory 8621 Georgia Avenue Silver Spring, Maryland 20910	1

	Copies
Curtiss-Wright Corporation Wright Aeronautical Division Woodridge, New Jersey Attention: G. Kelley	1
University of Denver Denver Research Institute P. O. Box 10127 Denver, Colorado 80210 Attention: Security Office	1
McDonnell Douglas Corporation Santa Monica Division 3000 Ocean Park Blvd. Santa Monica, California 94005 Attention: J. W. Price	1
General Dynamics/Astronautics P. O. Box 1128 San Diego, California 92112 Attention: Library & Information Services (128-00)	1
Convair Division General Dynamics Corporation P. O. Box 1128 San Diego, California 92112 Attention: R. Tatro Paul Stevens	1 1
General Electric Company Flight Propulsion Lab. Department Cincinnati 15, Ohio Attention: D. Suichu	1
Grumman Aircraft Engineering Corporation Bethpage, Long Island, New York Attention: Joseph Gavin	1
The Garrett Corporation 1625 Eye Street, N. W. Washington, D. C. Attention: G. R. Shepard	1

	Copies
IIT Research Institute Technology Center Chicago, Illinois 60616 Attention: Technical Library	1
Goodyear Aerospace Corporation 1210 Massillon Road Akron, Ohio Attention: Clem Shriver, Dept. 481	1
Marquardt Corporation 16555 Saticoy Street Box 2013 - South Annex Van Nuys, California 91404 Attention: Librarian W. D. Boardman, Jr.	1 1
Martin-Marietta Corporation Martin Division Baltimore 3, Maryland Attention: Science-Technology Library	1
McDonnell Douglas Corporation P. O. Box 6101 Lambert Field, Missouri Attention: R. A. Herzmark	1
North American Aviation, Inc. Space & Information Systems Division 12214 Lakewood Boulevard Downey, California 90242 Attention: Technical Information Center, D/096-722 (AJ01) H. Storms	1 1
Northrop Space Labroatories 1001 East Broadway Hawthorne, California Attention: Dr. William Howard	1
Purdue University Lafayette, Indiana 47907 Attention: Technical Librarian	1
Republic Aviation Corporation Farmingdale, Long Island New York Attention: Dr. William O'Donnell	1

	Copies
Rocketdyne Division of North American Rockwell, Inc. 6633 Canoga Avenue Canoga Park, California 91304 Attention: Library, Department 596-306	1
Stanford Research Institute 333 Ravenswood Avenue Menlo Park, California 94025 Attention: P. R. Gillette	1
TRW Systems, Incorporated 1 Space Park Redondo Beach, California 90200 Attention: G. W. Elverum STL Tech. Lib. Doc. Acquisitions	1 1
Union Carbide Corporation Linde Division P. O. Box 44 Tonawanda, New York 14152 Attention: G. Nies	1
United Aircraft Corporation Corporation Library 400 Main Street East Hartford, Connecticut 06118 Attention: Dr. David Rix Erle Martin	1 1
United Aircraft Corporation United Technology Center P. O. Box 358 Sunnyvale, California 94088 Attention: Librarian	1
Cryonetics Corporation Northwest Industrial Park Burlington, Massachusetts Attention: James F. Howlett	1
Martin-Marietta Corporation Denver Division Denver, Colorado Attention: Library D. W. Murphy	1 1

	Copies
National Research Corporation 70 Memorial Drive Cambridge, Mass.	1
New York University University Heights New York, New York Attention: P. F. Winternitz	1
National Aeronautics and Space Administration Flight Research Center P. O. Box 273 Edwards, California 93523 Attention: Library	1
Commander U. S. Naval Missile Center Point Mugu, California 93041 Attention: Technical Library	1